IMPACTS OF MICROGRID INTEGRATION ON DISTRIBUTION SERVICE RESTORATION UNDER COLD LOAD PICKUP CONDITIONS

A Thesis Submitted to the
College of Graduate and Postdoctoral Studies
In Partial Fulfillment of the Requirements
For the Degree of Master of Science
In the Department of Electrical and Computer Engineering
University of Saskatchewan
Saskatoon

By

MARIO ANDRES GONZALEZ CARRANZA

PERMISSION TO USE

In presenting this thesis in partial fulfillment of the requirements for a Postgraduate degree from the University of Saskatchewan, I agree that the Libraries of this University may make it freely available for inspection. I further agree that permission for copying of this thesis in any manner, in whole or in part, for scholarly purposes may be granted by the professor or professors who supervised my thesis work or, in their absence, by the Head of the Department of the Dean of the College in which my thesis work was done. It is understood that any copying or publication or use of this thesis or parts thereof for financial gain shall not be allowed without my written permission. It is also understood that due recognition shall be given to me and to the University of Saskatchewan in any scholarly use which may be made of any material in my thesis.

Requests for permission to copy or to make other use of material in this thesis in whole or part should be addressed to:

Head of the Department of Electrical and Computer Engineering
University of Saskatchewan
57 Campus Drive
Saskatoon, Saskatchewan, S7N 5A9, Canada

OR

Dean
College of Graduate and Postdoctoral Studies
116 Thorvaldson Building.
University of Saskatchewan
110 Science Place
Saskatoon, Saskatchewan, S7N 5C9, Canada

ABSTRACT

Although most distribution systems have benefited from state-of-the-art microprocessor-based devices and modern communication technologies, their design, operation, and control principles have remained unchanged for decades. However, with the deregulation of energy markets and the world being pushed towards the sustainable use of resources and renewable energies, an ever-increasing number of small-scale generation projects are being developed and incorporated into the distribution level, bringing with them a great deal of technical challenges, and defying the traditional operation of the distribution system.

In this research work, a protection and control strategy based on the microgrid concept is proposed for a MV feeder containing distributed generation with the aim of attaining a superior integration with the grid when compared to traditional radial distribution systems. To accomplish this, the functional requirements, and the architecture for a microgrid control system are defined based on IEEE Std. 2030.7. Then, the performance of the distributed generation during steady-state and the transition between microgrid operation modes is assessed under the IEEE Std. 1547 requirements.

Subsequently, the impact of the proposed microgrid islanding strategy on service restoration and interruption costs is evaluated for the severe cold load pickup (CLPU) conditions that may ensue during restoration following extended outages. This analysis is carried out for typical weather conditions in the winter season in Canada when the penetration of heating load is higher than other seasons. In this context, a detailed overview of the CLPU phenomenon is presented beforehand, including a recompilation of several models intended for power system planning and operation purposes, giving particular attention to the physical modelling of thermal loads.

ACKNOWLEDGEMENTS

Foremost, I cannot begin to express my deepest gratitude to my supervisor, Dr. Sherif Faried, not only for having accepted me as his student, but also for his guidance, support, and unwavering diligence throughout the completion of this work. I am also extremely grateful for the financial support he was able to provide me during the program, which was crucial during the unprecedented times the world is living.

I would like to express my most sincere gratitude to Dr. Keaton Wheeler, whose academic and professional advice was extremely valuable for the materializing of this research work. I would also like to express my appreciation for his help in the editing of this thesis and the insightful suggestions he provided during this process.

I would also like to gratefully acknowledge Dr. Mohamed Elsamahy. His guidance during the first stages of this research was the stepping-stone for the realization of this work.

Last but not least, my special thanks go to the people that never stopped believing in me: my parents, my sister, and my life-partner, Mayra. Without their support, unrelenting encouragement, and unconditional love, this would not have been possible.

DEDICATION

To my family and friends.

TABLE OF CONTENTS

LIST OF TABLES

LIST OF FIGURES

LIST OF ABBREVIATIONS

AVR	Automatic Voltage Regulator
CLPU	Cold Load Pickup
CTI	Coordination Time Interval
DER	Distributed Energy Resources
DFIG	Doubly-fed Induction Generator
DG	Distributed Generator
DMS	Distribution Management System
DSO	Distribution System Operator
EPS	Electric Power System
ENS	Energy Not Supplied
GOOSE	Generic Object-Oriented Substation Event
GOV	Machine Governor
LAN	Local Area Network
LV	Low Voltage
MGCS	Microgrid Control System
MV	Medium Voltage
OVMM	Overvoltage Mitigation Module
SCADA	Supervisory Control and Data Acquisition
TOC	Time Over-current Characteristic

Chapter 1

INTRODUCTION

1.1. Distribution Systems

After bulk power generation, and high-voltage power transmission, distribution is the last stage in the power delivery process, attaining the ultimate purpose of every power system: supplying the electric load when required and within adequate power quality margins.

Primarily, the distribution system infrastructure is in charge of reconditioning electric power to make it suitable for consumer-end equipment use. Distribution substation transformers step down the transmission voltage levels to a lower magnitude (henceforth called medium voltage, MV) so that power can be transported in packed urban and rural areas through primary distribution lines, called feeders. Finally, distribution transformers deployed along the feeders reduce the voltage magnitude to utilization level and energize secondary distribution lines to which most users are connected. Typical line-to-line voltage levels for primary MV distribution lines range from 4 kV to 35 kV [1], while voltage levels in secondary LV lines are normally 120/208 V, or 120/240 V.

1.1.1. Radial distribution system

In general, primary and secondary distribution circuits are operated radially. In this configuration, the feeder load is supplied from the distribution substation, which is the only source. As a result, current flows in one direction as shown in Figure 1.1. Usually, radial feeders are linked to others from the same or from a different substation by normally open circuit breakers to guarantee service continuity. If the main source is not available, or if the feeder has been sectionalized upstream due to maintenance or short circuit events, these ties are closed, and a portion of the load is supplied radially from a neighboring feeder, given that it has the capacity to do it.

Radial feeders are conventional and more common among many utilities because of their low cost and operation simplicity [2]. Some of the advantages of this configuration, compared to looped systems, are:

- Simpler protection requirements
- Easier voltage and power flow control
- Lower short circuit currents
- Reduced network complexity

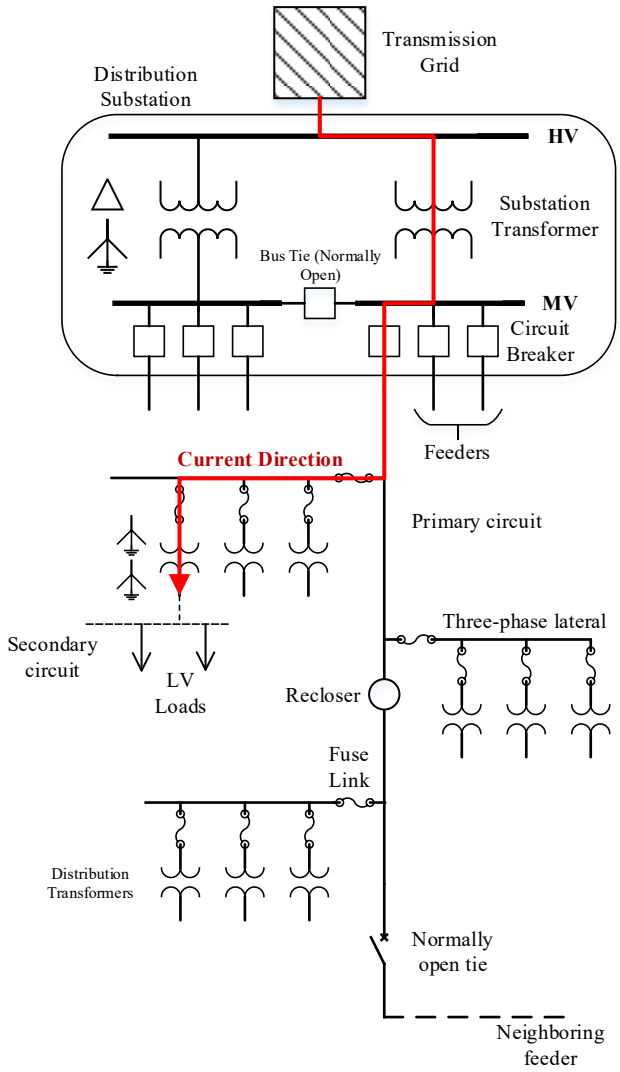

Figure 1.1. Typical radial distribution feeder configuration.

The major drawback of radial circuit configurations is the potentially low reliability (when compared to meshed networks), as downstream customers will experience service interruptions for upstream protection operation due to short circuits. For faults close to the circuit breaker, the whole feeder might lose supply. Feeder sectionalizing along with open ties with adjacent feeders greatly reduce the restoring time for portion of feeder load; however, manual or remote operation of the switching gear may require physical inspection of the line first, which might take some time. Thus, it is not a perfect solution. Meshed configurations are rare, but they offer improved reliability; however, they require more complex and expensive equipment, and in general, are more difficult to operate.

1.2. Protection of Radial Feeders

Distribution infrastructure is exposed to external and internal factors that can cause its equipment to fail or damage, and endanger personnel and customer lives. These factors include adverse weather, physical contact by animals or trees, contamination, and human errors, etc. [3]. In a distribution feeder, the main effects of faults are abnormally high currents and voltage dips caused by short circuits between phases and the ground.

The objective of the protection scheme in a distribution feeder is to properly identify a wide range of short-circuit currents (protection sensitivity) and interrupt them as fast as possible (protection speed) with the least effect to service supply (protection selectivity).

1.2.1. Overcurrent protection

In a traditional radial circuit, the fault current also flows in the same direction as the load current does in normal conditions. Additionally, its magnitude is inversely proportional to the total equivalent impedance from the source to the fault point and proportional to the voltage at the latter. This means that for the same type of fault, the current magnitude decreases when the fault location drifts away from the distribution substation as the impedance increases and the voltage drops if no regulation is present. Conversely, faults occurring closer to the distribution substation yield larger short-circuit current magnitudes as shown in Figure 1.2.

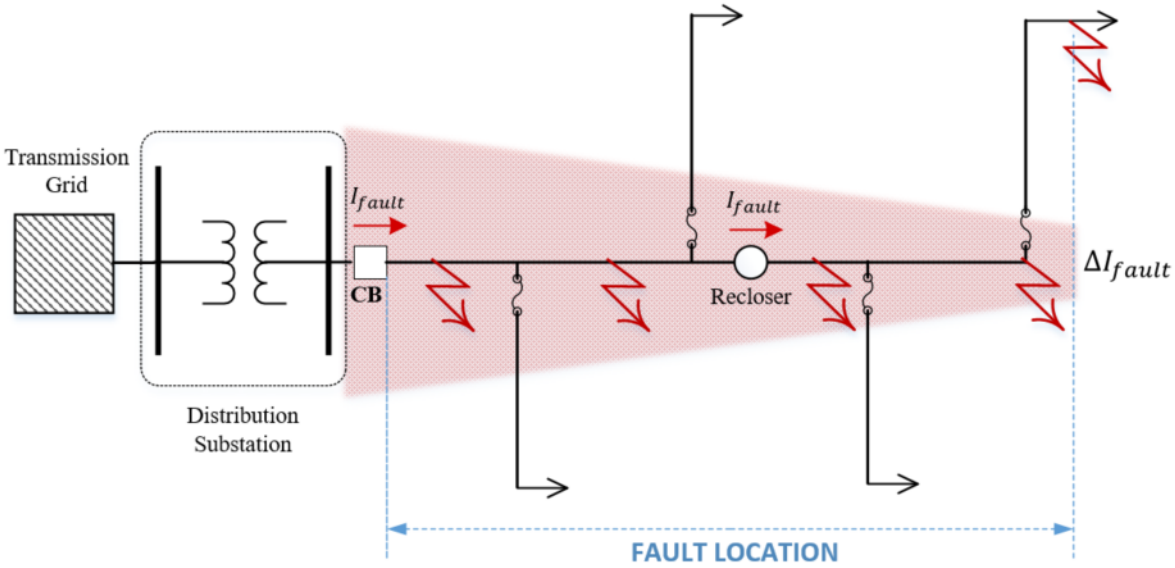

Figure 1.2. Variation of the fault current magnitude with the fault location.

As mentioned in the previous section, the protection strategy is to identify fault currents by measuring and comparing its magnitude. The basic overcurrent protection devices to perform this function are electromechanical relays, microprocessor-controlled relays, and fuses. In the case of overcurrent relays, when a fault is detected, a tripping command is generated (a trip coil is energized in electromechanical relays) and transmitted to the corresponding interrupting gear, such as circuit breakers or reclosers in order to clear the fault. On the other hand, fuses have a circuit-opening fusible part that melts when overheated by over-currents passing through it [4].

Normally, overcurrent protection devices operate under inverse time-overcurrent characteristic curves (TOC), as illustrated in Figure 1.3. This feature enables faster operation of the relay for high fault currents and slower for light currents [3]. In digital relays, these curves primarily resemble the typical operation of electromechanical induction relays, but other customized curves, including definite time and instantaneous curves can also be selected or programed depending on the features of the relay.

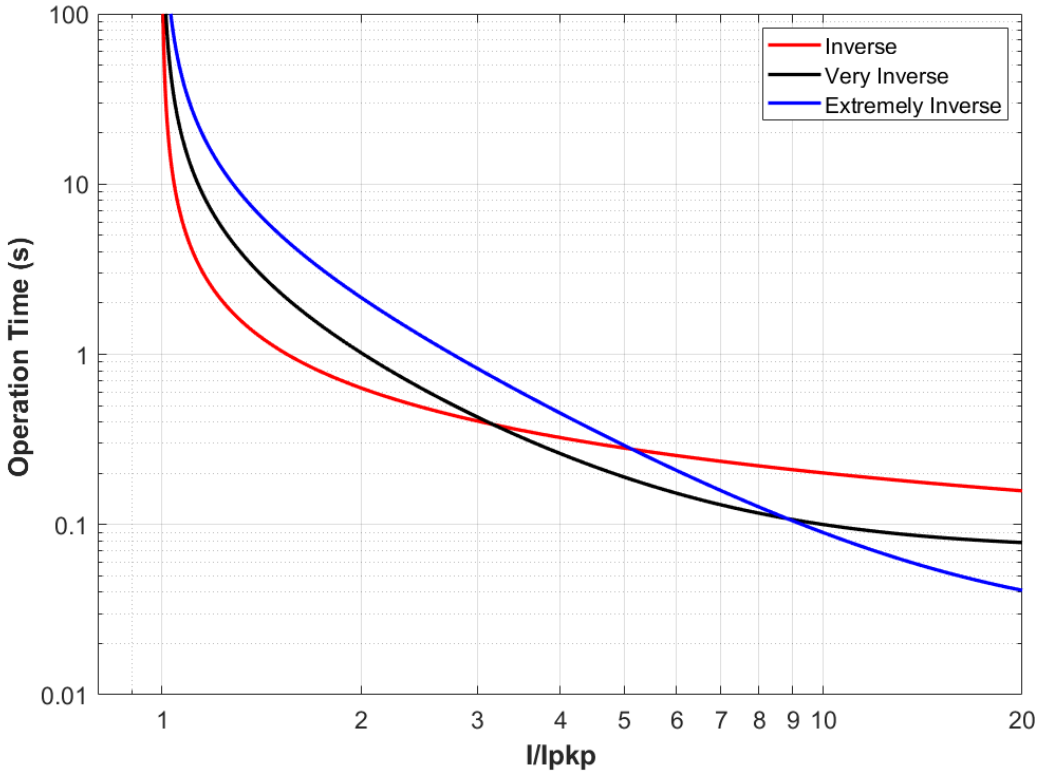

Figure 1.3. Example of time-overcurrent characteristic curves.

The standard operation curves for relays can be approximated using Equation (1.1) [1]. The pickup current setting, I_{pkp}, defines the sensitivity of the relay as it is defined as the minimum current for which the relay must operate accordingly with the curve. Additionally, the time dial setting, TD, allows the curves to be shifted vertically, reducing or increasing the protection speed. The parameters A, B, and p for multiple curves are tabulated in [5].

$$t = TD\left[\left(\frac{A}{\left(\frac{I}{I_{pkp}}\right)^{p} - 1}\right) + B\right] \tag{1.1}$$

The relay pickup setting must be selected such that the relay does not operate for transient or short time currents. There are many criteria to select an adequate value for I_{pkp}; however, the industry standard settings for phase and ground distribution feeder protection, are recommended as follows [1]–[3]:

Phase faults: $I_{pkp} \geq 1.5\, I_{load}$ (1.2)

Ground faults: $I_{pkp} \geq 0.75\, I_{load}$ (1.3)

Where I_{load} is the maximum current expected to be sensed by the relay during the peak load of the system. It must be taken into consideration that large pickup values reduce protection sensitivity.

1.2.2. Protection coordination

To ensure selectivity of the protection system, multiple devices are deployed along the feeder, including relayed circuit breakers, reclosers, and fuses. Then, relay settings and fuse sizes must be properly selected to clear the faults occurring downstream of their installation point, and if possible, provide backup protection for other downstream devices as well. In a radial distribution circuit, selectivity is achieved when fault clearing is performed by the first available device upstream to the fault location while avoiding false tripping of other devices in the same current path. To accomplish that, upstream and downstream devices must be coordinated by means of proper sizing, and adequate selection of TOC curves and time dial settings.

1.2.2.1. Fuse – fuse coordination

Most fuse types for feeder protection applications have extremely inverse time-overcurrent characteristics defined by the melting time and the total clearing time curves. K and T links are the most common fuse types used in feeder protection.

To coordinate two adjacent fuses in the same current path, as shown in Figure 1.4, the total clearing time of the downstream fuse must be not greater than 75% of the melting time of the upstream fuse, to avoid permanent damage of the latter due to short circuit currents outside of its reach [1], [6].

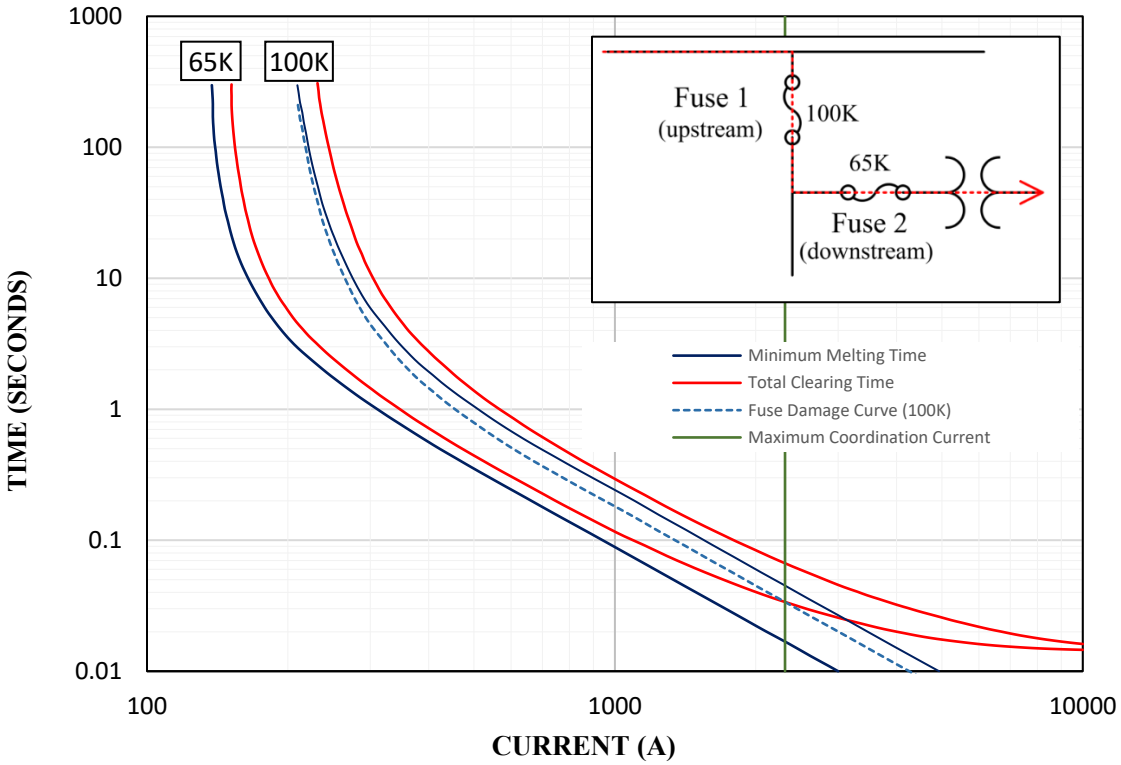

Figure 1.4. Coordination between a 100K and 65K fuse link. The maximum coordination current for these fuses is 2310 A.

1.2.2.2. Recloser-fuse coordination

The main purpose of a recloser is to discriminate temporary from permanent by momentarily interrupting short-circuit currents using a fast TOC curve or an instant element. The interruption must last enough time to allow the arc to extinguish and the air to de-ionize before automatically reclosing. If the short circuit persists after a fixed number of operations, the fast curve (or the instant element) is disabled. Subsequently, the recloser is forced to operate with a delayed or slow curve and lock in the open position afterwards, clearing the fault permanently.

In a recloser, the slow operation curve is used for coordination purposes as it allows the downstream fuses to operate first and clear the fault only if it is permanent. This coordination strategy is known as fuse-saving as its objective is to avoid fuse blowing for temporary faults. Conversely, in a fuse-blowing scheme, the recloser allows the fuse to clear the fault first, whether the fault is temporary or permanent, and performs the reclosing operations only for faults not

protected by other devices. The fuse-recloser coordination curves for both strategies are depicted in Figure 1.5.

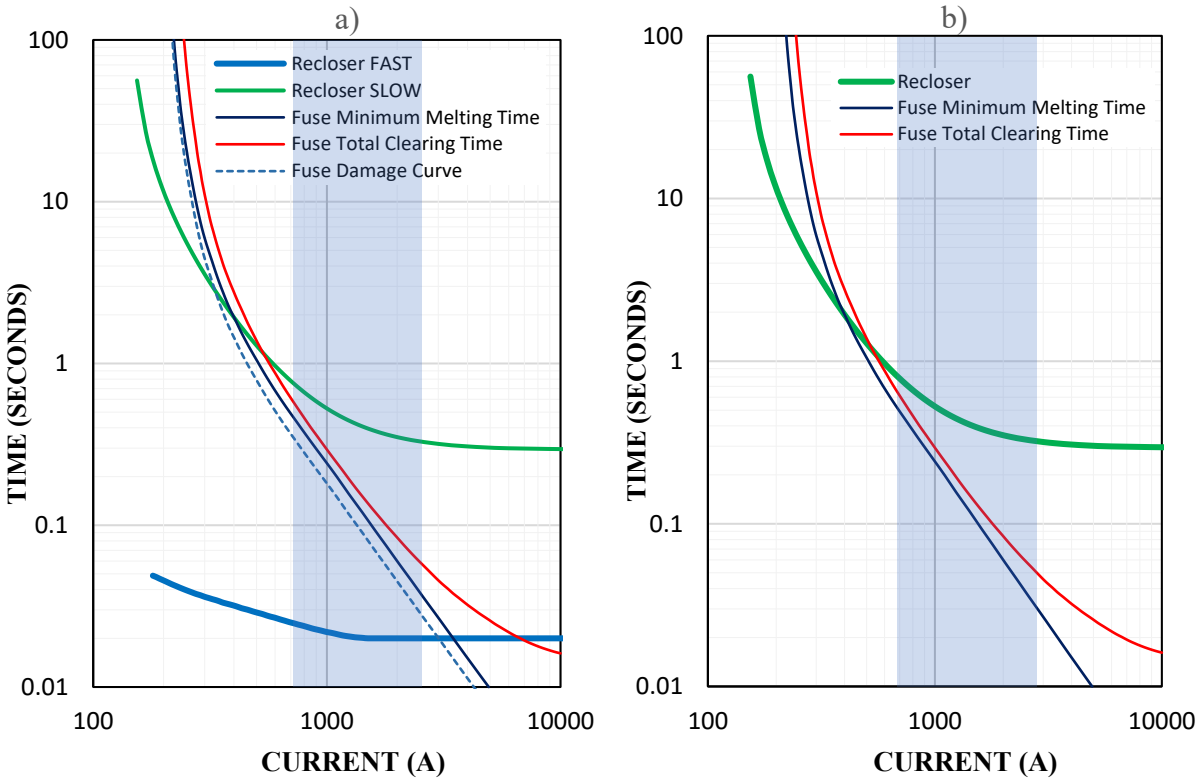

Figure 1.5. a) Fuse-saving scheme, and b) Fuse-blowing scheme.

For a fuse-saving scheme [6], one approach is to coordinate the recloser fast curve, including the breaker interrupting time, with the fuse damage curve (75% of the minimum melting time or as specified by the fuse manufacturer) if the recloser is electronic. The maximum short-circuit current must not exceed the intersection between these curves. For the slow operation, a common approach is to select a time dial setting such that the relay detection time is two times the fuse total clearing time for the minimum short circuit current. Recommended coordination practices for electromechanical relays are reported in [1].

1.2.2.3. Relay-relay coordination

For a proper coordination of two series-connected relayed protective devices, a minimum coordination time interval, CTI, must be maintained for fault current levels for which the upstream relay overreaches the downstream relay protection zone as shown in Figure 1.6. The CTI takes

into account the breaker interrupting time, the relay overtravel (for electromechanical relays) and a safety factor to compensate current transformer saturation and setting errors [7].

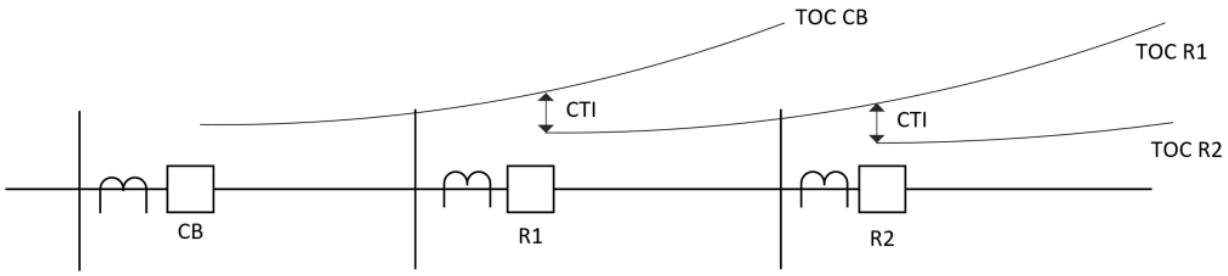

Figure 1.6. Relay-recloser and recloser-recloser coordination using CTI.

For the protection of radial feeders, a CTI of 0.26 second is recommended for coordinating two microprocessor-based multifunction relays for circuit breakers with an interrupting time of three cycles [7]. Additional 0.05 second may be deducted from the CTI if the relays are properly calibrated and tested in field.

1.3. Distributed Generation

Distributed generation refers to any kind of generation technology installed at the distribution level, including distribution substations, and distribution feeders. Traditionally, as passive distribution systems are designed to operate radially, their infrastructure is not normally intended to accommodate distributed generation [8]. For this reason, the presence of distributed generation, especially within feeders has been mostly limited to industrial facilities. However, with market deregulation, climate-change concerns and the need for increased reliability and lower operating costs, an ever-increasing number of small-capacity generation projects are being developed and incorporated to the distribution level, increasing network complexity and defying the traditional operation of distribution systems [9].

There are several types of distributed generator technologies (DG), classified in several groups depending on the generation principle, source type, interconnection with grid, etc. In general, two major groups stand out: conventional and non-conventional generation. Conventional distributed generation encompasses hydropower, and diesel generation, while non-conventional generation refers to renewable energies, such as wind, solar, geothermal, tidal, etc. [9]. For these two types,

the connection with the grid can be either synchronous, for rotating machines at system frequency, or asynchronous through power converters typically for renewable energies as shown in Figure 1.7.

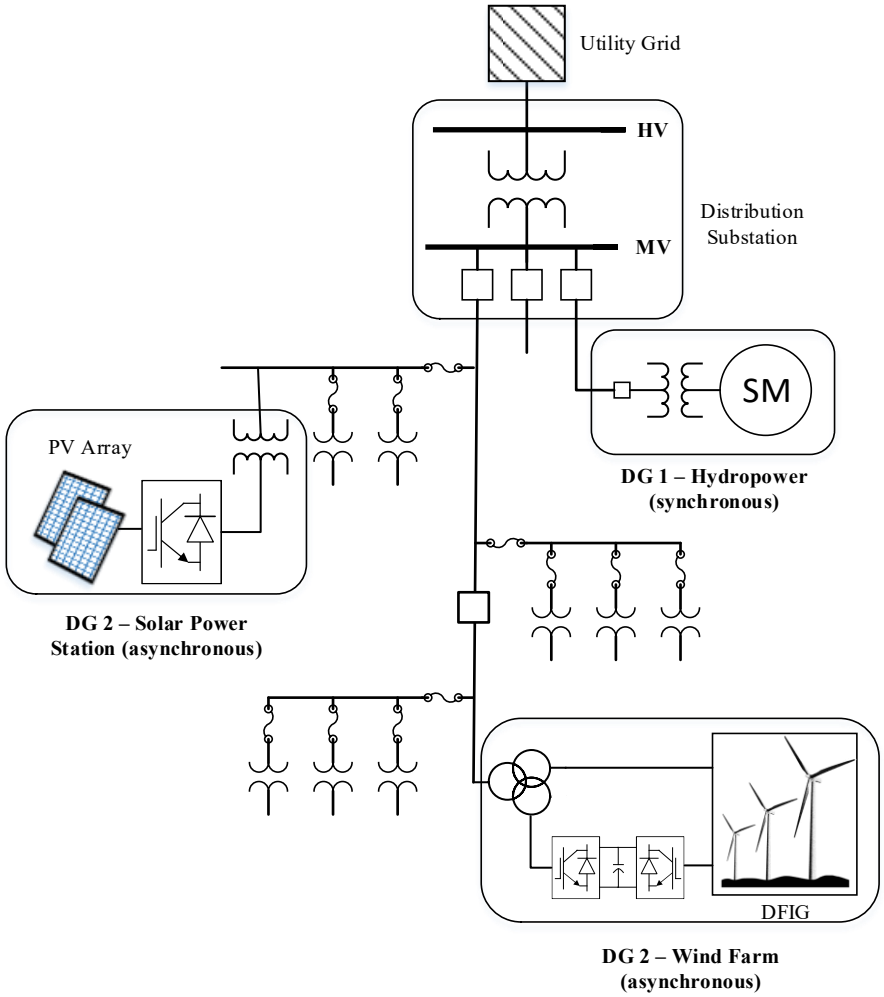

Figure 1.7. Examples of different DGs installed at the MV level.

1.3.1. Impact of distributed generation on MV circuits

The increased network complexity resulting from the presence of distribution generation in the MV level brings about several technical challenges for utilities. Depending on the location and capacity of the DG station the following problems might arise [9]:

- Risk of overvoltages as a result of unexpected unbalance between load and generation, especially with the unpredictable behavior of renewable sources.

- Power quality disturbances during unintentional islanding of the DG with utility load, or during other major switching events, such as a sudden disconnection of generating units.
- Erroneous operation of traditional overcurrent protection devices caused by the increased short circuit levels and loss of radiality.

In the following section, the particular impact of distributed generation on traditional overcurrent protection schemes is presented.

1.3.2. Impact of distributed generation on protection

Typically, the incorporation of distributed generation in a traditional distribution system (primary and secondary) is not compatible with the overcurrent-based protection schemes. As mentioned earlier, this protection concept is based on circuit radiality, and its coordination is only possible due to the predictable change of the short-circuit current magnitude with the fault location. However, with the introduction of distributed generation in the distribution level, both load and fault currents may flow in two directions as in meshed configurations. Consequently, the use of non-directional overcurrent protection for these cases may become troublesome or, in some cases, not suitable. The common problems in feeder protection associated with distributed generation are outlined below [10]–[13]:

- **Protection blinding:** A high contribution from the DG to the fault may reduce the fault current supplied from the utility substation; therefore, protection devices in the path between the substation and the fault may not be able to identify and clear the fault. This problem is more common for faults located near the end of the feeder.
- **Sympathetic tripping:** Faults at adjacent feeders may cause the protection devices in the feeder containing the DG to operate. Sympathetic tripping mainly affects protection selectivity.
- **Loss of recloser-fuse coordination:** Increased fault levels may cause that short-circuit current exceeds the maximum coordination current limited by the intersection point of the fast curve and the fuse damage curve shown in Figure 1.5.
- **Unsynchronized reclosing:** When a distributed generator is separated from the utility by a reclosing device (DG is no longer in parallel with the utility), the DG voltage and angle

may drift away from those of the utility; thus, automatic fast reclosing could not be performed unless synchronism conditions are checked first. Unsupervised reclosing may result in severe power disturbances and mechanical stress in rotating units that could lead to unit shutdown or equipment damage.

During major system disturbances resulting in protection tripping, a DG may continue to energize a portion of the feeder, affecting power quality and interfering with normal service restoration. In order to tackle this problem, most utilities incorporate anti-islanding protection in their schemes to disconnect or shutdown the DG during these scenarios to avert possible islanding conditions. As a result, the DG is prohibited from supplying the grid during outages for as long feeder restoration takes, even when there is sufficient generation capacity to hold an island.

When adequate automated control can be implemented on both utility and DG infrastructure, planned and unplanned islanding operation (e.g., due to protection tripping) could be allowed. A network prepared to allow this type of operation is known as a *microgrid,* which concept, operation and control fundamentals are covered in Chapter 3.

1.4. Research Objective

This research project has two main objectives:

The first objective is to develop a novel protection and control scheme based on the microgrid concept for a typical Canadian MV feeder containing a synchronous-machine-based DG. To accomplish this, a selective and fast protection scheme is designed for the distribution feeder to properly accommodate the DG while also coping with the technical challenges listed in Section 1.3.2. Subsequently, a control scheme is proposed to allow DG islanding for scheduled and unscheduled events, such as protection operation after short circuits, converting a portion of the original feeder into a microgrid. The functional requirements for the control system are specified under the recommendations presented in IEEE Std. 2030.7 [14]. Moreover, the approach for the mitigation of the power quality issues that may arise during unbalanced transitions is design to comply with IEEE Std. 1547 [15]. For validation purposes, the protection and control schemes proposed in this research work are implemented and simulated (time domain) in the EMTP-RV program.

The second objective is to investigate the impact of microgrid islanding on service restoration under the significant cold load pickup (CLPU) conditions that may ensue following extended outages. In this context, a load model is presented to physically emulate the behavior of residential heating load amid typical weather conditions in the Canadian winter season, including the severe loss of load diversity that occurs during prolonged interruptions, normally leading to significant overcurrents during restoration. The approach for the assessment of the level of impact is aimed at the estimation of restoration times, energy not supplied during the interruption, and the corresponding costs to utilities.

1.5. Organization of the Thesis

This thesis is organized into five chapters, as follows:

In Chapter 1, the basic concepts and notions of the conventional operation and protection of distribution systems are introduced, including a brief description of the technical challenges and effects of introducing generation in the distribution level.

In Chapter 2, a detailed overview of the cold load pickup phenomenon is provided, covering its components, causes and effects on distribution systems. Additionally, a recompilation of several CLPU models intended for power system planning and operation studies is presented, giving particular attention to the physical modelling of thermostat-controlled residential load.

In Chapter 3, the microgrid concept is introduced, including the fundamentals of microgrid operation and control. Subsequently, the specifications for a protection system and the functional requirements for a microgrid controller are defined for a MV distribution network containing a microgrid with a synchronous-machine-based distributed generator. The performance of the proposed approach is evaluated during transitions between operation modes.

In Chapter 4, the physical load model presented in Chapter 2 is used to evaluate the effect of the unintentional microgrid islanding strategy proposed in Chapter 3 on service restoration under the severe CLPU conditions that may arise after extended outages. A quantitative assessment focusing on the estimation of restoration times and interruption costs is presented.

Finally, in Chapter 5, the conclusions derived from this research work are listed.

Chapter 2

COLD LOAD PICKUP MODELING

2.1. Introduction

The instantaneous load in a distribution feeder is the sum of all the individual customer loads connected to it at the same time. Whereas it is possible to stochastically predict the daily load behavior of a group of customers with similar characteristics, it is technically difficult to predict the behavior of single customers due to their unique consuming habits. For instance, the operation cycles of several thermostat-controlled household appliances such as baseboard heaters, water heaters, or refrigerators are constantly being altered as a result of random customer usage during the day. For this reason, individual peak loads tend to be non-coincident with one another, and consequently, with the peak load measured at the distribution transformer or at the feeder to which they are connected. Hence, as the number of customers increases, the probability of having coincident peaks decreases, and the load become more diversified. To measure the diversity of the load, two factors are used: the diversity factor (DF), and the coincident factor (CF) [1], [2] defined as:

$$DF = \frac{\sum_{i=1}^{N} D_{\max i}}{D_{peak}} \geq 1 \tag{2.1}$$

$$CF = \frac{D_{peak}}{\sum_{i=1}^{N} D_{\max i}} = \frac{1}{DF} \tag{2.2}$$

Where,

D_{max} individual non-coincident peak load,

D_{peak} system peak load, and

N number of customers connected to the system.

For example, a diversity factor of 1.0 (lowest diversity) means that the individual peak loads coincide 100% during the system peak load while a diversity factor of 3.0 ($CF = 1/3 = 0.333$) represents that only 33.3% of each customer's peak load coincide during the system peak. Table 2.1 shows the diversity factor at different levels of a distribution system [14]–[17].

Table 2.1. Diversity Factors in a distribution system.

Component	Diversity Factor	
	Reported in [19]	Reported in [17][1]
Individual Customer	1.0	1.0
Distribution Transformer	1.44	1.67
Primary Lateral	-	1.86
Feeder	1.95	-
Substation	2.24	2.00

[1] For urban areas during summer or winter

Although diversity and coincident factors are mostly used by distribution engineers to assess the loading of distribution transformers and feeders, their concept can be used to illustrate the causes and effects of cold load pickup.

2.2. Cold Load Pickup

Usually, following extended outages, the restored load is considerably higher than the pre-outage load as a consequence of the loss of diversity of the load and magnetizing inrush currents. This phenomenon is known as *cold load pickup* (CLPU). The term refers to the attempt of picking up load after it has reached a "cold" state when supply has been interrupted for a prolonged period of time [20].

A cold load could reach magnitudes of over three times the pre-outage load and progressively decay back to normal as it regains diversity; this process may take from a few minutes to several hours [21]. In general, the magnitude and duration of the CLPU effect depend on many factors, such as the composition of the load, the weather conditions, season, and the duration of the outage [22]. These factors are covered in more details in the following sections.

Figure 2.1 shows a CLPU event in the BC Hydro distribution system during the reconnection of a 69 kV subtransmission line radially supplying a rural substation and a small customer-owned substation [23]. The current was measured by the line relay and corresponds to the total load of both substations. As it can be observed, after a four-hour outage, the CLPU magnitude reached 2.22 times the pre-outage load, decaying back to normal conditions in approximately 45 minutes.

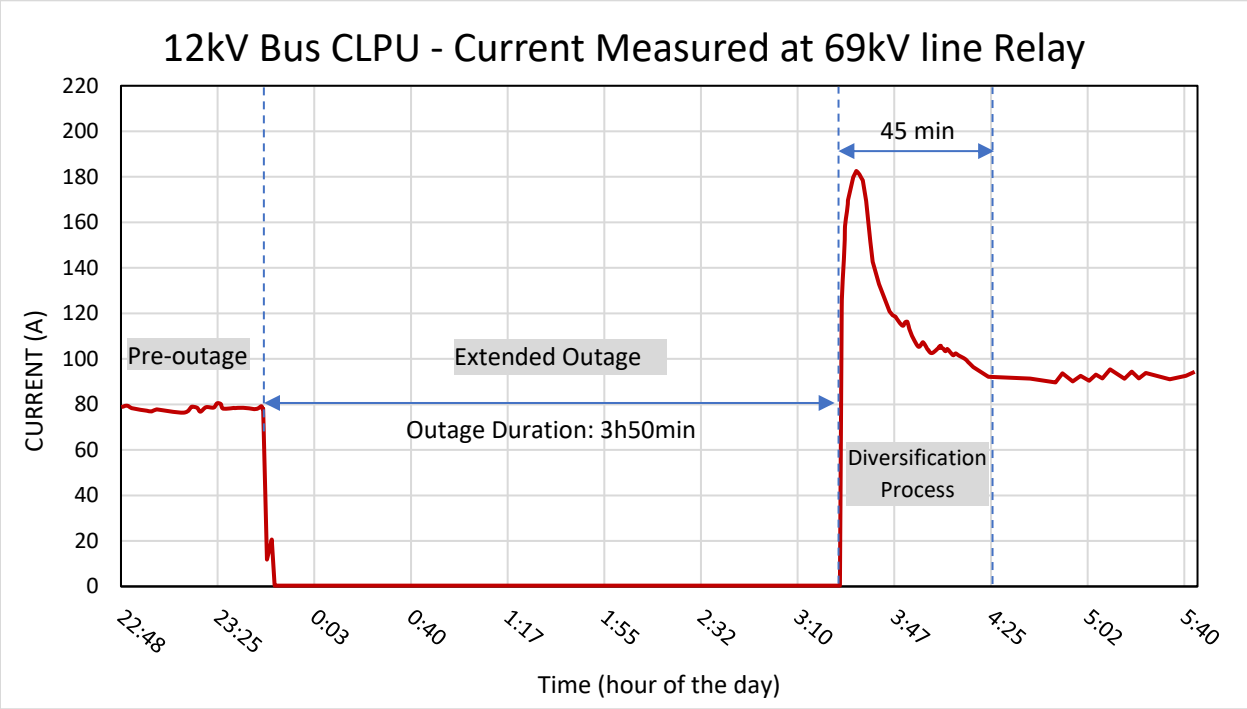

Figure 2.1. CLPU effect after a 4-hour outage.

CLPU can be divided into two stages: the inrush phase, and the enduring phase. During the inrush phase, the current magnitude can reach up to 15 times the pre-outage level [24]. The main components of the first phase are the transformer magnetizing currents, motor acceleration inrush currents and electrical lighting inrush currents. Usually most of these currents die out in less than 5 cycles, but overall, the inrush phase ends in few seconds after motors have reached steady-state operation (less than 15 seconds) [25]. Conversely, in the enduring phase, currents could be above 2 to 3 times larger than the pre-outage level. However, as mentioned before, this current returns to normal in a slow process that may last several hours depending on the severity of the loss of load diversity.

2.3. Factors Affecting CLPU

2.3.1. Thermostat-controlled loads

Even though the CLPU phenomenon is common among utilities, it is more significant in distribution systems with large penetration of electric thermostat-controlled HVAC loads, such as air conditioning, baseboard heaters, and water heaters. These types of appliances operate in highly variable cycles, maintaining diversity in normal conditions [24]. When power supply is lost, temperature changes will occur due to the natural heat transfer between inside spaces and the outside, either by conduction, convection or radiation [26]. The appliance and building insulation help reduce the incoming or outgoing heat flow; however, as insulation is not perfect, considerable variations in temperature will eventually occur during extended outages. When service is restored, thermostats will try to recover pre-outage temperature conditions simultaneously, resulting in significant coincidence of the load (loss of load diversity), and consequently, higher load demand. The severity of the loss of diversity will depend also on the outside temperature, season of the year and duration of the outage.

2.3.2. Outage duration

One of the main factors affecting the load diversity, and thus CLPU is the outage duration [20]. Thermal or weather-sensitive loads do not instantly reach a "cold" state since the temperature can be held within thermostat limits for some time depending on the level of insulation of the appliance or the building. As a result, diversity is not significantly impacted during short interruptions. However, this condition cannot be maintained if the outage is extended for long periods, increasing the severity of CLPU during restoration. Likewise, other small appliances will lose diversity if their operation intervals are shorter than the outage duration as their cycles will restart simultaneously when service is re-established. In general, the outage duration depends on many factors, such as the outage cause and location of the fault, factors that have a direct repercussion on repairing times.

2.3.3. Weather conditions and season of the year

Ambient temperature is another significant factor that affects both the duration and magnitude of CLPU. Moderate to extreme ambient temperatures (summer or winter) directly impacts the behavior of weather-sensitive loads (HVAC) as they accelerate the heat transfer between inside

and outside spaces. As a result, the operating cycles of these devices are affected along with diversity of the load. Additionally, weather-related conditions, such as storms, snow, and reduced visibility, can affect repairing times of faulted outdoor equipment, prolonging the outage duration.

2.3.4. Magnetizing inrush currents

Distribution transformers can draw high inrush currents for several cycles to magnetize their cores when re-energized. The magnitude and duration of the inrush give shape to the initial CLPU magnitudes and depend on the magnitude of the voltage, the reclosing instant, and the system relative impedance to the transformer size. Whereas energizing a single distribution transformer may cause inrush currents up to 30 times its full-load current, energizing multiple transformers at once (e.g., a lateral tap or a whole feeder) reduces the system voltage, and therefore, less inrush current is drawn from each transformer. The inrush current while picking up the load of a whole feeder is estimated to be 5 times the total installed kVA [1].

2.3.5. Electric lighting

Lighting load, usually connected to the utilization voltage, also draws short-lived inrush currents [20]. Field tests have determined that the inrush current to heat the resistance of tungsten filament lamps may be over 7 times its nominal value. Depending on the size of the lamp, the duration may last over 12 cycles before stabilizing. Similarly, the ballasts of pressure discharge lamps can draw over 20 times the steady state current, yet the duration is usually less than two cycles [27].

2.3.6. Motors

Motors for residential, commercial, and industrial applications may draw five to eight times the rated current during start-up. Nonetheless, motor contribution to CLPU is not significant since large industrial motors are commonly protected with contactors to prevent automatic re-starting after service is restored. On the other hand, low power motors for residential use, such as small water pumps, and cooling fans have a small share in the composition of the load, so they are negligible.

2.3.7. Distributed generation

As discussed in Subsection 1.3.2, anti-islanding protection disconnects the DG from the distribution network during system disturbances and outages. Normally, service is restored by the

main grid alone, and DGs are reconnected afterwards when conditions allow it [13]. This results in the utility being forced to pick up its own load in addition to the load supplied by the DG before the outage, causing a significant difference between the pre-outage load and the load during restoration. The CLPU level reached to compensate the delayed contribution of distributed generation during the restoration depends on the DG size, the power dispatched before the outage and how long it takes to reconnect it after service is re-established.

It is important to mention that utility infrastructure is typically able to endure the extra load indefinitely without risking overloading as their components are designed not only to operate without the presence of distributed generation, but also to allow normal load growth. However, the current level during service restoration may interfere with non-adaptive protection systems designed specifically to accommodate distributed generation.

On the other hand, DG units allowed to operate in an island with utility load are beneficial to reduce the effect of CLPU as they reduce the loss of load diversity severity by keeping clusters of loads supplied during outages. This is explored in the next chapters.

2.4. Adverse Effects of Cold Load Pickup on Distribution Systems

The cold load pickup phenomenon is inherently an overcurrent condition. Hence, the effects of CLPU on a distribution system derive from the circulation of high currents through its elements. In the following sections, the most relevant adverse effects are presented.

2.4.1. Transformer overloading and aging

The impact of CLPU on distribution and substation transformers has been widely studied in the literature [22], [28]–[30]. During restoration under CLPU conditions, the transformers in the grid, including the substation transformer must endure high currents, above two times their rated value for several minutes (even hours) while the load regains diversity, especially in distribution networks with high penetration of electric heating (slow diversification). As a result, high temperatures in the windings and the oil might arise, degrading the insulation, and reducing their life expectancy. Figure 2.2 shows the relation between the pre-outage load, the appearance of hot spots and the loss of life of oil-immersed transformers for different outage durations [30].

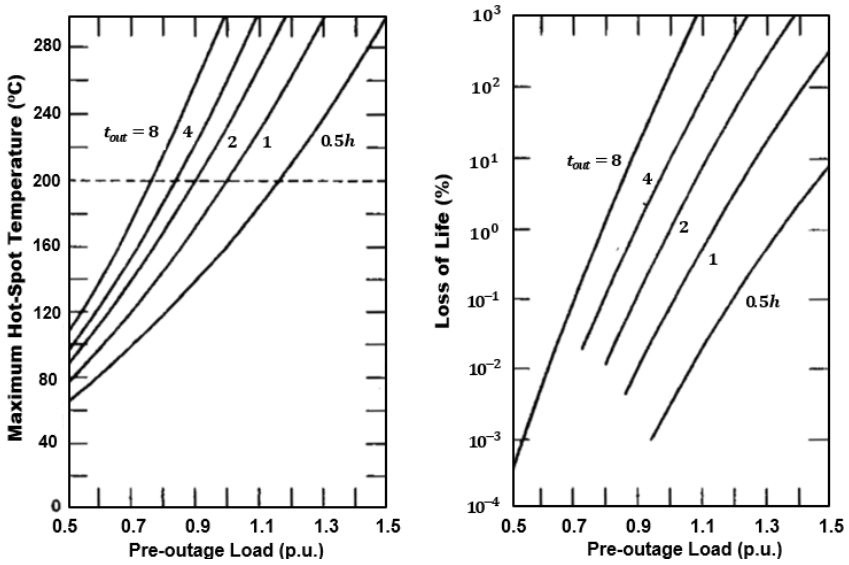

Figure 2.2. CLPU effect in loss of life of distribution transformers.

2.4.2. Increased power losses

Active power losses in passive elements such as lines and transformers are directly proportional to the square of the current circulating through them (I^2R). During the system peak load, losses are predominantly from primary lines [1]. A study from EPRI revealed that 75% of the analyzed distribution circuits presented losses over 3.0% during the system peak [31]. In CLPU conditions, the losses could reach k^2 times the losses during the system peak load, where k is the ratio between the CLPU current and the peak load current. For example, if the current during a CLPU event is two times the peak load current, the losses will increase 4 times. The increased losses during CLPU will persist until the current settles back to normal.

2.4.3. Nuisance tripping of protection devices

As an overcurrent condition, CLPU may potentially cause the false tripping of inverse-time and instant overcurrent relays as well as fuse blowing for non-fault currents. This situation may arise when the CLPU level is higher than the expected minimum short circuit current or the relay pickup setting [23]. Based on the current magnitude, the inrush phase of CLPU could affect the instant element of overcurrent relays while the enduring phase mainly affects inverse-time relays and fuses.

CLPU affects fault detection as it could reach levels that can be easily mistaken as fault currents, causing the re-opening of circuit breakers and reclosers during service restoration. Therefore,

CLPU may result in the lengthening of the outage duration, and consequently, further loss of load diversity, making subsequent attempts to re-stablish service less probable to succeed. Figure 2.3 shows a sequence of multiple attempts to restore a feeder in a distribution substation radially supplied by a single 69 kV line [23], [32]. Since SCADA was not available in this substation, the effect was recorded by the telemetry of the subtransmission line. In total, nine unsuccessful reclosing attempts were performed before CLPU-related protection tripping was deemed to be the cause. In this particular case, CLPU resulted in an outage extension of more than one hour for a total outage time of around five hours. The feeder load was finally restored by sections, starting with the areas close to the substation.

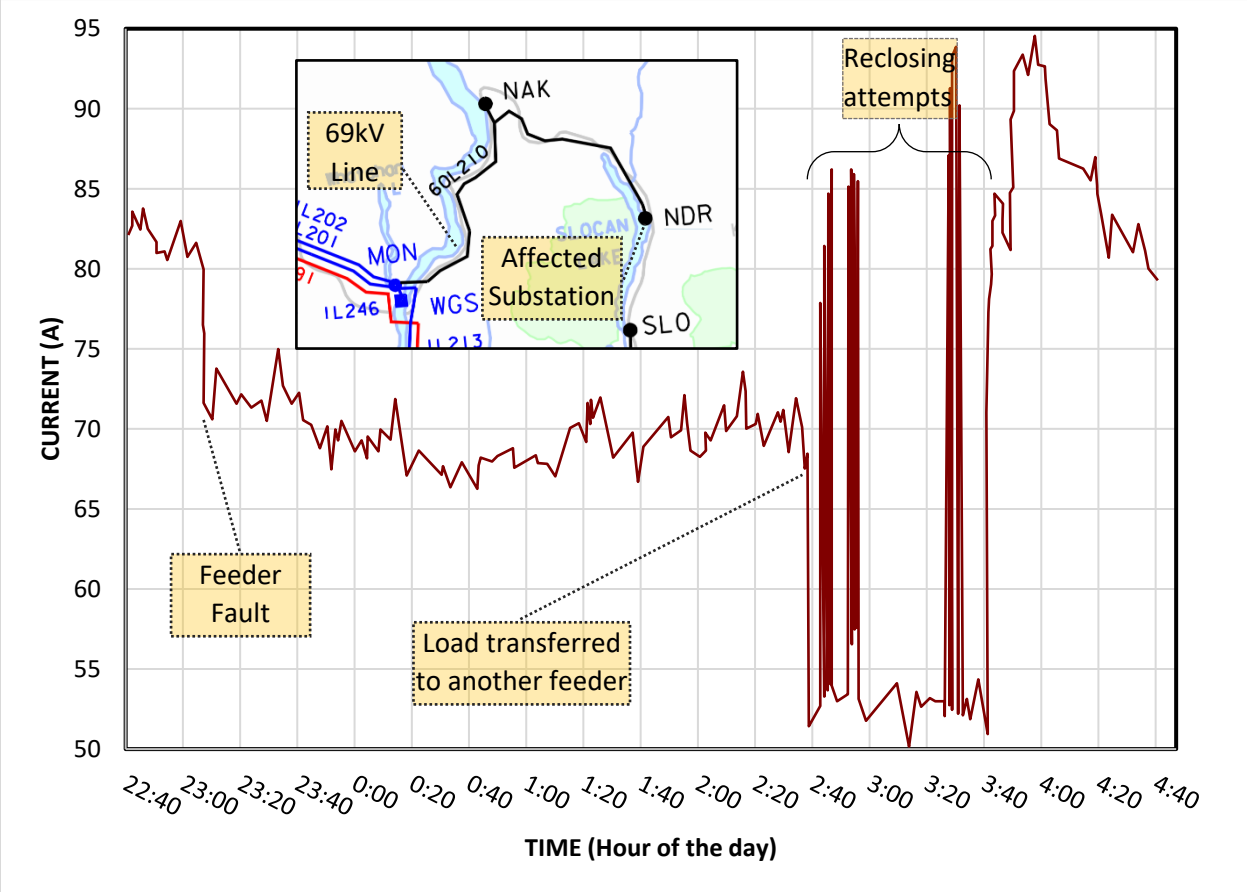

Figure 2.3. Several failed attempts to restore a feeder during CLPU seen from the upstream subtransmission line 60L210.

Protection issues related to CLPU are, in fact, quite common. In a IEEE Survey [33], 75% of 102 responding utilities reported that they have had problems associated with CLPU. Of these utilities, 87% reported tripping of time-overcurrent relays, 60% of which reported phase relay operation,

10% ground relays, and 30% both phase and ground relays. Moreover, the same survey revealed that 62% of the cases were associated with outages lasting more than 45 minutes. To cope with nuisance protection tripping during CLPU, utilities usually resort to one or more of multiple restoration methods discussed in the following section.

2.5. Traditional Restoration Practices

2.5.1. Feeder sectionalizing

The most common practice to restore a feeder following an extended outage is to sectionalize it and re-establish it by parts. With this approach, the cumulative effect of CLPU on upstream devices can be reduced, as shown in Figure 2.4. In this example, the feeder load is divided into two sections. Instead of picking up the whole feeder load at once, a smaller load encompassed in a section of the feeder is restored first. The second section is re-established after enough diversification has been achieved in the previously restored section. Note that if the feeder is not restored by parts, the head-end relay may trip during restoration if the initial CLPU level persists above the pickup setting, within the time-overcurrent operation threshold.

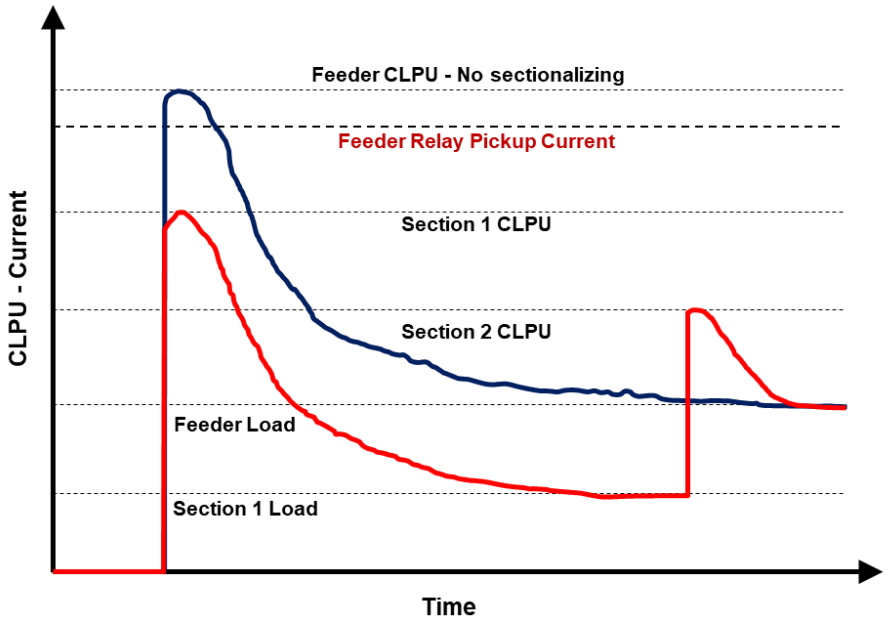

Figure 2.4. Effect of restoration by sections on CLPU level.

The drawback of this approach is that restoration may take up to several hours before all sections are restored depending on the length of the feeder. Since sufficient time must elapse to allow

diversification of one section before energizing the adjacent next, customers in the tail-end sections of the feeder may experience prolonged service interruptions.

2.5.2. Reducing feeder voltage

As discussed in Section 2.3.1, the largest contributors to CLPU in terms of power and affectation to loss of diversity are resistive heating loads, such as space and water heaters. As these types of devices behave as constant-impedance loads (mostly resistive), the drawn power is proportional to voltage square. Thus, reducing the voltage during restoration will decrease the CLPU magnitude as less power and current are drawn. In [22], a reduction of around 20% of the initial CLPU magnitude was achieved by reducing the voltage 15% of its rated value.

Conversely, this approach is not always feasible to execute for several reasons. The most important is that the higher demand during CLPU results in higher losses, and thus, significant voltage drops occur along the feeder. This means the system voltage magnitude may be already compromised and further reduction may result in power quality issues, especially for customers far from the distribution substation. Additionally, constant power loads such as motors will draw more current when voltage is reduced. However, this effect is less significant because their share in the total load is low. Moreover, a reduced voltage also affects thermostat-controlled loads as their operating cycles may become longer in order to compensate for a lower power consumption, resulting in slower diversification of the load and a longer enduring phase [22].

2.5.3. Adjusting protection settings

Directly adjusting protection settings to inhibit its operation during CLPU is usual practice among utilities. There are several approaches to mitigate CLPU-related tripping of protective devices, such as adjusting relay parameters (pickup setting and time dial), tailoring CLPU curves, and even disabling protections during restoration.

The most common approach is to permanently increase the pickup current setting of relays and reclosers above the expected CLPU level. Several studies [1], [3], [19] recommend using pickup settings up to 2 times the peak load current along with extremely inverse TOC curves to override CLPU. However, if CLPU is higher than the pickup setting, this solution is ineffective if the inverse-time characteristic does not allow the current magnitude to subside before tripping. On the other hand, using a pickup setting above $2 \times I_{load_{max}}$ will cause loss of sensitivity (protection

blinding), and thus, it is not recommended. Figure 2.5 shows a family of extremely inverse curves (different time dials) with a pickup setting of 2 times the maximum load current. As it can be observed, none of the curves will pick up CLPU levels up to $2 \times I_{load_{max}}$ since there is an asymptote at $1 \times I_{pkp}$. For CLPU currents above twice the maximum load, the uppermost curve will allow diversification of the initial CLPU between 5 to 15 minutes (for CLPU levels up to $2.5 \times I_{load_{max}}$) whereas the bottom curve may cause tripping if current has not dropped below the pickup value as fast as 10 seconds.

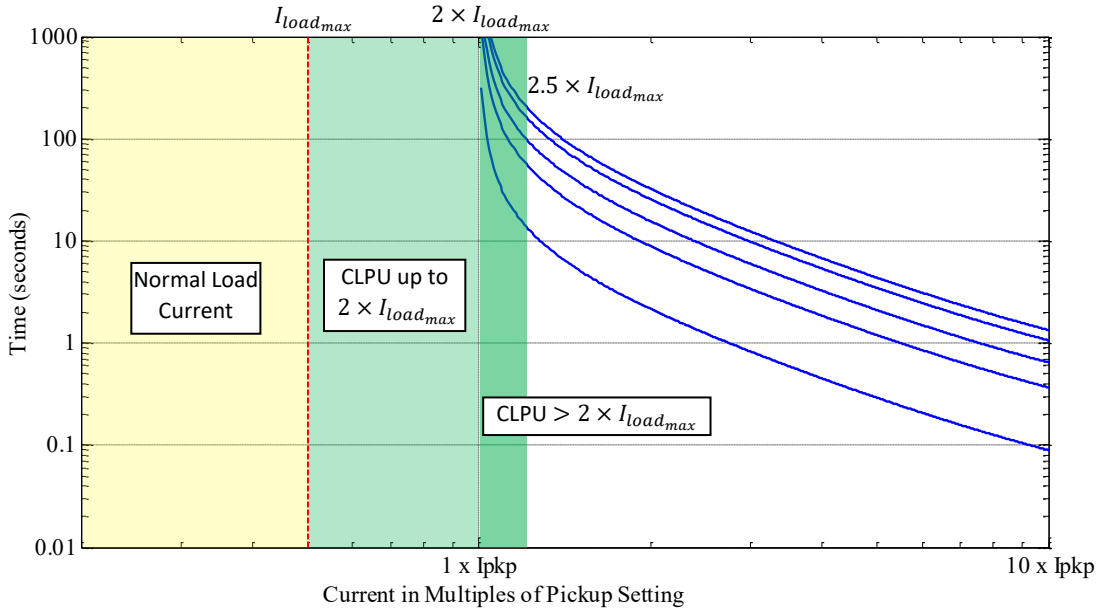

Figure 2.5. Normal Load and CLPU current ranges sensed by protective relays.

The major drawback of this approach is that using pickup settings above $1.5 \times I_{load_{max}}$ (industry standard) reduces protection sensitivity as discussed in Section 1.2.1, especially for high impedance faults. Additionally, the selection of the TOC curve and the time dial may be limited by protection coordination and speed requirements. For instance, using the uppermost curve in see Figure 2.5 would result in slow detection and clearing of high-current faults.

Another approach to overcome the speed problems caused by using extremely inverse curves with high time dials is to tailor the protection curves to override CLPU [20]. Modern microprocessor-based multifunction relays allow the customization of TOC curves to fit a particular need such as maximizing protection speed under CLPU conditions [34]. Figure 2.6 shows a customized time-overcurrent curve comprising an extremely inverse curve with a time dial of 10 for CLPU current

levels up to $2 \times I_{load_{max}}$. For higher short circuit currents, a faster extremely inverse curve (lower time dial) and an instantaneous element are used. This guarantees fast operation for short circuit currents while allowing some diversification time for the initial CLPU.

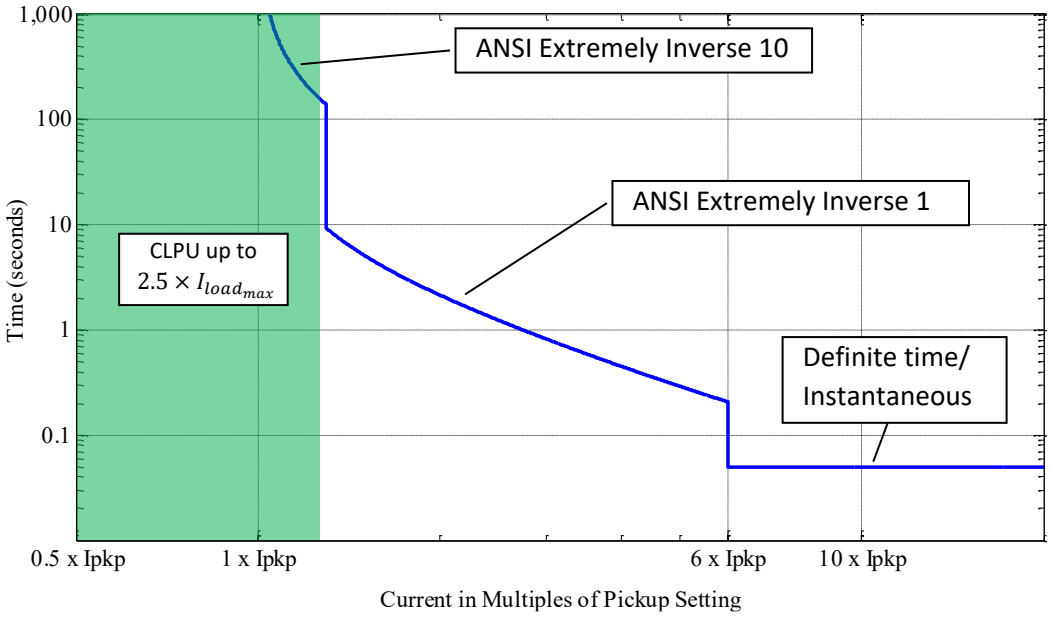

Figure 2.6. TOC customization for CLPU overriding**.**

Even though this approach solves the protection speed problem for short circuit currents higher than the expected CLPU levels, the protection operation speed and sensitivity for high-impedance faults remains low.

Disabling protections to avoid nuisance tripping during restoration under CLPU conditions is the least recommended practice of all, as it leaves the system vulnerable to faults for as long this measure is taken. In cases in which the fault has not been properly repaired or removed due to human error, faulty replacement equipment, or because the outage cause was not properly identified, a subsequent fault upon restoration may occur. Thus, if protections are inhibited or disabled, faults during service re-establishing may go off undetected, posing a high danger to lives, property, and equipment. Consequently, the application of this approach is limited to instant elements in overcurrent relays and fast curves in reclosers, which could be temporarily disabled only if their protection zones are thoroughly backed up by inverse-time elements or other upstream devices.

2.6. Cold Load Pickup (CLPU) Modeling

2.6.1. General CLPU model

Estimating the CLPU level following an outage is imperative for multiple purposes, such as predicting transformer and feeder overloading, sizing conductors, determining feeder configurations, and anticipating tripping of protective devices. Several models have been developed to estimate the power or current during CLPU conditions [20], [33]–[36]. Some of these models are based on the quantification of previous measured events while others focus on the composition of the load and the physical behavior of heating loads.

The estimation approach presented in [28] and generalized in [30] has been widely used by utilities to predict and analyze the CLPU effect on distribution feeders and transformers. The model aims to estimate the power demand in a feeder after service interruption by means of physically modeling weather and non-weather sensitive loads under different weather conditions. Although the physical models are not shown in detail, a piecewise linear representation of the CLPU shown in Figure 2.7 is presented [30].

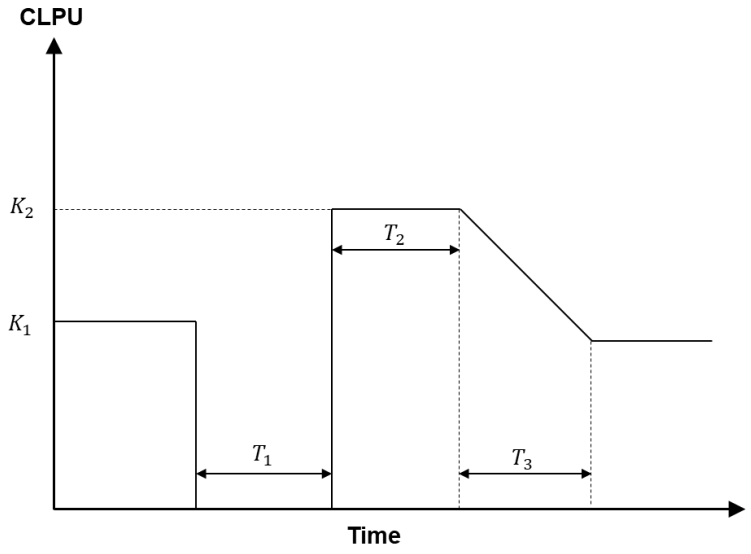

Figure 2.7. Piecewise linear representation of CLPU**.**

The model considers the following parameters:

T_1 duration of the outage,

T_2 duration of the overload (initial CLPU),

T_3 duration of the re-diversification process,

K_1 pre-outage load, and

K_2 initial CLPU magnitude.

Sets of values for multiple winter temperatures are shown in Table 2.2 [30].

Table 2.2. CLPU parameters different ambient temperatures.

Temperature (°C)	$\boldsymbol{T_1}$ $\boldsymbol{(h)}$	$\boldsymbol{T_2}$ $\boldsymbol{(h)}$	$\boldsymbol{T_3(h)}$	$\boldsymbol{K_1/K_2}$
0	1	0.17	0.17	3.70
-20	1	0.34	0.34	2.74
-40	1	0.52	0.52	2.10

While the estimation of these parameters is empirical, CLPU for different outage periods and ambient temperatures can be approximated using Equation (2.3).

$$T_3 = T_2 = 0.0083(20 - \theta)T_1 \tag{2.3}$$

Where θ is the ambient temperature in degrees Celsius.

This model is usually agreed upon by Canadian utilities as it provides relevant information to system operators to estimate CLPU when information is insufficient to build more precise models [22]. In the following sections, extensions to this model to include the stochastic behavior of the load and the non-linearity of the diversification process are presented.

2.6.2. Extension to the general model

2.6.2.1. Non-linear diversification

The general model presented in the previous section considers a linear re-diversification process with duration T_3 as shown in Figure 2.7. Conversely, recorded CLPU events in several utilities [22], [23], such as the one presented in Figure 2.1, have shown that in fact, the load decays exponentially before settling back to normal.

In [39], the delayed exponential CLPU model shown in Figure 2.8 is presented. Note that the CLPU is built piecewise, similar to the general model, yet only two sections are considered: the initial CLPU for $T_i \leq t < t_i$ and the diversification process for $t \geq t_i$.

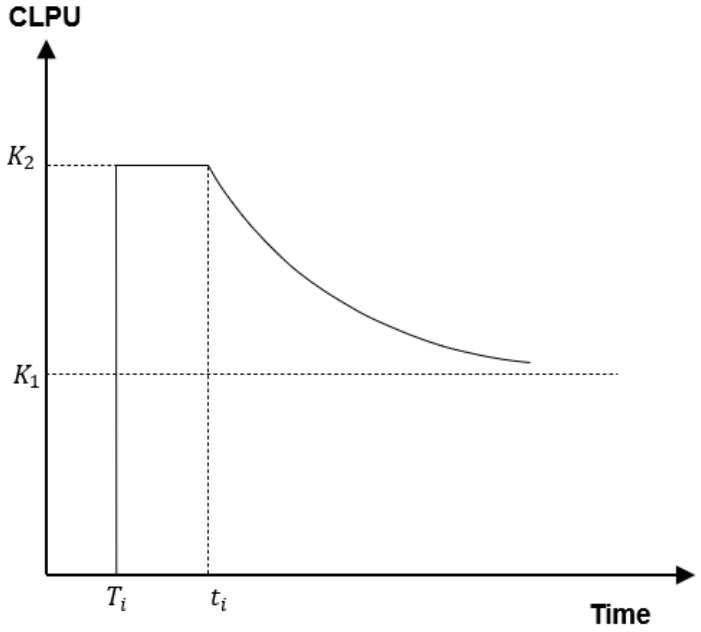

Figure 2.8. Delayed Exponential CLPU Model.

The mathematical expression for this model in terms of the variables of the general model can be written as follows:

$$CLPU = I(t) = \left[K_1 + (K_2 - K_1)e^{-\alpha(t-t_i)}\right]u(t-t_i) + K_2[1-u(t-t_1)]u(t-T_i) \qquad (2.4)$$

Where,

$u(t-\tau)$ unit step function with delay τ, and

α rate of load decay.

Figure 2.9 shows the approximation of the real CLPU case from Section 2.2 using both models. The maximum CLPU current magnitude is 180 A (K_2) and the diversified load is around 90 A (K_1). As it can be observed, using the general piecewise linear model, such that $T_2 = T_3$ as suggested by Equation (2.3), results in an underestimation of the total time to reach complete diversification.

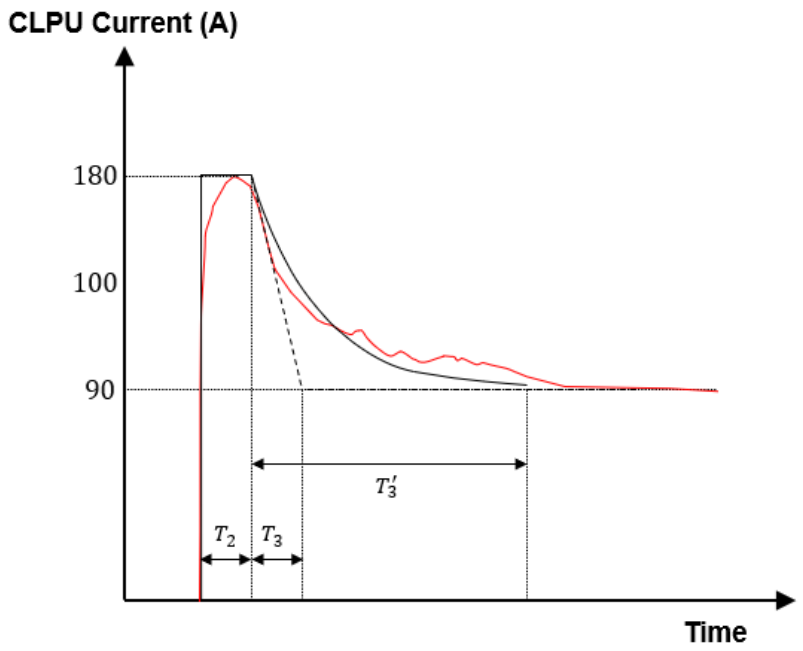

Figure 2.9. Comparison between the general and the delayed exponential CLPU models.

For this model, the decay rate can be approximated as follows:

$$\alpha = \lim_{\gamma \to 1^-} \frac{-\ln(1-\gamma)}{T_3'} \tag{2.5}$$

Several plots are presented in [22] on how to estimate T_3' for different outage durations (constant temperature) and different ambient temperatures (constant outage duration).

2.6.2.2. Stochastic behavior of the load

Aggregate power and current in a feeder vary in a stochastic fashion due to the random, manual operation of switch-governed loads and the random, automatic operation of cyclic loads, both at the customer end. The stochastic behavior of the load can be incorporated into the CLPU model by defining a stochastic process for (2.4), such as the Ornstein-Uhlenbeck process [38].

An Ornstein-Uhlenbeck process, X_t, can be denoted by the following stochastic differential equation (SDE):

$$dX_t = \beta(\mu - X_t)dt + \sigma dW_t \tag{2.6}$$

Where W_t corresponds to a Wiener process for $t \geq 0$. The solution for this equation in the integral form is:

$$X_t = X_0 e^{-\beta t} + \mu\left(1 - e^{-\beta t}\right) + \sigma e^{-\beta t} \int_0^t e^{\beta_s} dW_s \tag{2.7}$$

If the integral term (Wiener process) is ignored, it can be observed that the function approaches the mean value μ with a rate β. Using the Euler-Maruyama Method [40], the integral term from SDE (2.6) can be discretized as follows:

$$W_{n(t+1)} = W_{n(t)} + e^{-\beta t} \cdot N(0, \Delta t) \tag{2.8}$$

Where $N(0, \Delta t)$ is a normally distributed random variable with zero mean and variance Δt.

Figure 2.10 shows the realization of the CLPU model using the Ornstein-Uhlenbeck process. β and σ are adjustable parameters to control the load variation with respect to the mean value. The parameters for this example are: $\beta = 0.002$, $\sigma = 0.35$, $X_0 = K_2$, and μ is denoted by (2.4). The step time Δt is one minute.

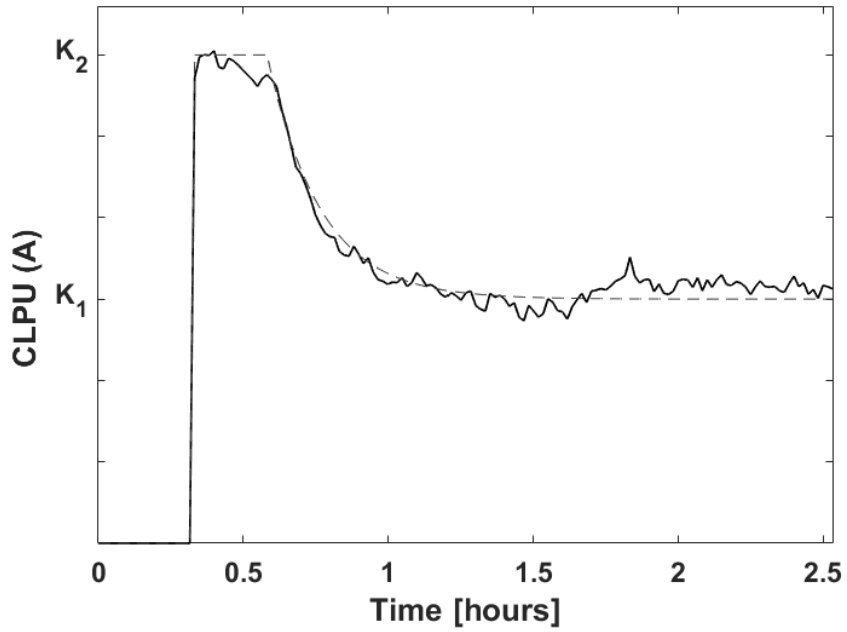

Figure 2.10. CLPU model using the Ornstein-Uhlenbeck process.

A comparison between the real CLPU case from Section 2.2 and the stochastic model is depicted in Figure 2.11. The dashed line corresponds to the mean value of the function with parameters $K_1 = 90\ A$, $K_2 = 180\ A$, $T_i = 20$ min, $t_i = 27.94$ min. The duration of the diversification process was assumed to be 80 minutes, resulting in a decay rate of $\alpha = 0.0015$.

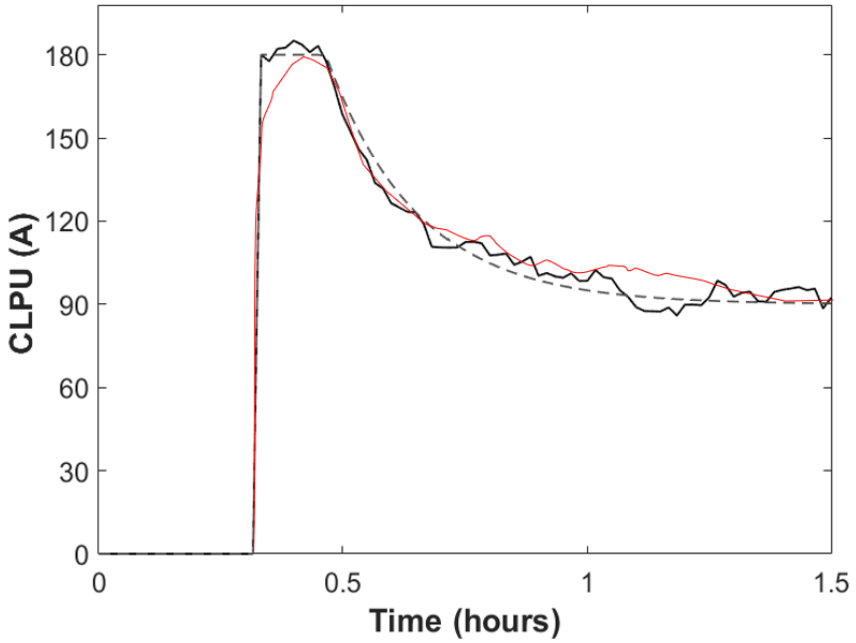

Figure 2.11. Stochastic model applied to a real CLPU case.

It has to be taken into consideration that this model generates stochastic CPLU changes around an assumed mean value. Therefore, the load profile generated is unique for each simulation, resulting sometimes in slight over or under estimation of some of the parameters, such as the maximum CLPU level, which can be compensated by slightly increasing or reducing K_2. This model is intended for applications where load changes are relevant, such as analyzing transformer aging due to internal temperature changes.

2.6.3. Physical modeling of CLPU

2.6.3.1. Thermostat modeling

As it has been discussed previously in this chapter, a large and significant contributor to CLPU is electric heating load. The operation cycle of this type of loads is normally governed by thermostats with a hysteresis loop similar to the one depicted in Figure 2.12 [41]. Normally, the temperature

setpoint $T_{setpoint}$ is a configurable setting while the temperature deadband ΔT is specific for each thermostat design.

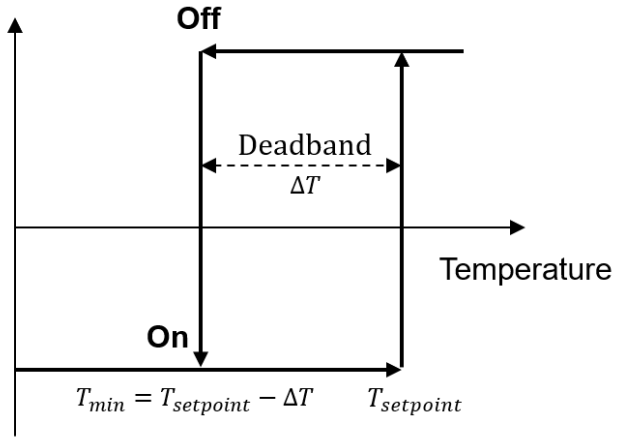

Figure 2.12. Hysteresis loop of a thermostat.

The thermostat turns on the controlled device (e.g., baseboard heater), allowing current to flow through its heating element. When the temperature setpoint is reached, the thermostat turns the heating device off until the temperature falls below the minimum threshold; then, the cycle starts over.

In the following sections, the modeling for each of the principal thermal, weather-sensitive loads that contribute to CLPU is introduced. Subsequently, an aggregate load built up from these components, for multiple customers connected to a feeder (or a feeder section) is presented.

2.6.3.2. Space heating modeling

Space or zone heating is usually performed by electric baseboard devices with a resistive heating element controlled by a thermostat. The heat that builds up in the resistive element due to the circulation of current is dissipated by the natural circulation of air (convection), warming up interior areas with a certain degree of insulation.

In order to reproduce the behavior of a thermostat-controlled baseboard heater, a physical model that includes all the involving variables must be defined. In [41], the equivalent circuit for a residential space heater shown in Figure 2.13 is presented. The model considers the outside temperature T_{out} $(°C)$ and the heater capacity Q_{sh} (kW) as input variables. Furthermore, the building insulation parameters are also taken into account; R_b corresponds to the building

equivalent thermal resistance ($°C/kW$) and C_b represents the building equivalent thermal mass ($kWh/°C$). A list of typical values for these parameters can be found in [22] and Appendix A.

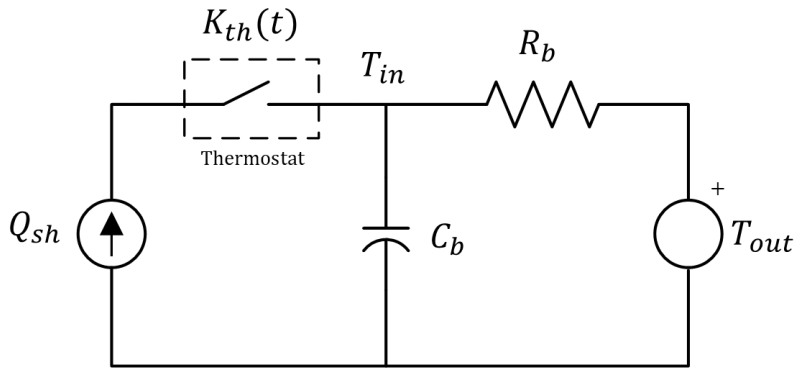

Figure 2.13. Equivalent thermal model for residential heaters.

The time intervals when the heater injects Q_{sh} kW into the building are controlled by the thermostat, denoted by the Boolean function $K_{th}(t)$ as shown in Figure 2.14.

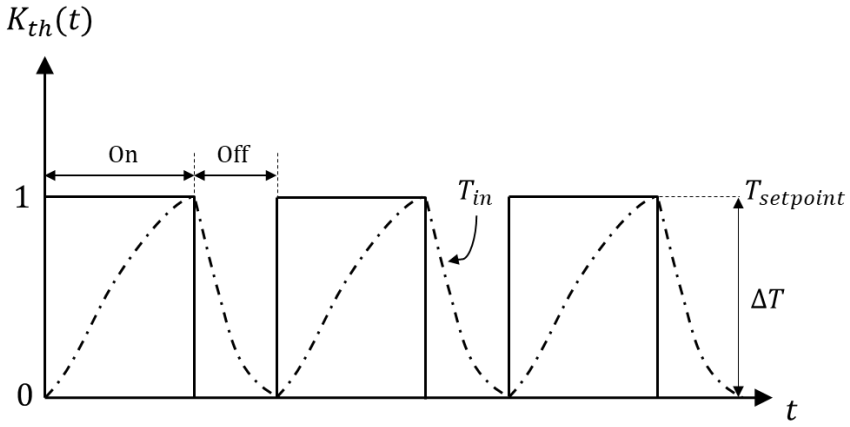

Figure 2.14. Boolean function of a thermostat.

Then, the mathematical model that describe the operation of a baseboard heater for a customer i can be written as follows [22]:

$$C_{b_i}\frac{dT_{in_i}}{dt} = -\left(\frac{1}{R_{b_i}}\right)\left(T_{in_i}(t) - T_{out}(t)\right) + Q_{sh}K_{th}(t) \tag{2.9}$$

The integration of this differential equation was performed using Euler's method with a time step of 60 seconds. The following conditions were assumed:

- The baseboard heaters in a household are assumed to be identical but independent from one another. This means that all the heaters share the same setpoint and deadband, but the initial inside temperature and state may differ.
- The initial inside temperature T_{in} for a customer i is a random, normally distributed number with mean value $T_{setpoint} - \Delta T/2$ and variance $(\Delta T/6)^2$. This guarantees that the probability that the initial inside temperature is within T_{min} and $T_{setpoint}$ is at least 99.7%.
- The probability that a thermostat is initially ON ($K_{sh} = 1$) is 20%.

Figure 2.15 shows the operation of a single, 4 kW residential baseboard heater. The thermostat deadband is 0.55 °C and the temperature setpoint during the day (winter) is 19.5 °C. A two-hour outage is assumed to occur at 11 AM. During the outage, the room cools down, reaching a temperature of 16 °C. When the power is restored at 1 PM, the cycle resumes immediately. As it can be observed, the ON state of the heater after power is restored is significantly longer (>1h) than the others as the temperature must be recovered to the thermostat predefined setting.

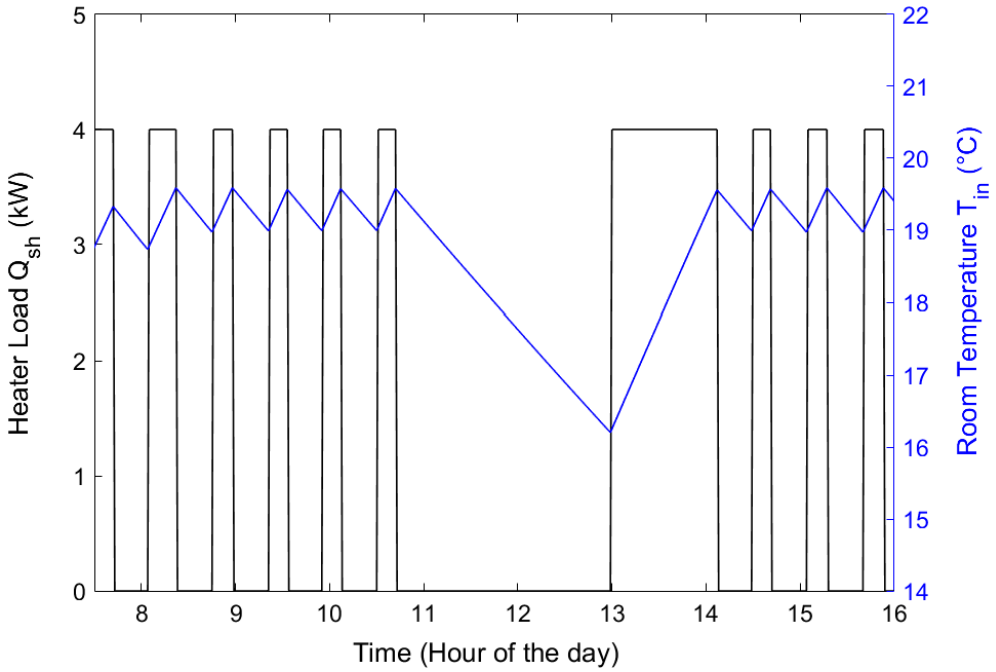

Figure 2.15. Cyclic operation of a single 4kW baseboard heater during an outage.

Figure 2.16 shows the heating load of four different residential customers. The same installed heating capacity (12 kW) and number of baseboard heaters per household (4) were assumed. The

building insulation parameters for each household were assigned stochastically. For this particular scenario, the non-coincident peak loads for each customer resulted to be 12 kW, which means that in each household, the four baseboard heaters were ON simultaneously at some point. As the system peak load in normal condition only reached a maximum of 40 kW, the diversity factor of the heating load is 1.2 (83% of coincidence). Nevertheless, after a two-hour outage, the system peak reached 48 kW as result of the total loss of diversity (100% coincidence).

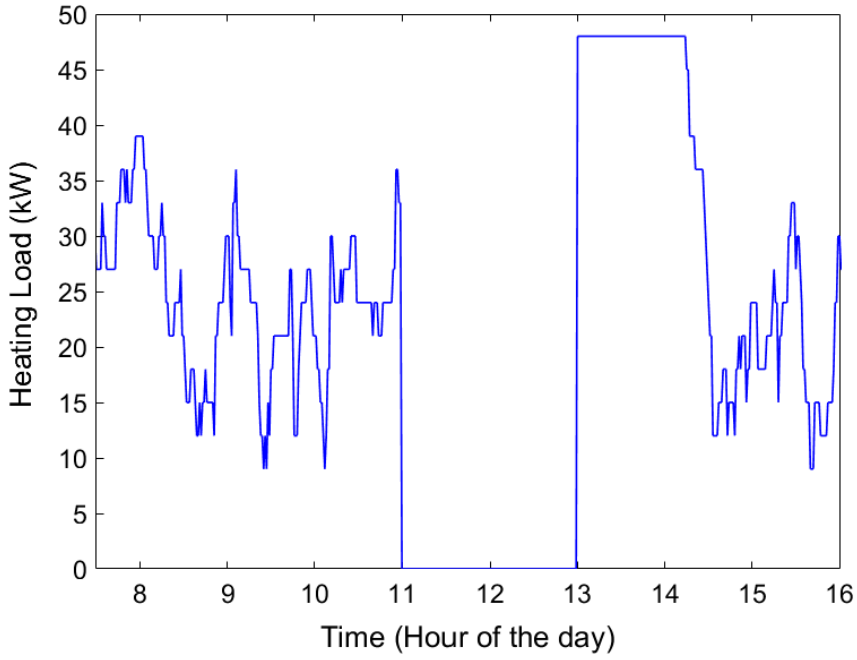

Figure 2.16. Space heating load of four residential customers.

2.6.3.3. Water heating

Another significant contributor to CLPU is electric water heating. In order to define an equivalent model for a water-heating tank, the thermal energy losses must be defined. Normally, two sources are responsible for the energy losses in a water heating tank [42], the thermal convection (heat transfer from the tank surface to its surrounding air) and water demand (cold water replacing hot water after usage).

The instantaneous convection losses in kW can be calculated as follows:

$$P_1(t) = \frac{1}{R_{wh}}(T_w(t) - T_{room}) \tag{2.10}$$

$$\frac{1}{R_{wh}} = SA\left(\frac{1}{R_{tank}}\right) \tag{2.11}$$

Where,

SA tank surface area (m^2),

R_{tank} thermal resistance of tank insulation ($m^2°C/kW$),

T_w water temperature in tank ($°C$),

T_{room} room temperature where the tank is installed ($°C$), and

$1/R_{wh}$ water heater equivalent thermal conductance ($m^2°C/kW$).

Moreover, the instantaneous power loss of regular water usage is denoted by the following equation:

$$P_2(t) = \rho \cdot C_p \cdot W_D(t)(T_w(t) - T_{int}) \tag{2.12}$$

Where,

ρ water density equal to $1\ kg/l$,

C_p isobaric specific heat of water equal to $0.00167\ kWh/kg°C$, and

T_{int} inlet water temperature ($°C$).

Using an analog model to the one presented in Figure 2.13 for a space heater, the differential equation describing the temperature changes in a water heater can be described as follows [22]:

$$C_{wh}\frac{dT_{wh}(t)}{dt} = -\left(\frac{1}{R_{wh}}\right)(T_w(t) - T_{room}) - C_pW_D(t)(T_w(t) - T_{int}) + Q_{wh}K_{th}(t) \tag{2.13}$$

C_{wh} is the water equivalent thermal mass (0.351 kWh/°C). Similar to the space heater model, the power injection to the water heater is controlled by a thermostat with parameters T_{ref} and ΔT_{wh}. Moreover, the instantaneous water demand, $W_D(t)$, is determined using the Monte Carlo rejection

method along with the stochastic data from the load control experiment presented in [42]. Typical values for a residential water heater tank can be found in [22] and in Appendix A.

The integration of Equation (2.13) was performed using Euler's method with a time step of 60 seconds. The following conditions were assumed:

- The inlet water temperature is constant over time and equal to 5 °C.
- The room temperature T_{room} is not affected by the water heater, but it is affected by the outside temperature.
- The probability that the water heater thermostat is initially ON ($K_{sh} = 1$) is 10%.

Figure 2.17 shows a daily load profile of 300 water heaters of similar characteristics, obtained with the model presented in this section. The typical rated power of each tank is 4.5 kW; therefore, the total installed water heating capacity is 300 × 4.5 kW = 1350 kW. As it can be observed, the peak load is only 373.5 kW corresponding to 83 heaters operating at the same time in one particular instant. This reflects the high diversity of the water heating load as only 27% of the water heaters coincide during the peak (DF = 3.6).

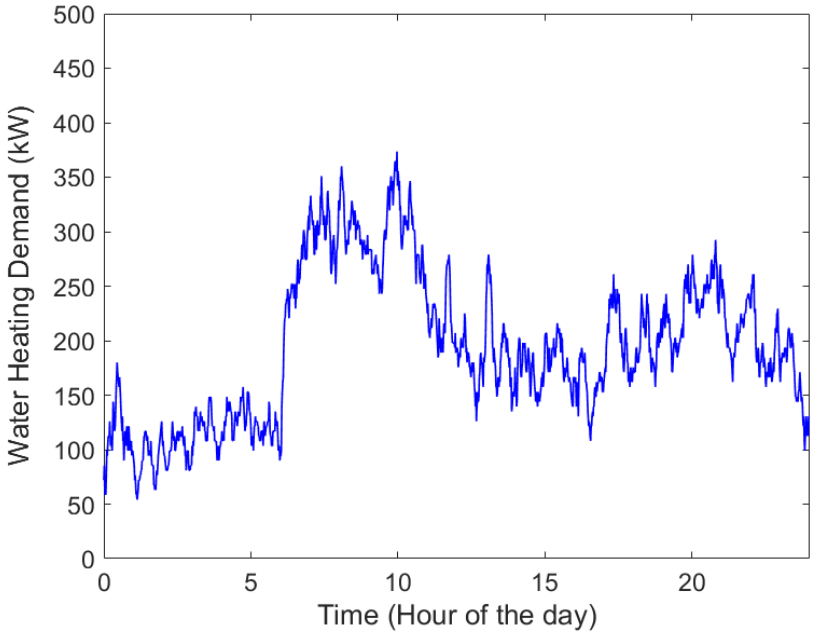

Figure 2.17. Combined load of 300 residential water heaters.

Water heating load is less susceptible to severe loss of diversity during short outages, even in geographic zones with extreme winter temperatures. Figure 2.18 shows the loss of diversity of the water heating load for multiple outage durations. Assuming a typical winter day with a mean ambient temperature of -24 °C during the outage, the load losses diversity completely in about three hours (DF = 1.0; CF = 100%). The loss of diversity is faster if the outside temperature is lower (higher convection losses) and if the outage occurs during peak hours, when the probability of hot water usage is higher (higher water demand losses).

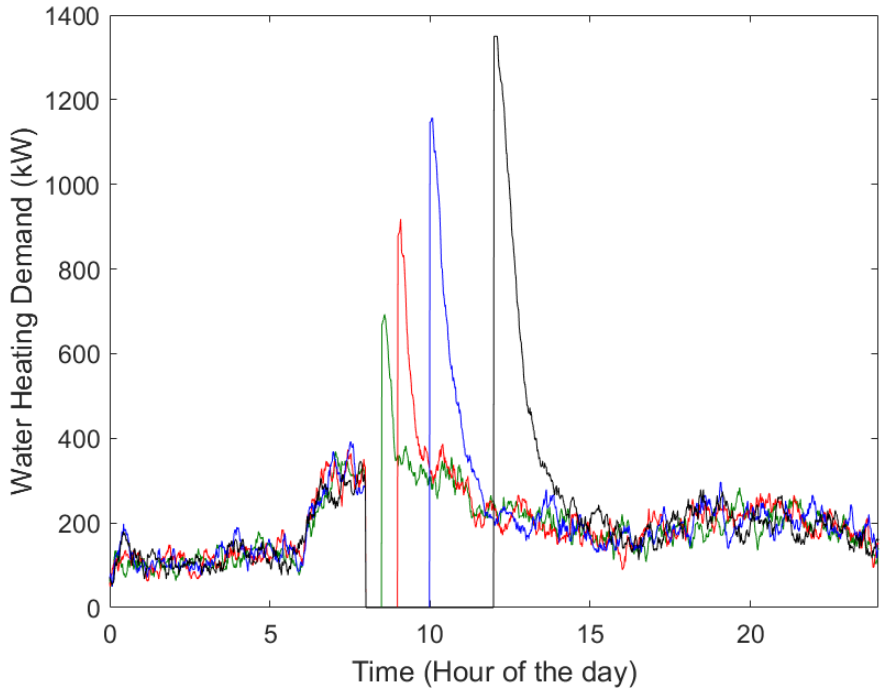

Figure 2.18. Water heating load response for a 30-min, 1-hour, 2-hour and 4-hour outage.

2.6.3.4. Aggregate model

In order to estimate the total feeder load and its response to outages, its main components must be defined. In this work, the aggregate load is assumed to be composed of space heating, water heating and miscellaneous loads. In [22], statistical data for residential customers in the Hydro Quebec distribution network is presented; based on this study, the installed load of a typical residential customer was determined to be 18.5 kW with the following composition: 12 kW for space heating (64.9%), 4.5 kW for water heating (24.3%) and 2 kW for miscellaneous loads (10.8%).

In [22], the miscellaneous component was obtained by subtracting the space and water heating load from the total load from a large group of monitored residential customers as shown in Figure 2.19. For this work, an Ornstein-Uhlenbeck process ($\beta = 0.05$ and $\sigma = 0.05$) was introduced to the average value (dashed line) to consider a certain degree of stochastic variation.

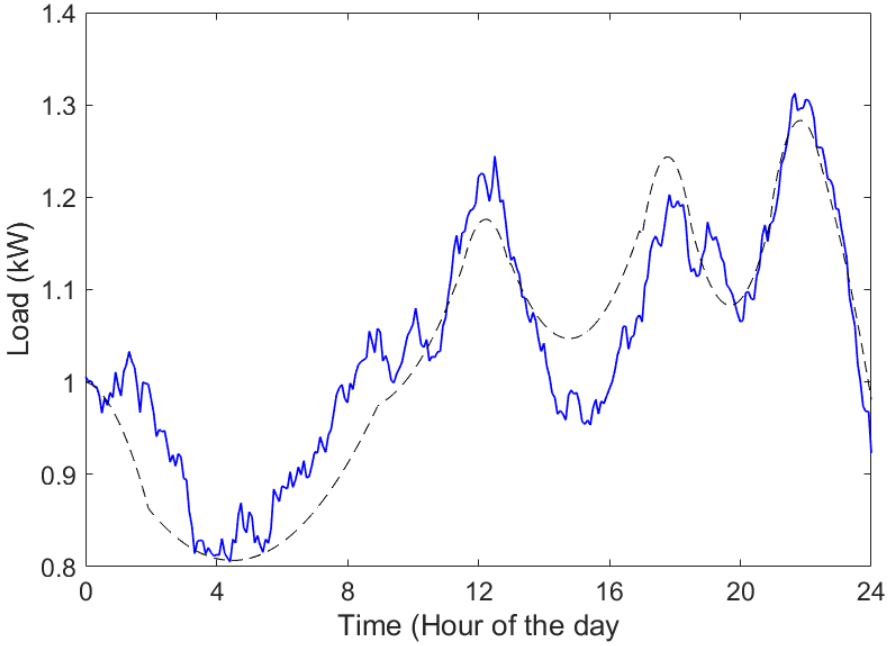

Figure 2.19. Average miscellaneous load per customer.

Since the average load is the result of dividing the total measured miscellaneous load to the number of customers, this stochastic load profile can be used to estimate the total miscellaneous load for N customers as long as they have the same characteristics, such as geographic location and composition of the load.

Regarding CLPU, the miscellaneous load is assumed to be composed only of breaker-governed loads not sensitive to weather variations; thus, there is no loss of diversification during outages. Figure 2.20 shows the CLPU response of the aggregate load of a feeder comprising 1000 residential customers with the load composition determined in [22]. The outage was assumed to happen at 8 AM when the space heating load is high, and the water heating is in its peak. The pre-outage load is 8.2 MW and corresponds to the daily peak load while the maximum CLPU level reached 16.9 MW (2.06 times the pre-outage load).

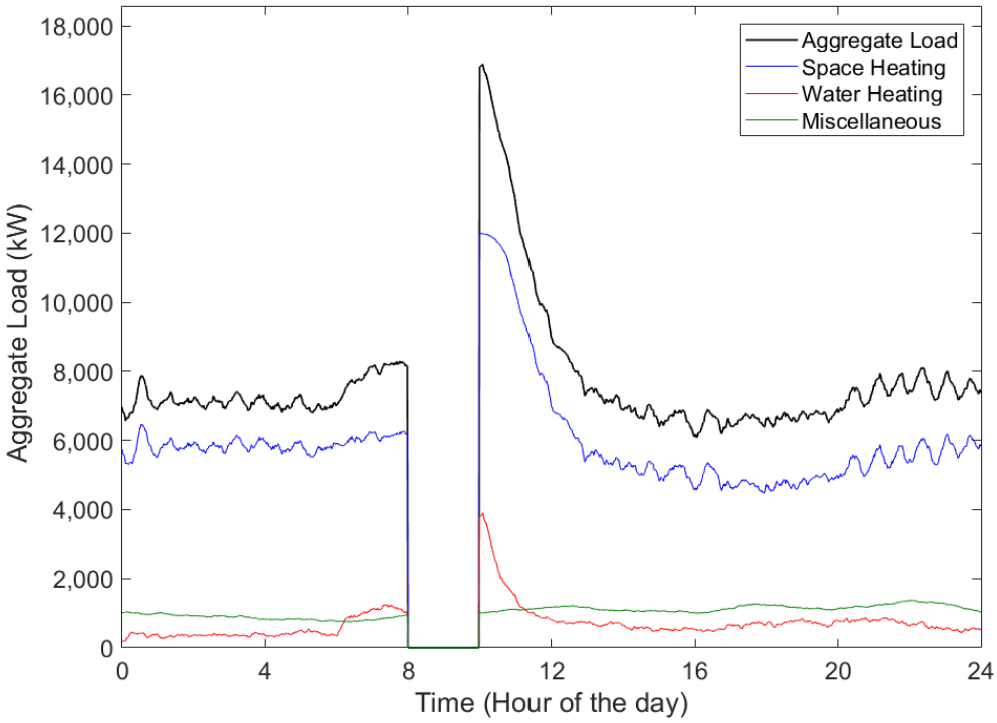

Figure 2.20. Aggregate load for 1000 residential customers during a 2-hour outage (winter).

For this simulation, the outage duration, T_1, was assumed to be two hours, and the average ambient temperature -20 °C. The duration of the initial CLPU, T_2, was 6 minutes (0.1 h) and the diversification process, T_3, lasted around three hours. A comparison between the CLPU general model and the physical model are presented in section 2.6.1 is presented in Table 2.3.

Table 2.3. Comparison between the physical model and the general model

Parameter	General Model	Physical Model	Error (%)[1]
K_1/K_2	2.74	2.06	-24%
$T_1(h)$	2	2	0
$T_2(h)$	0.66	0.1	-84.84%
$T_3(h)$	0.66	2.92	342.42%

[1] The results from the physical model are assumed to be the observed values.

Even though the general model is widely used by Canadian utilities, the empirical parameters defined by equation (2.3) and shown in Table 2.2 have not been validated with field measurement, usually resulting in overestimating the overload (K_2) and significantly underestimating the

diversification time. On the other hand, results from simulations using the physical load model presented in this section have proven to be more accurate to replicate the CLPU effect when compared to real recorded events [22]. In general, the CLPU piecewise linear model can be useful for diverse applications in power system analysis; however, its parameters should be selected to match the results of physical models in order to have a more accurate representation of the CLPU phenomenon.

2.7. Summary

In this Chapter, the causes, and effects of cold load pickup (CLPU) in distribution systems are discussed. Additionally, several load models are presented for different applications in power system analysis, focusing mainly in a physical and stochastic model for distribution feeders with high penetration of electric space and water heating. This model is used later in Chapter 4 to analyze the effect of microgrid islanding on service restoration under severe weather conditions reflecting typical Canadian winter climate.

Chapter 3

MICROGRID CONTROL AND PROTECTION

3.1. Introduction

In order to cope with the technical challenges caused by the presence of embedded generation in the distribution level, utilities are usually forced to resort to rigid operation practices during disturbances and outages. Traditionally, most DG units do not feature automatic voltage and frequency regulation capabilities; consequently, they are not allowed to island with utility load to avoid severe power quality and service restoration issues [43]. Thus, the power disturbances and switching events that may potentially result in islanding operation are averted by automatically disconnecting the involved DG units from the main grid. For this reason, the benefits of distributed generation have been mostly limited to steady-state operation.

On the other hand, in deregulated and liberalized markets, one of the major drivers of the increased interest in distributed generation is reliability [44]. With the introduction of additional power sources in the distribution level, the inherent disadvantages of radiality, such as reduced reliability, could be addressed. However, actual improvements in this matter are usually not significant as the operation practices regarding distributed generation are not flexible, especially during power outages, when DG units are normally prohibited from providing support to the grid [45]. Thus, the presence of distributed generation may become rather detrimental for the overall system reliability as the resulting increased network complexity may compromise the stability and seamless operation of the network [46].

Nevertheless, with the research on distributed generation shifting towards attaining a more robust integration with the grid [45], the technical gap limiting complex applications continues to narrow. In this context, with the support of state-of-the-art computing and communication technologies, the operation and control of distributed generation can achieve a greater degree of automation, and flexibility, allowing the distribution system to benefit from it even during power disturbances and

outages. This has led to the continuous consolidation of the *microgrid* concept, which will be further expanded in the following sections.

3.2. Basic Definitions

In [14], IEEE defines a microgrid as "*a group of interconnected loads and distributed energy resources with clearly defined electrical boundaries that acts as a single controllable entity with respect to the grid and can connect and disconnect from the grid to enable it to operate in both grid-connected or island modes.*" This definition is congruent with the one proposed by CIGRÉ in [47] that states: "*Microgrids are electricity distribution systems containing loads and distributed energy resources, (such as distributed generators, storage devices, or controllable loads) that can be operated in a controlled, coordinated way either while connected to the main power network or while islanded.*" Although there are many discrepancies in other definitions for a microgrid in the literature [48], most agree in two points: a microgrid comprises load and distributed generation, and it is capable of operating both in parallel with the main grid as well as an island. Figure 3.1 shows different microgrid topologies with different DG technologies.

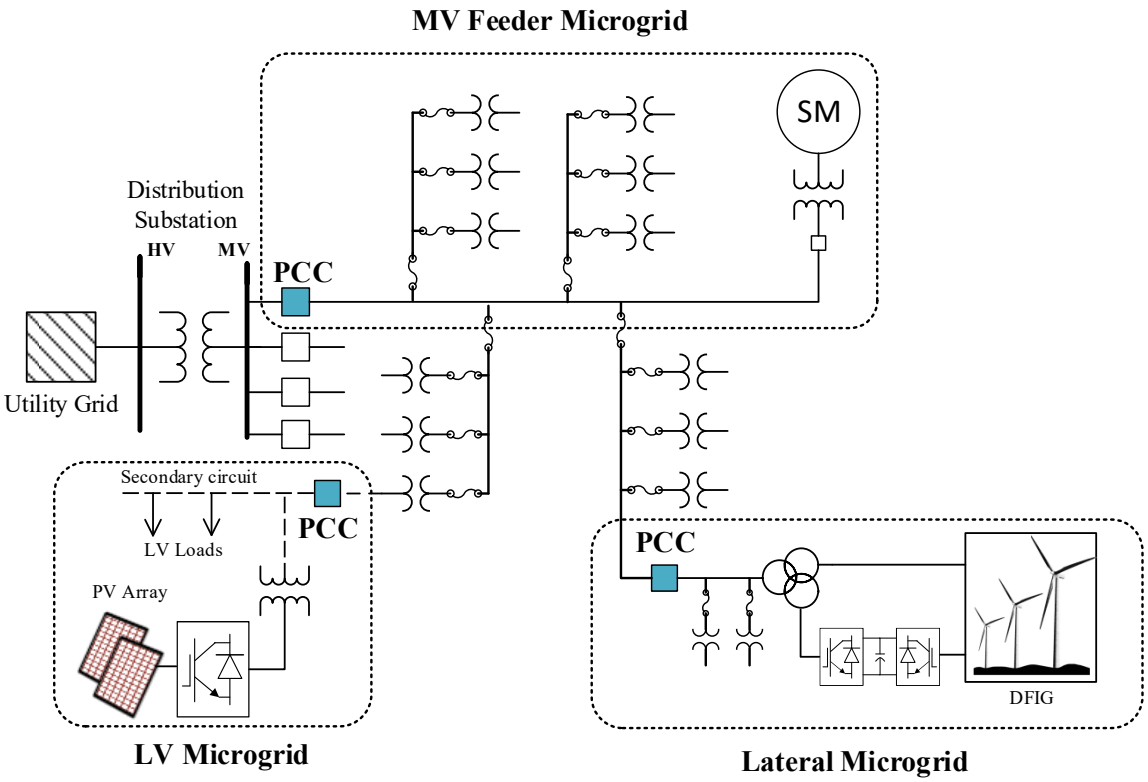

Figure 3.1. Examples of microgrids connected to an AC distribution system.

The microgrid is connected to the main grid through the point of common coupling (PCC), also known as the point of interconnection (POI) [49]. The PCC is the electrical point, normally comprising on-load switchgear, at which the microgrid connects to, or disconnects from the main grid [14]. When the microgrid is connected to the main grid (closed PCC), it operates in parallel with the area EPS (electric power system). This operation mode of a microgrid is usually referred to as the *grid-connected mode*. Likewise, when the microgrid operates isolated from the area EPS (open PCC), voltage and frequency regulation is performed by the DER (distributed energy resources) within the microgrid boundaries. This operation mode is referred to as the *island mode*.

3.3. Functional Requirements of a Microgrid

As mentioned in the previous section, a fundamental component of a microgrid is the distributed generation. However, the defining element which differentiates a microgrid from a facility island is the microgrid control system (also referred to as microgrid controller). The microgrid control system contains the functions that enable the microgrid, as an independent controllable entity, to operate either in parallel with the distribution network or isolated from it upon request. In general, the microgrid control system functions supervise other lower-level functions while receiving information and requests from higher-level functions, usually pertaining to the distribution system operator (DSO) as shown in Figure 3.2. IEEE Std. 2030.7 [14] defines two core functions for the microgrid control system: the dispatch function and the transition function.

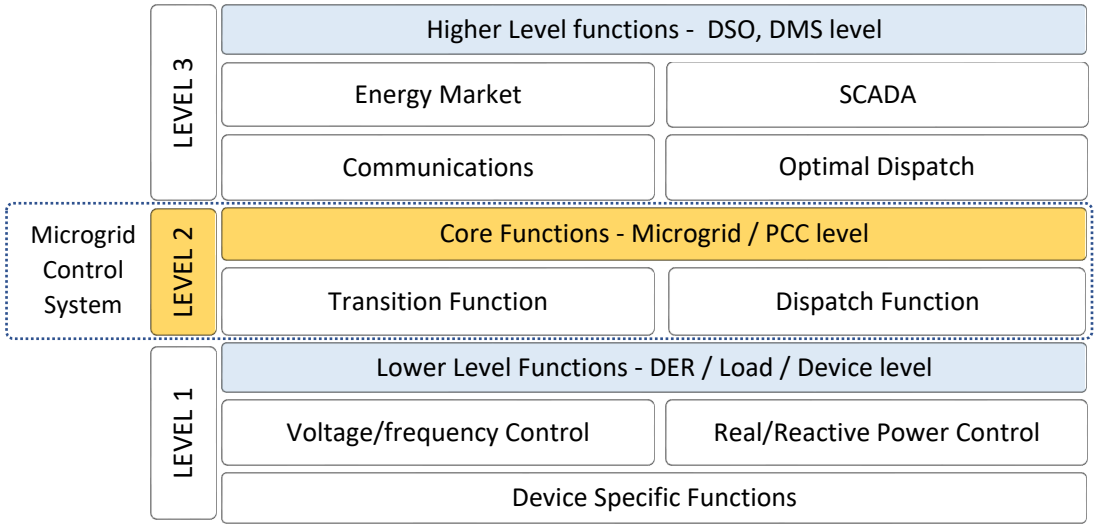

Figure 3.2. Modular integration of the microgrid control functions in a distribution system.

3.3.1. Dispatch function

The dispatch function module generates and transmits dispatch orders to the DER assets and controllable loads within the microgrid boundaries to satisfy the specific operation requirements for each operation mode (grid-connected and island mode). Table 3.1 shows the typical functionalities provided by the dispatch module [14].

Table 3.1. Functional specifications of the dispatch function

General Functions (Both operation modes)	**Specific Functions**
• Individual or coordinated DER control/command. • Load Management. • Operation of circuit breakers, switches and control devices. • Lookup-table-based or optimization-based dispatch control. • Voltage regulation (including DER Var control, capacitor switching and transformer tap changing).	**Grid-connected mode:** • Control of real and reactive power import/export at the PCC (to meet the interconnection agreement with DSO). **Island mode:** • Frequency regulation • Steady-state power quality control

For unplanned transitions (unscheduled or unintentional islanding) the dispatch function may also generate and execute emergency dispatch orders (EDO). Usually, these orders are temporary and are effective until adequate operating conditions are achieved in the microgrid. A set of EDOs may include actions such as temporary dispatch rules and temporary load shedding.

3.3.2. Transition function

The transition function module commands the sequence of actions required to ensure a seamless transition between operation modes. These actions include, but are not limited to adjusting controllers, modifying the protection system parameters, enabling or disabling functions in the microgrid control system and updating and instructing the dispatch function. Under normal

conditions, the transition sequence is initiated upon external request (e.g., from the DSO). In this scenario, the microgrid operating conditions at the PCC are progressively adjusted prior to the transition to achieve a smooth shift between operation modes while ensuring adaptability.

Furthermore, a specific string of actions must be also included in the transition function to rapidly recover adequate operating conditions following unintentional islanding events while in the grid-connected mode as shown in Figure 3.3. Unplanned or unintentional islanding occurs when the circuit interconnecting the area EPS with the microgrid inadvertently opens at one or multiple points simultaneously. Handling unintentional islanding plays an important role in the transition function module as the normal sequence of actions required to ensure a seamless transition and subsequent adequate operation of the microgrid cannot be taken in a timely manner, which could potentially lead to stability and power quality issues within the island if they are not addressed properly. The main cause of unintentional islanding is protection tripping, either in the utility side or at the PCC.

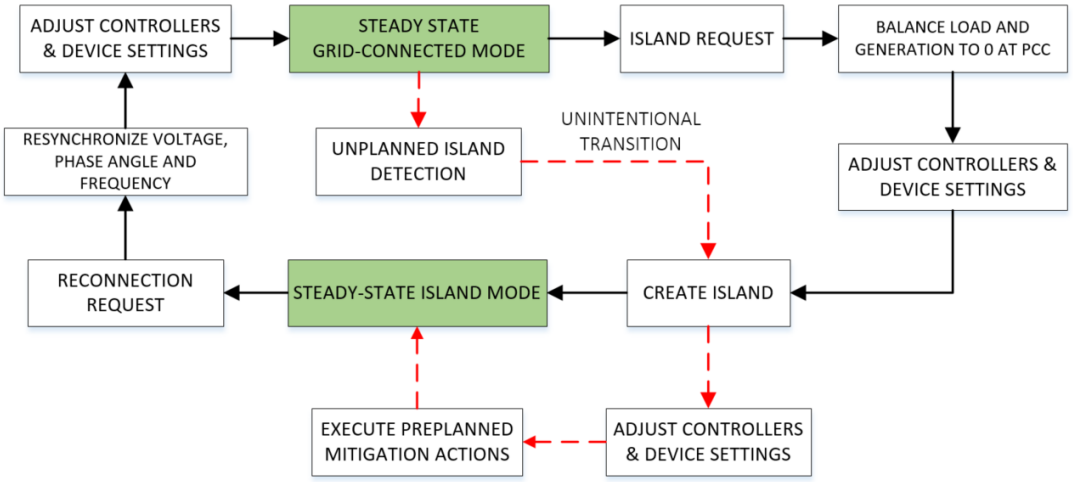

Figure 3.3. Predefined sequence of actions in the transition function.

In order for the microgrid control system to execute the required actions to recover steady-state operating conditions in the microgrid following an unplanned transition, the islanding condition must be detected soon after it occurs. In this context, the transition function must also include an islanding detection module. There are multiple local and remote islanding detection techniques in the literature [50]–[52] and its selection depends mostly on the DG technology and the assets available in the microgrid. IEEE Std 1547-2018 [15] stipulates that an unintentional island must be detected within 2 seconds.

In general, the selection of the specific features for the dispatch and transition functions and its interactions within the control system depend on the available resources in the grid and the intended application for which the microgrid is designed. Additionally, a modular approach for the design of the microgrid control system is recommended in order to attain cohesion and interoperability while allowing future expansion of the control features [14]. Figure 3.4 depicts the interoperability of the core functions in a microgrid control system. In the following sections, a complete example of the specification and operation of a microgrid control system is provided.

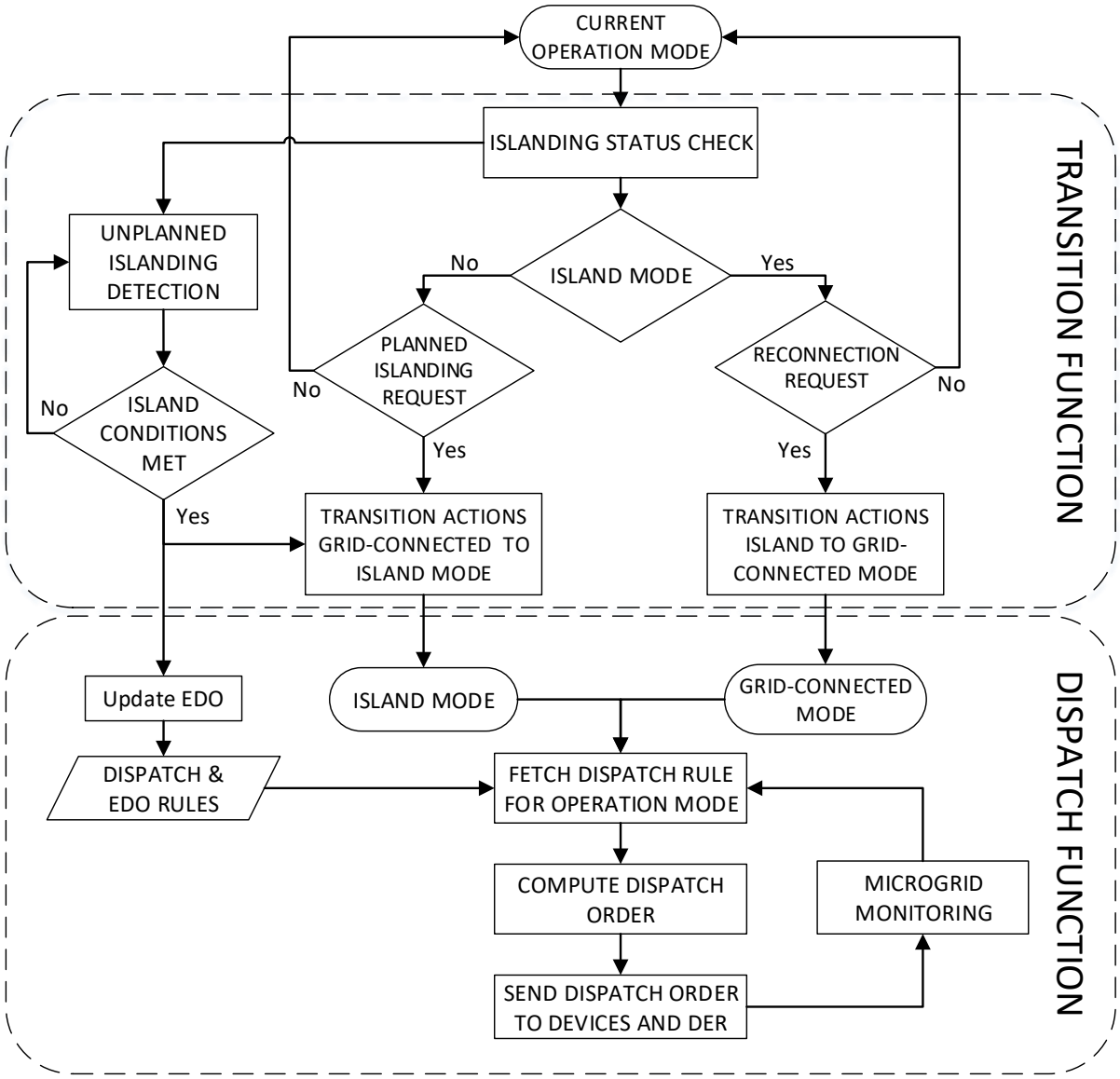

Figure 3.4. Flowchart of the core functions in a microgrid control system.

3.4. System Under Study

In this research work, a modified version of the MV benchmark network presented in [53] is used to analyze the design and incorporation of a microgrid into a distribution system. The original benchmark aims to resemble a typical Canadian MV distribution feeder and it is intended for research purposes involving DER integration to the grid including operation and control, planning and design, power quality and protection. Figure 3.5 shows the original grid with the additional elements added in the studies conducted in this thesis.

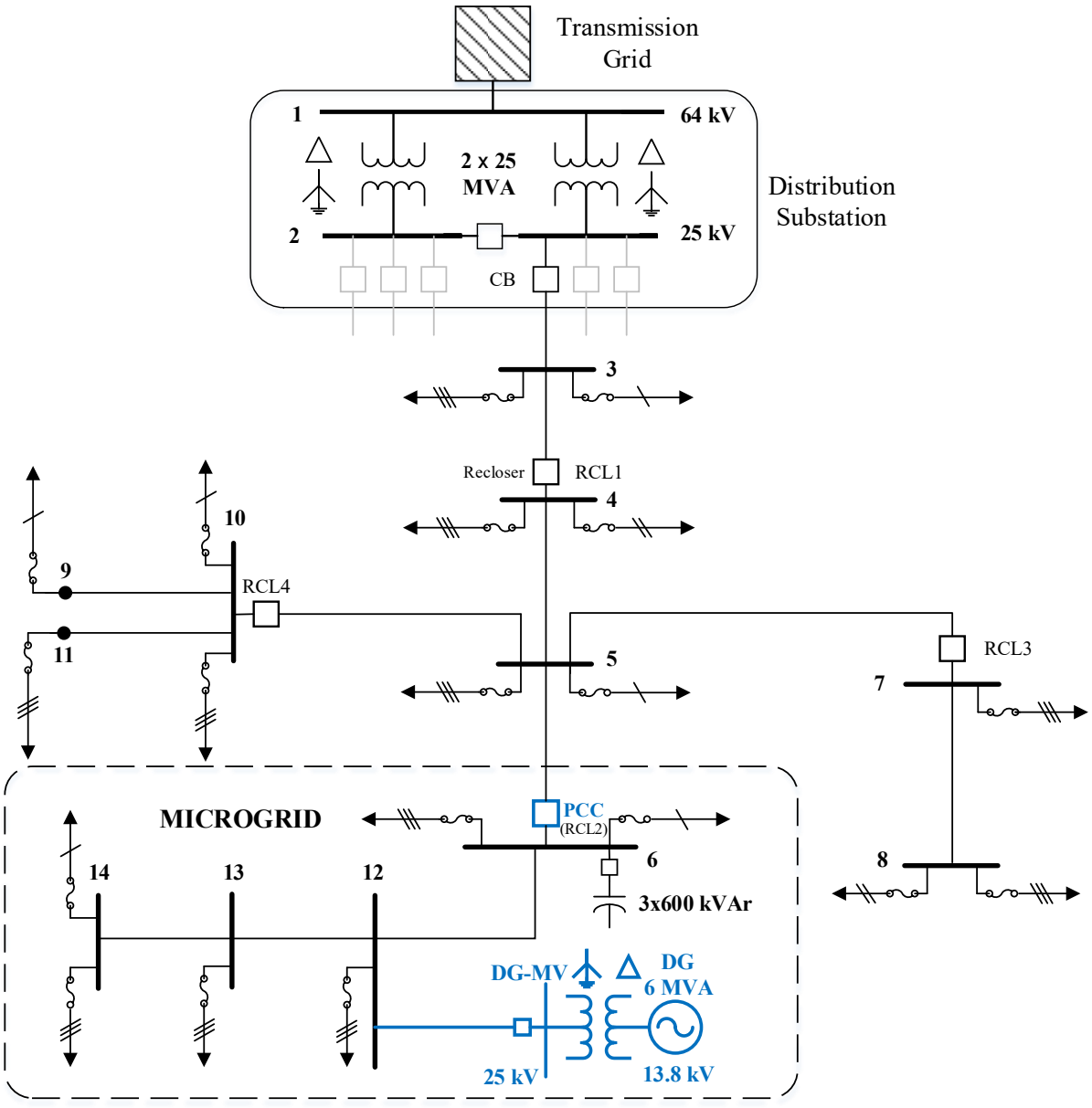

Figure 3.5. Single-line diagram of the modified MV feeder benchmark.

A 6 MVA synchronous-machine-based DG station (hydro) was incorporated to node 12 through a four-wire MV overhead line with similar electrical characteristics to the main feeder. Additionally, Recloser 2 (RCL2) is henceforth considered as the PCC, delimiting the boundaries of the microgrid. Furthermore, open ties with adjacent circuits have been neglected in order to limit the analysis to the standalone operation of the feeder with the microgrid. A complete description of the electrical parameters of the system is reported in [53], and the parameters for the newly incorporated equipment are tabulated in Appendix B. The system presents the following characteristics:

- The feeder is comprised of four-wire overhead lines with three-phase and single-phase laterals.
- The feeder has a total load of 12.7 MVA, unbalanced for a more accurate representation of voltage drops.
- The feeder has a head-end relayed circuit breaker. Additionally, it comprises four electronically controlled reclosers. For this work, one of them is considered as the PCC, and it is treated as a relayed circuit breaker instead.
- A three-phase shunt capacitor bank with a capacity of 600 kVAr per phase is installed Node 6 (within the microgrid boundaries).

When the microgrid operates in island mode (open PCC), the loads are radially supplied by the DG. Hence, the line configuration composed of the DG-MV bus (node 15), and nodes 6, 12, 13, and 14 with their corresponding laterals are referred to as *the microgrid feeder*. The peak load encompassed in the microgrid is 2 MVA.

3.5. Protection Strategy

With the incorporation of the DG unit to the system, the radiality of the former feeder is lost as both load and fault currents may flow upstream. While the reversal of the power flow is not an inconvenience during steady-state operation, dealing with fault currents may become troublesome for traditional non-directional overcurrent schemes. As the fault drifts away from the utility substation and approaches the microgrid, the contribution from the main grid dwindles whereas the contribution from the microgrid increases. As a consequence, the coordination of non-

directional overcurrent devices becomes challenging and problematic since the variation of the fault current magnitude with the fault location is not homogenous, opposed to the case of radial systems as shown previously in Figure 1.2. For these reasons, additional elements, such as directional overcurrent and pilot protection, must be considered when designing a protection scheme for a distribution feeder comprising multiple sources, or in this case a microgrid.

3.5.1. Directional overcurrent protection

Under normal conditions, AC power systems, including distribution systems are inherently inductive; thus, the phase current lags its corresponding phase voltage with an angle displacement ϕ between 0° and 90°. Hence, in a positive-sequence phasor diagram rotating in a counter clockwise direction, a forward current phasor is normally located in the fourth quadrant if the reference voltage phasor is set to 0° as shown in Figure 3.6 (a). This characteristic normally remains unchanged during short-circuits, when the current phasor tends to shift towards the purely inductive axis ($\phi = 90°$) as the resistive part of the load is lost. However, if the polarity of the current measuring device (e.g., a current transformer) is reversed, as if the current were flowing in the opposite direction in the coil, the new measured angle displacement corresponds to the supplementary angle of ϕ. In this context, the direction of the current can be estimated if its phasor angle and a reference voltage phasor are known [3].

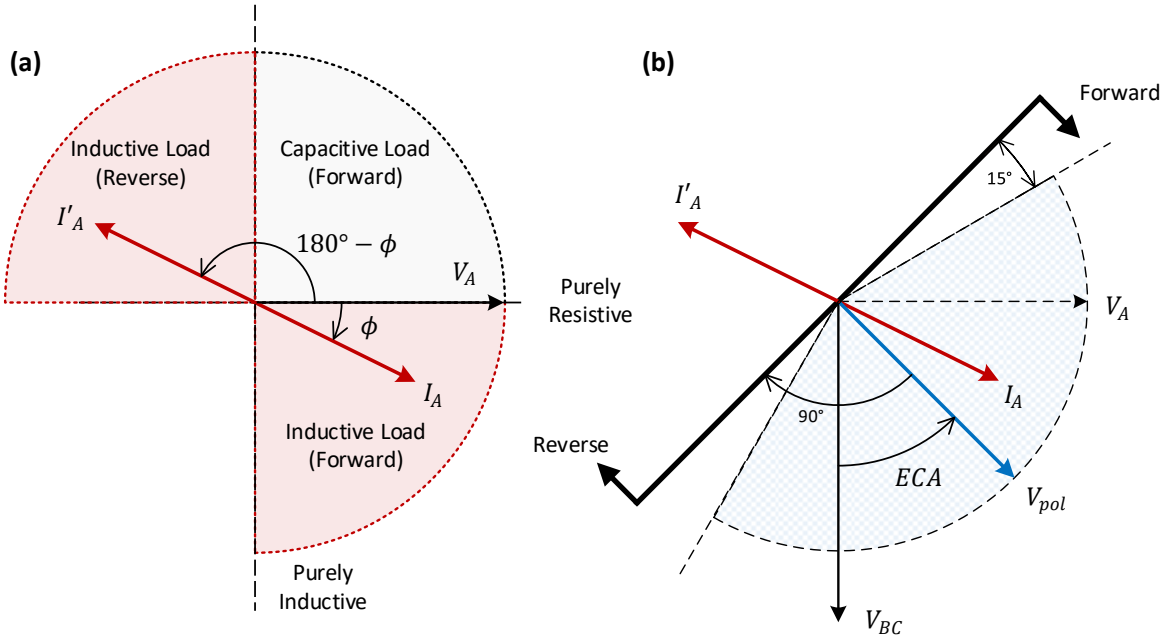

Figure 3.6. (a) Phasor diagram during normal operation, and (b) Directional element logic.

Typically, for a particular phase, the line-to-line voltage phasor of the remaining two phases (e.g. V_{BC} for I_A) is typically selected as reference signal, as shown in Figure 3.6 (b), to prevent the loss of voltage reference for the faulted phase [54]. To determine the current direction for a specific phase, its phasor angle is compared to the polarizing signal (V_{pol}) angle, which corresponds to the voltage reference phasor shifted ECA degrees counterclockwise (directional element characteristic angle). If the displacement of the current angle compared to the polarizing phasor is not greater than the comparator angle ($\pm 75°$ or $\pm 90°$) the current is assumed to flow in the forward direction; otherwise, current is assumed to flow in the reverse direction. To cover the full inductive quadrant and a small region of the adjacent capacitive quadrants (unusual operation but possible), typical values for the ECA are 30°, 45°, and 60° [55].

Directional phase overcurrent protection includes two components: an overcurrent function, including instant and time-inverse overcurrent elements (functions 50P/51P) and a directional element (function 67) [56]. The directional element does not generate a tripping signal on its own, but it enables or inhibits the tripping command generated by the 50P/51P functions based on the direction of the overcurrent (forward or reverse) [3], [7], [55]. Most microprocessor-based relays allow the use of multiple overcurrent sets and programmable logic to enable specific operation for each current direction as shown in Figure 3.7. Multiset directional overcurrent protection is an important element in the definition of the protection concept for the microgrid presented in Section 3.4.

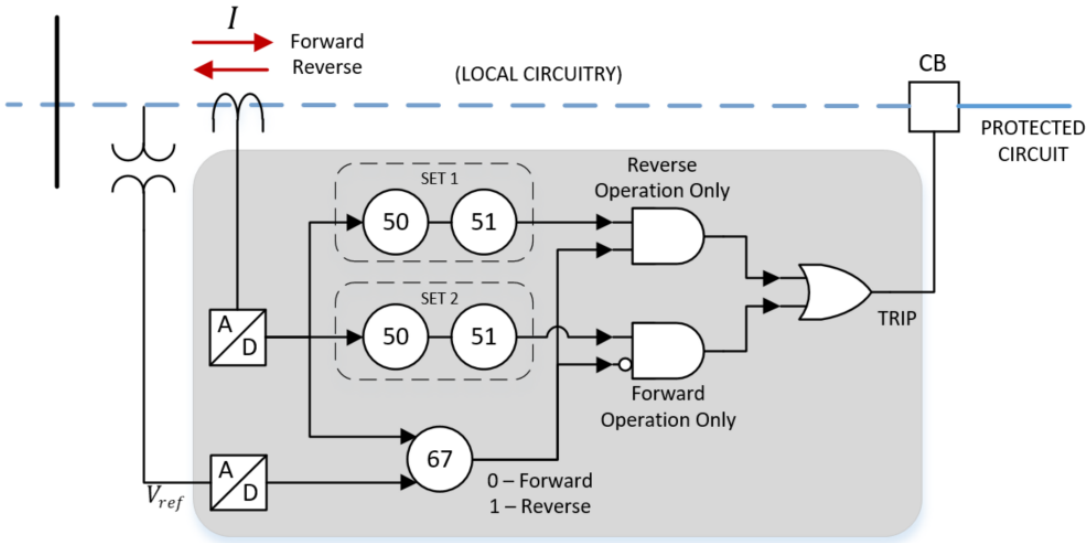

Figure 3.7. Multi-set directional overcurrent protection logic.

3.5.2. Directional earth-fault overcurrent protection

Short circuit currents involving ground are characterized for the presence of zero-sequence current as a result of unbalance in the form $I_0 = (I_A + I_B + I_c)/3$, as shown in Figure 3.8 (a). In this context, earth-sensitive overcurrent protection (50N/51N) estimates $3I_0$ based on phase-current measurements and operates whenever it exceeds a predetermined threshold, usually with a sensitive pickup setting set above the maximum current unbalance during normal operation.

For the protection of power systems with multiple sources, such as the study case depicted in Figure 3.5, estimating the direction of $3I_0$ (function 67N) can also be required to achieve selectivity. Like directional phase overcurrent protection, to determine the direction of the zero sequence current a polarizing quantity is required. Normally, the zero-sequence voltage phasor, $3V_0$, is selected as reference since its rotation does not depend on the direction of the current, and it can also be calculated by phase measurement ($3V_0 = V_A + V_B + V_C$) [54]. In electromechanical relays, to estimate the direction of $3I_0$, the polarizing voltage for angle comparison is normally obtained by inverting and rotating $3I_0$, ECA degrees towards the inductive region as shown in Figure 3.8 (b), to produce torque in one direction. In microprocessor-based relays, this comparison is performed digitally.

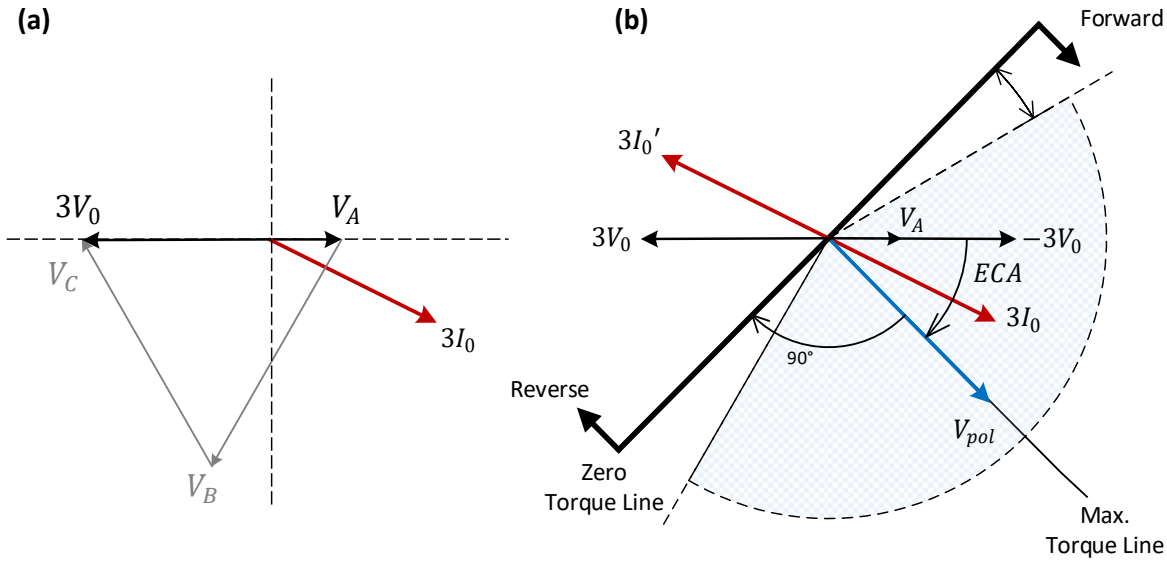

Figure 3.8. (a) Phasor diagram for a single-phase to ground fault (b) Operation of a directional earth-fault overcurrent relay.

3.5.3. Pilot protection

Pilot protection, also referred to as “teleprotection”, is a communication-assisted strategy for line protection, based on the exchange of information (analog or digital) between two or more remote relays [3], [7], [54]. In a pilot protection scheme, the required electrical quantities involved in fault detection (e.g., voltage and current) are processed by the local relays and transmitted to their corresponding remote counterparts through a communication channel; subsequently, the local and remote information is compared, and a tripping decision is made in both terminals, as shown in Figure 3.9. The communication channel used for pilot relaying can be established through pilot wires, power-line carrier (PLC), microwave and digital channels (optical fiber or multiplexed networks) [3]. The objective of pilot protection is to achieve selective, high-speed fault clearing by means of using the tripping information of multiple relays to identify the faulted line segment and the involved clearing devices, accurately and fast [3], [7].

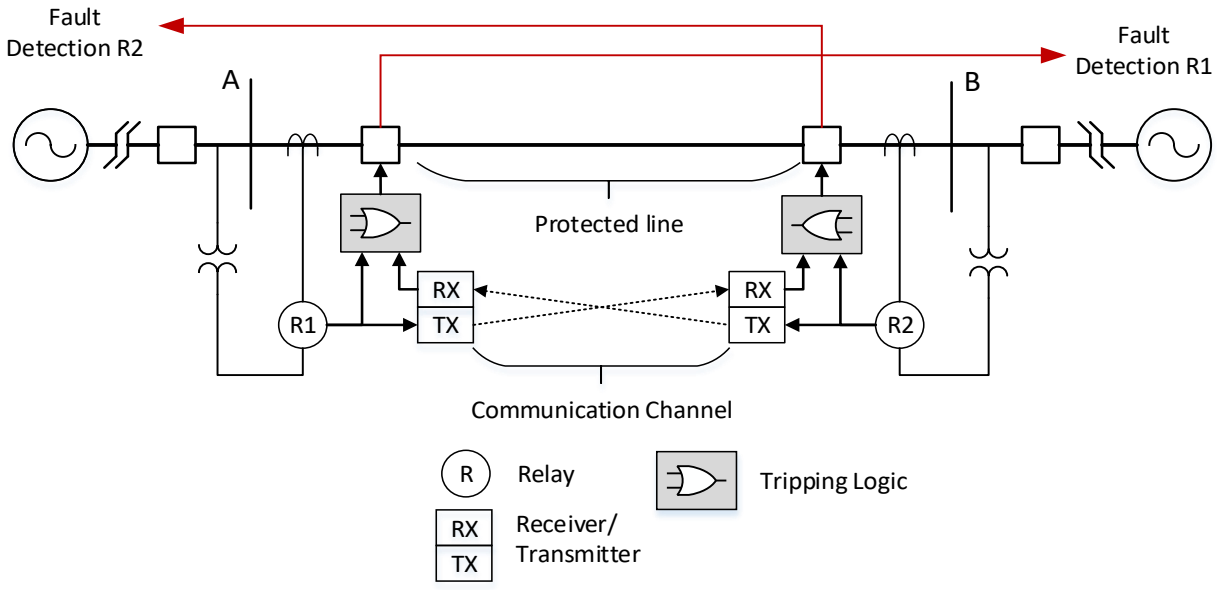

Figure 3.9. Pilot protection scheme.

There are multiple types of pilot protection schemes; however, they can be classified in two major groups: tripping and blocking schemes [7], [54]. In a tripping scheme, a trip signal is transmitted from one terminal to the other upon fault detection in order to initiate tripping of circuit breaker. This type of pilot protection is also referred to as *transfer trip*. On the other hand, in a blocking scheme, a signal is transmitted through the communication channel to prevent the remote relay

from operating. The selection of the pilot scheme usually depends on the type of the communication channel. Typically, when the communication channel is an integral part of the protected line, such as a PLC channel, a blocking scheme is preferred since it will not interfere with protection tripping for internal faults [54]. Conversely, if a separate medium is used for communication, such as an independent optical fiber channel a transfer trip scheme is viable. In this work, a hybrid tripping-blocking scheme is used for the protection of modified distribution system depicted in Figure 3.5.

3.5.4. Protection concept

The design of the protection system for the distribution feeder comprising the microgrid shown in Figure 3.5 is performed in two stages. First, an integral protection scheme based on pilot relaying involving internal and external devices to the microgrid is proposed for the whole system while the microgrid operates in the grid-connected mode. Second, an independent protection strategy is designed for the microgrid when it operates isolated from the distribution feeder. The transition between the two protection strategies (adaptive protection) is performed by the microgrid control system via the transition function, as described in Section 3.3.2.

3.5.4.1. Grid-connected mode

In order to maintain the parallel operation of the DG unit with the main grid and to ensure that the microgrid operates in the grid-connected mode, all the circuit interrupting devices in the straight path between the utility substation and the DG must remain closed during normal operating conditions. For the network benchmark presented in Figure 3.10, corresponding to the study case of this Chapter, these devices are the feeder circuit breaker (CB), recloser 1 (RCL1), the point of common coupling circuit breaker (PCC), and the microgrid feeder circuit breaker (μGCB). In other words, whenever one or more of these devices are open and the DG is still in operation, an island condition will occur.

Additionally, the line sections interconnecting these devices are the only portions of the feeder where the load and fault currents can have a forward o reverse direction, depending on the load conditions and the power dispatched from the DG during normal conditions, and on the fault location during abnormal operation. Conversely, the laterals leading to reclosers 3 and 4 (RCL3 and RCL4 respectively) and the portion of the microgrid feeder encompassed between nodes 6 and

14 are still radial as only one current direction is possible. With these considerations, the protection strategy for the grid-connected mode consists in a directional pilot relaying scheme for the portion of the feeder with bi-directional currents and a traditional overcurrent protection for the radial sections.

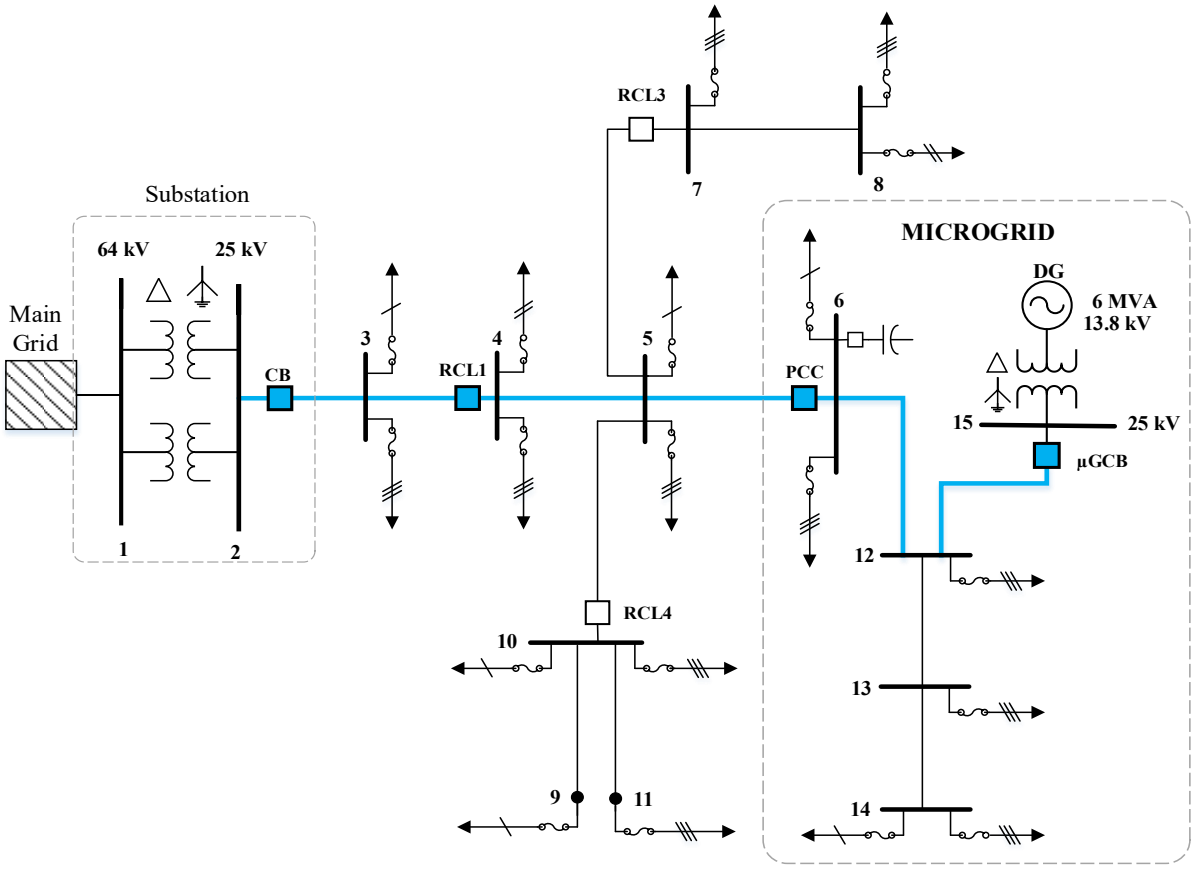

Figure 3.10. Feeder segments and interrupting devices with bi-directional currents.

The pilot protection scheme is based on a variant of a Directional Comparison Unblocking scheme (DCU) combined with a Direct Transfer Trip scheme (DTT). For this approach, a multifunctional microprocessor-based relay or intelligent electronic device (IED) is required for each circuit interrupting device along the blue line in Figure 3.10. The required functions for each IED are:

- 50P/51P – Instantaneous and time-inverse overcurrent protection phase faults.
- 50N/51N - Earth-sensitive ($3I_0$) instantaneous and time-inverse overcurrent detection for ground faults.
- 67P/67N - Directional phase and earth-fault overcurrent detection.

- Programmable tripping logic and communication capability based on IEC Std. 61850 [57].

For this directional pilot protection approach, the relayed devices along the blue line in Figure 3.10 are grouped in pairs, each one linked by a communication channel. The groups are formed as follows: CB-RCL1, RCL1-PCC, and PCC-µGCB. The main protection zone for each group is the feeder portion delimited by the two devices, as shown Figure 3.11. Additionally, the main protection zone of RCL1-PCC also encompasses the unprotected lateral sections without overreaching the protection zones of RCL3 and RCL4.

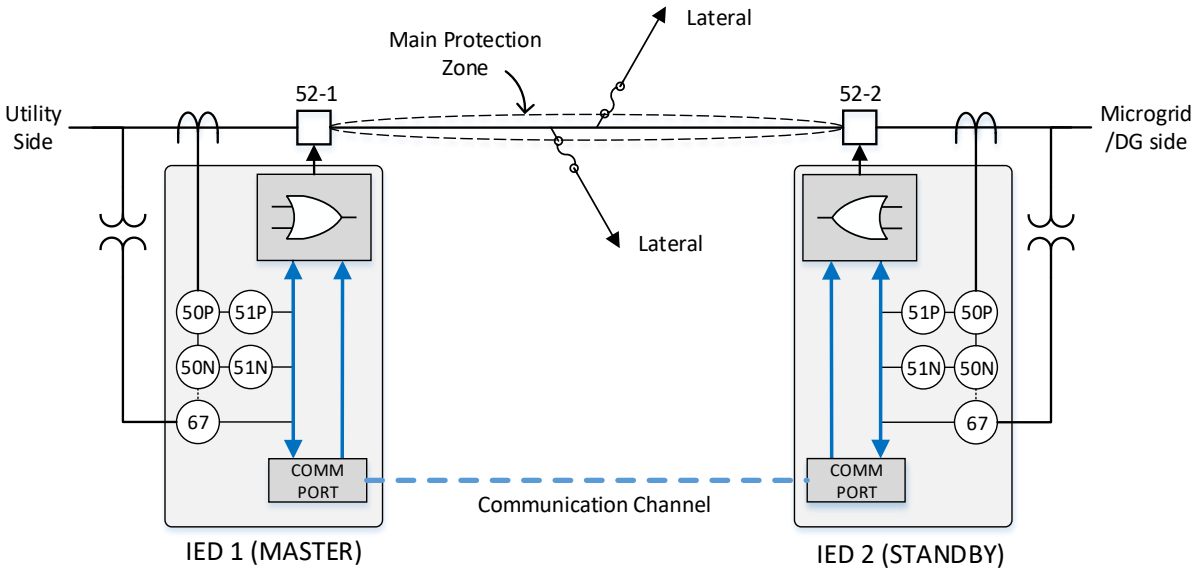

Figure 3.11. Pilot protection scheme for the grid-connected mode.

For each group, the IED in the utility side is identified as the MASTER relay, and the other, in the DG side, as STANDBY. In this protection strategy, the MASTER IED makes the tripping decision for the local and the remote circuit breaker while the STANDBY IED waits for a tripping command. Additionally, the current direction is considered as forward if it flows from the utility towards the DG. The protection logic for internal faults is described as follows:

- For an internal fault, the overcurrent protection in the MASTER relay detects the fault and generates a trip command (50P/51P or/and 50N/51N) that is transmitted to its corresponding circuit breaker if the fault current is sensed in the forward direction. In this condition, a flag is raised (condition 1).

- An internal fault will cause fault currents flowing from opposite directions in at least one phase depending on the fault type. If the phase current in a faulted phase (or phases) or the ground current ($3I_0$) is sensed in the forward direction by the MASTER relay, and in the reverse direction by the STANDBY relay, there is indication of a probable internal fault and another flag is raised in the DCU module (condition 2). The comparison between the 67P and 67N functions of each relay is performed in the MASTER IED only.

- If condition 1 and 2 (DCU) are met in the MASTER relay for at least one phase, the tripping command initially generated locally is transferred to the STANDBY relay without intentional delay (DTT), tripping the remote circuit breaker instantaneously and isolating the faulted portion of the feeder. This requires the MASTER relay to constantly read the current direction in the STANDBY relay through the communication link.

Figure 3.12 shows the tripping logic block proposed for this work for the IEDs in the backbone of the feeder shown in Figure 3.10. Note that the operation logic allows all the relays to operate both as master for a downstream relay and as standby for an upstream relay.

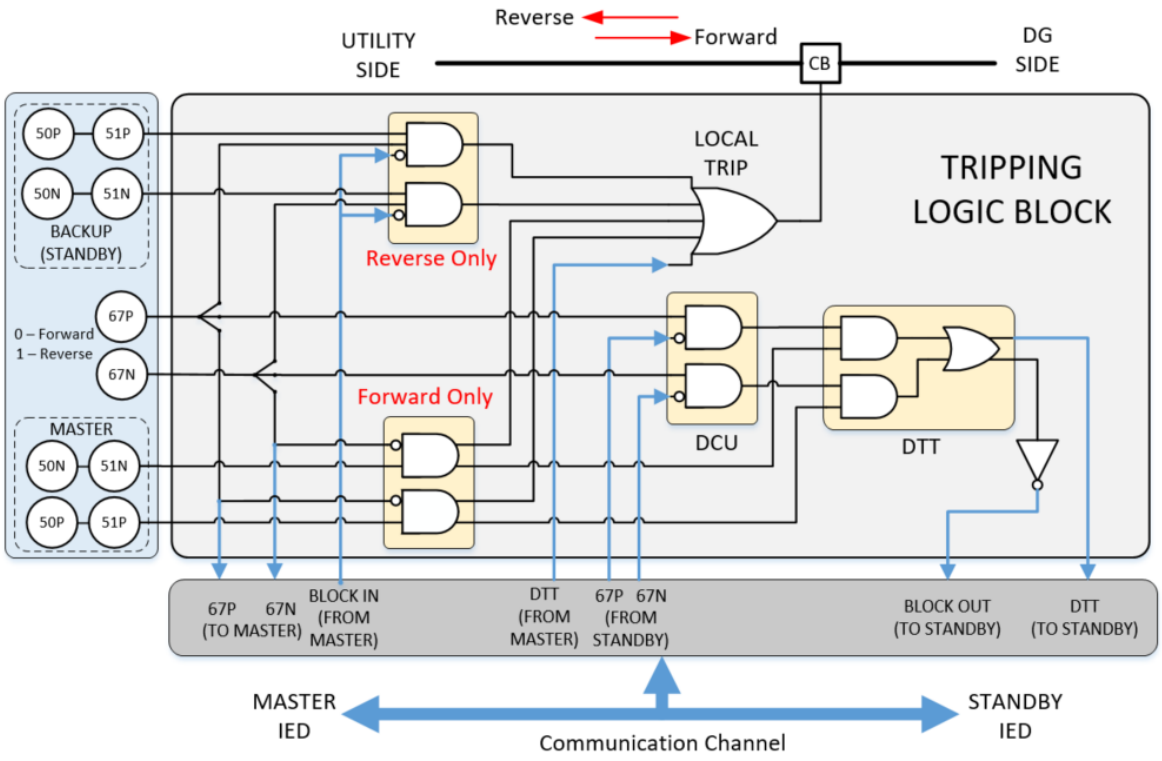

Figure 3.12. Tripping logic for each IED.

With this approach, the remote telemetry of the current direction for the DCU module does not affect the normal tripping of the master relay if the communication link is unavailable. However, since an active channel is required for the DTT, the standby relay will not receive the remote tripping command if the communication link is down. For this reason, a slower backup directional overcurrent protection in the reverse direction must be included in the standby relay to provide security to the protection scheme. However, this function must be blocked if the communication link is active to avoid uncoordinated tripping with lateral fuses. To achieve this, the inverted DTT command, corresponding to a logic 1 in normal conditions, is transmitted to the standby relay to act as a blocking signal. In this fashion, the standby relay is authorized to operate in the reverse direction if the channel is unavailable (blocking signal not received) or instantly when a remote tripping command in the master relay has already been generated.

To ensure that all the master relays operate only for faults within their protection zone, time-overcurrent coordination between them is required. As it has been previously discussed, as the fault location moves away from the utility substation towards the DG, along the blue line in Figure 3.10, the contribution to the fault from the latter increases whereas the contribution from the utility will decrease, making the use of traditional time-overcurrent coordination techniques more difficult. However, in the pilot protection strategy defined in this section, each master relay makes the tripping decision for its protection zone considering forward fault currents only, and thus, the contribution of the second source, in this case the DG in the microgrid, is neglected. Consequently, a conventional time-overcurrent coordination between the master relays is feasible if the calculated fault current contribution from the utility through each relay to each fault location is used as a reference for coordination instead of the short-circuit current calculated at the same locations, as it is common practice in the coordination of time-overcurrent protection in radial system as described in Section 1.2.2.

Figure 3.13 shows the time-overcurrent coordination for phase faults for the master relays (forward direction) for the grid-connected mode. It is worth noting that the PCC relay is the far-most device in the backbone for fault protection in the forward direction, so it must be the fastest to operate. This relay must coordinate only with the fuses within the microgrid (25T) in a fuse-blowing scheme. The reclosers in the radial laterals, RCL3 and RCL4, do not need to be coordinated with other devices other than the fuses in their protection zone (80T and 65T respectively) in a fuse-

saving scheme as they protect independent radial circuits. Next, RCL1 must coordinate with the slow operation curve of RCL3 (the slowest between RCL3 and RCL4) and with the fuses within its protection zone (80T) in a fuse-blowing scheme. Finally, the relay at CB must coordinate with RLC1 and the fuses in its protection zone (65T) in a fuse-blowing scheme. A CTI of at least 0.20 second was used for the coordination between these relays as recommended in [7]. It is important to mention that for faults within the protection zone of RCL3, the contribution from RCL1, the next upstream device, is only 70%; therefore, the predetermined CTI can be maintained with the selected TOC curves.

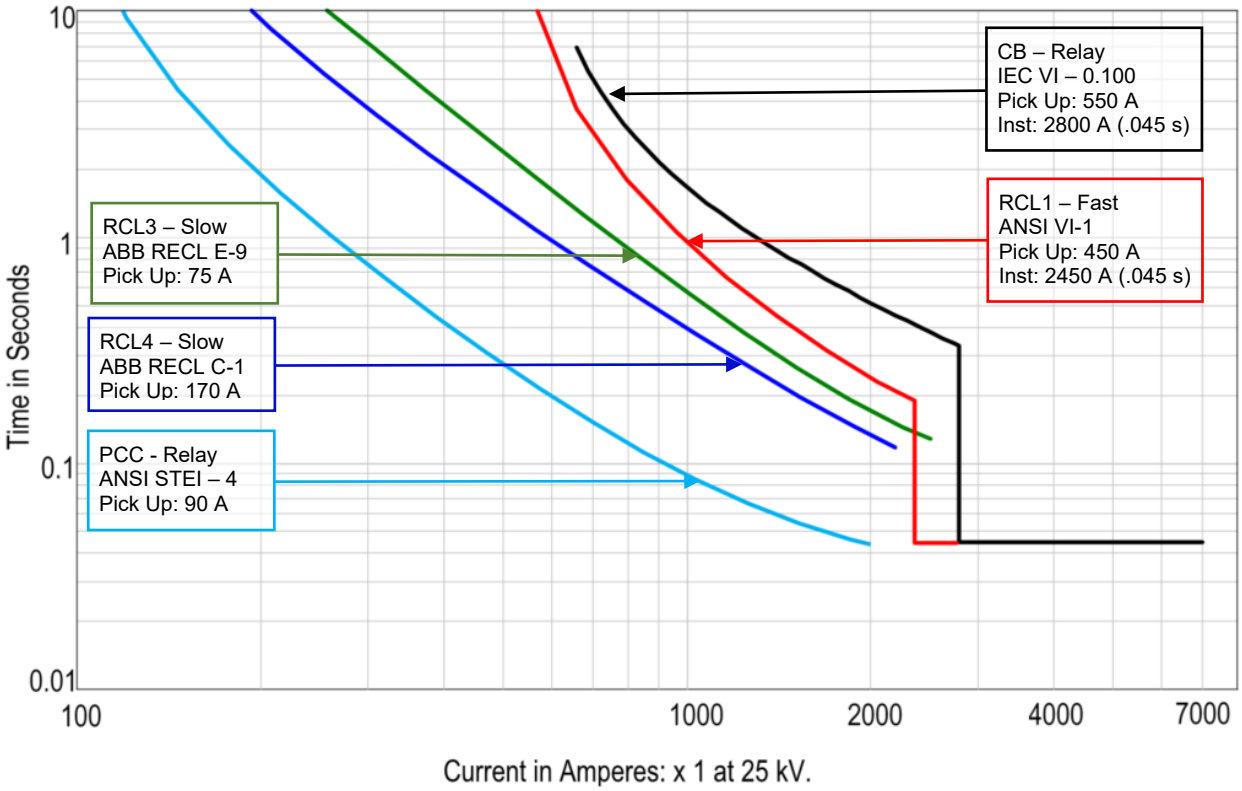

Figure 3.13. Phase time-overcurrent coordination - master relays (forward).

For the backup protection, normally blocked in the pilot protection system, a similar coordination process is followed as shown in Figure 3.14. RCL1, in the reverse direction, must coordinate with the fuses in the protection zone of its corresponding master relay, CB (65T), in a fuse-blowing scheme. Next, the relay at PCC must coordinate with RCL1 in the reverse direction, with a CTI of 0.20 second; additionally, it must also coordinate with the fuses in the protection zone of its corresponding master relay, RCL1 (80T) in a fuse-blowing scheme, and with the slowest curve

between RCL3 and RCL4, also maintaining a CTI of 0.20 second. Finally, the relay at the microgrid feeder circuit breaker, µGCB, must coordinate with the fuses in within the microgrid (25T) in a fuse-blowing scheme.

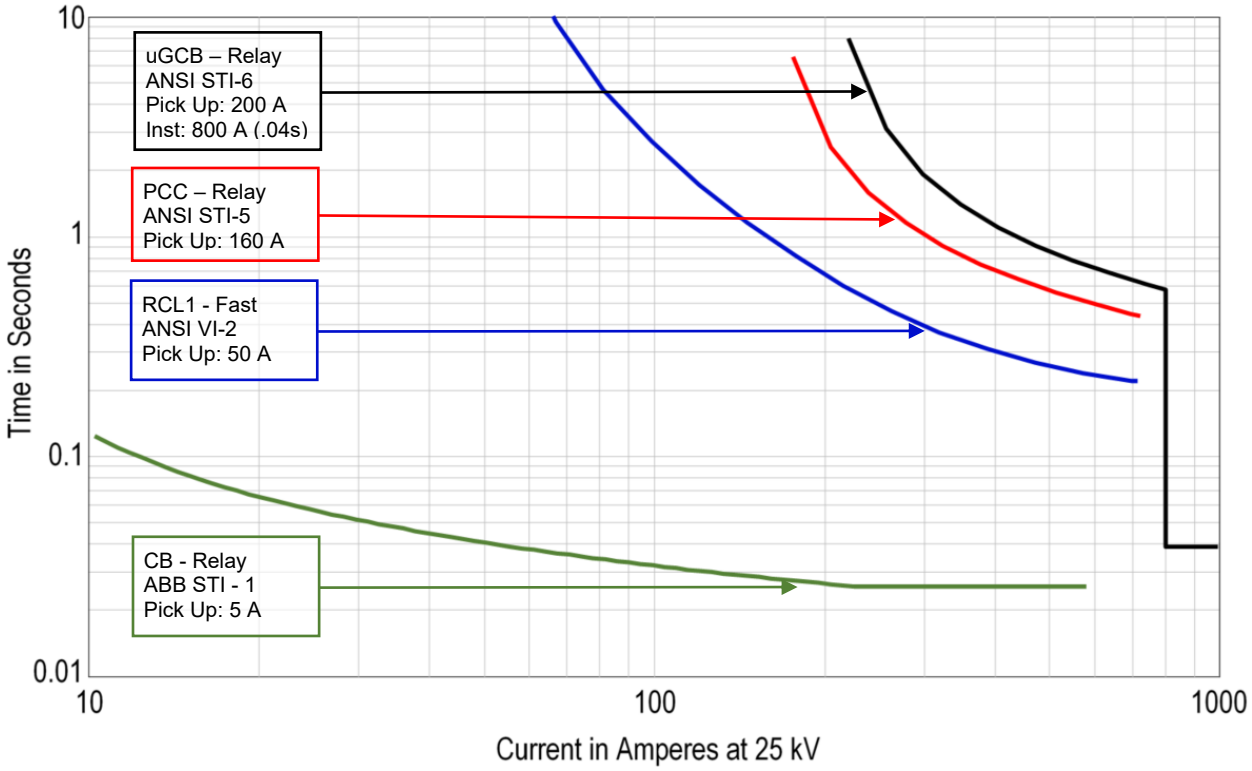

Figure 3.14. Phase time-overcurrent coordination – standby relays (reverse).

In normal conditions, the 6 MVA DG is only capable of supplying the totality of the microgrid load (2 MVA) and up to 4 MVA out of 10.7 MVA of the remaining feeder load during the system peak as shown in Figure 3.15. Therefore, the only case in which currents may flow in the reverse direction through the feeder circuit breaker (CB) is during short circuits in the utility substation, adjacent feeders or in transmission system level. If the fault occurs in the utility substation (e.g., at the MV busbar), its protection system may cause the disconnection of the transformer bay and the feeder CB, causing an unsustainable, significantly unbalanced island (12.7 MVA of load vs. 6 MVA of generation capacity) which may cause a severe disturbance in the DG and its subsequent disconnection. For this reason, a directional overcurrent element with a low pickup setting in the reverse direction must be also included in the CB relay as shown in Figure 3.14. However, the tripping commands generated following fault detection are not directly sent to CB, but instead, they are transferred to the PCC through the communication channel. In this scenario, the microgrid

will unintentionally shift to island mode during which the microgrid control system will be better able to restore balance and normal operating conditions. This feature is covered in Section 3.6.

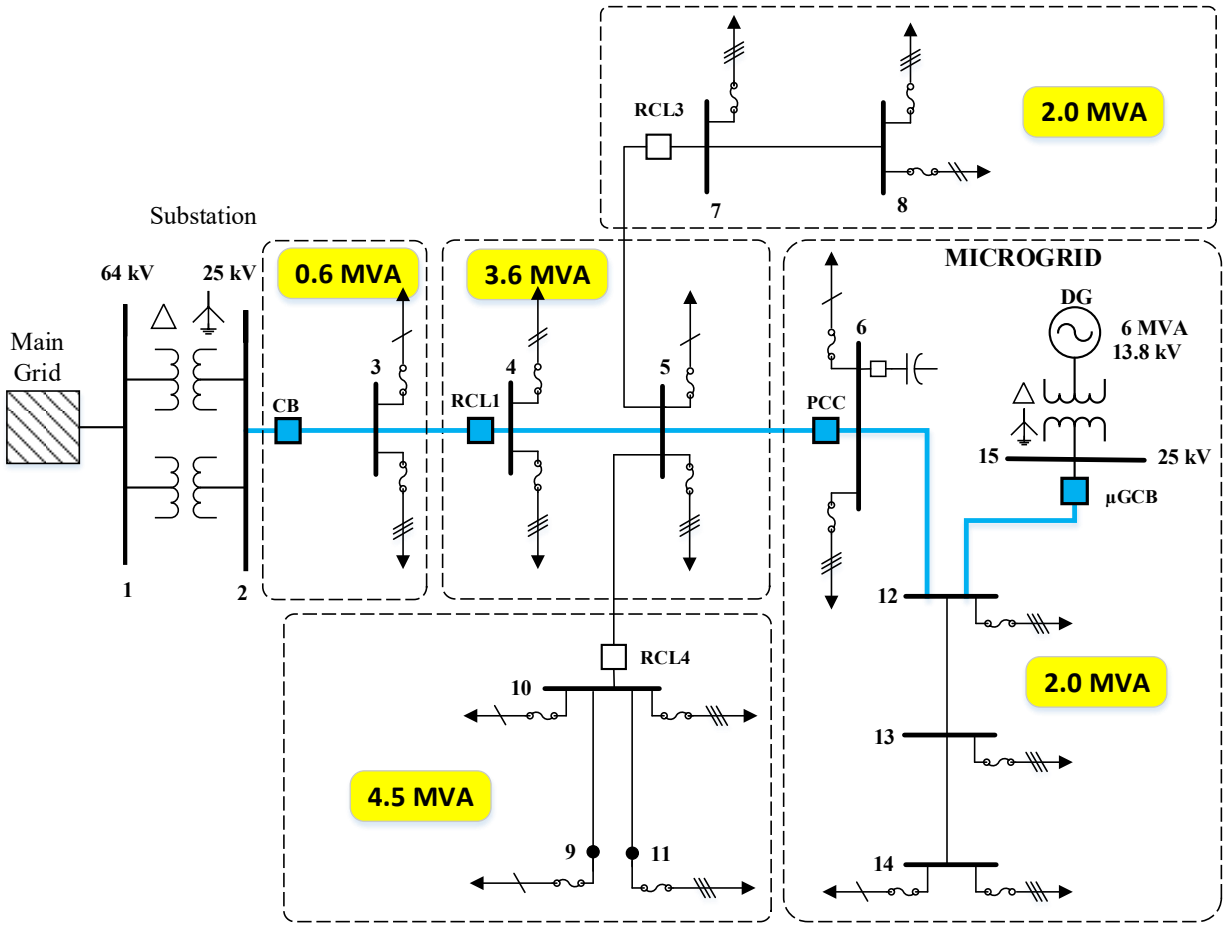

Figure 3.15. Load encompassed in each protection zone.

The coordination of the main and backup directional ground protection follows the same procedure as the phase coordination for the master and standby relays. A summary of the phase and ground protection settings for the grid-connected mode is presented in Appendix C.

Figure 3.16 shows the response of the master relay at PCC for a bolted, single-phase to ground fault at node 12, within the microgrid. Before the occurrence of the fault, the DG was dispatched to 80% of its capacity (4.8 MVA). Therefore, the pre-fault current through the PCC circuit breaker flows in the reverse direction (67A is logic 1) as the generation within the microgrid is greater than its load (2 MVA). When the fault occurs, a reversal of the current direction in phase A (faulted phase) at PCC takes place, as the utility EPS contributes to the fault. The phase element, 50/51A, is the first to pick up the fault, at $t = 1.082$ seconds, and local trip command is generated in

conjunction with the inverted 67A (forward direction). Simultaneously, the 67A element in the standby relay at µGCB is remotely monitored in the master relay at PCC. When the fault occurs, the current direction through µGCB remains unchanged as the DG contributes to the fault. Thus, the DCU for phase A is armed as soon as the fault occurs, unblocking the direct transfer trip module, which generates a transmits a remote trip command for µGCB as soon as the overcurrent protection element for the corresponding faulted phase picks up the fault, in this case 50/51A. At the same time, the backup blocking signal expires, allowing the relay at µGCB to operate in the reverse direction in case of DTT reception failure. For this scenario, the communication channel between PCC and µGCB was assumed to be active.

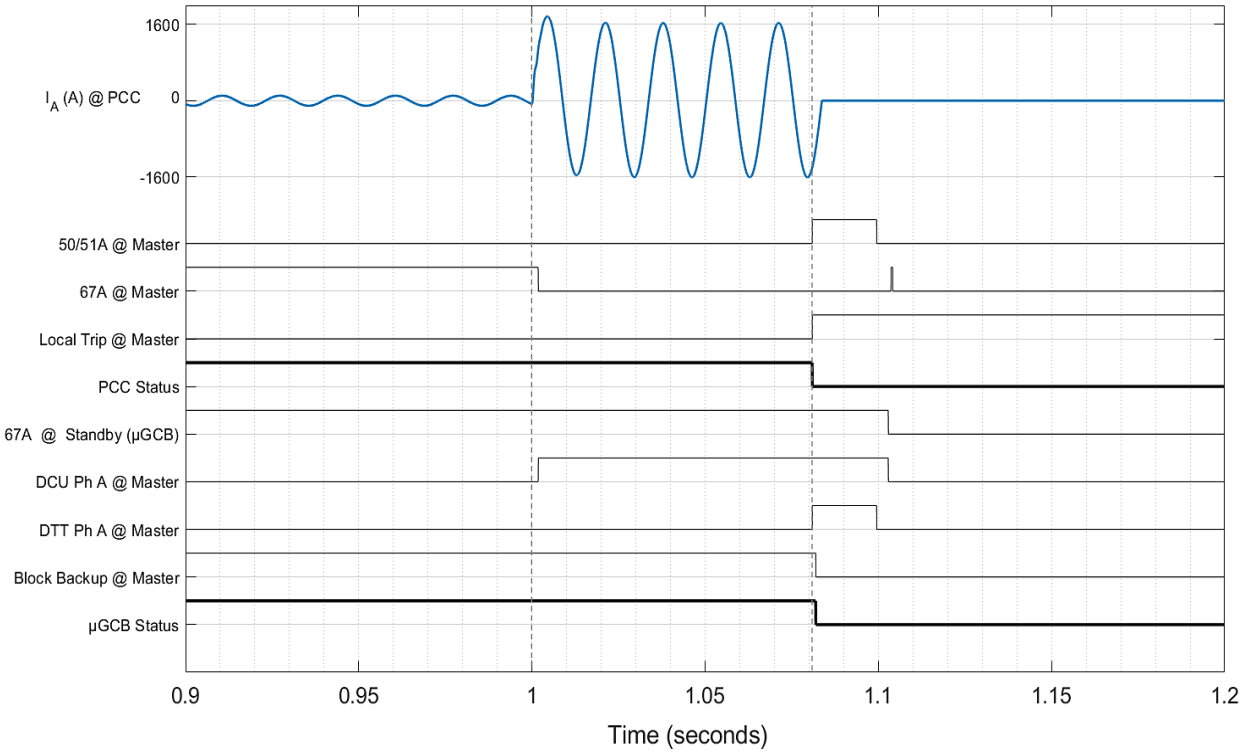

Figure 3.16. Tripping sequence in the master relay at PCC for a fault within the microgrid.

Figure 3.17 shows the response of the protection system for a single-phase to ground fault at node 5 that also causes the failure of the communication link between RCL1 and PCC, whose relays operate as master and standby respectively for this protection zone. As communication is lost shortly after the fault occurs, the remote telemetry of the current direction stops at the master relay. Thus, the DCU module is no longer able to unlock the DTT, so a remote trip command will not be generated. However, since the fault is detected in the forward direction by the phase element

50/51A in the master relay, a trip command is generated and sent to the local circuit breaker, cutting the fault contribution from the utility EPS. On the other hand, as the communication channel is lost, the signal blocking the backup protection in the standby relay is no longer detected in the standby relay, enabling its operation in the reverse direction. In this case, the ground element, 50N/51N, in the standby relay is the first to detect the fault in the reverse direction, tripping its corresponding circuit breaker.

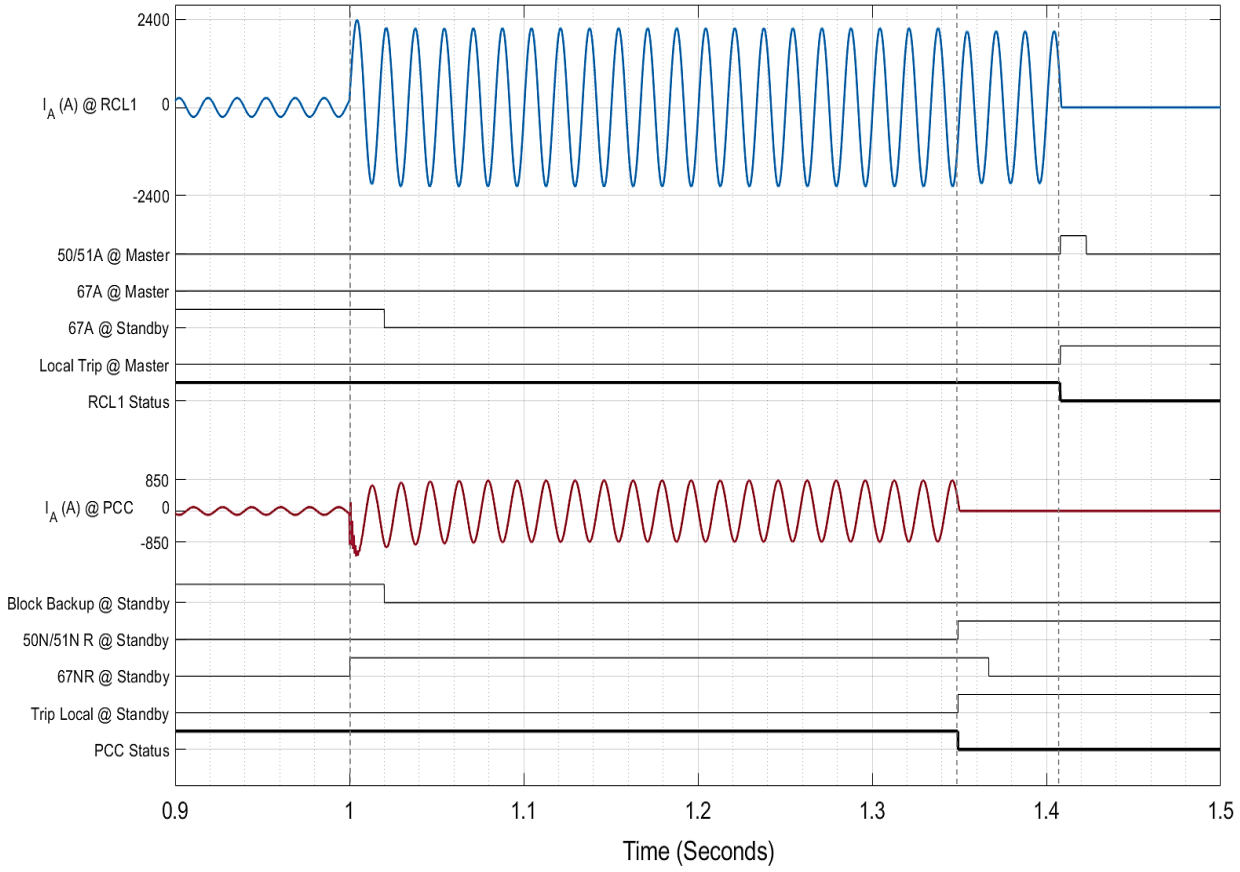

Figure 3.17. Protection performance during failure of the communication link.

The objective of the pilot protection scheme designed for the grid-connected mode is to take advantage of the fast fault detection in the forward direction for faults close to the microgrid and to the DG unit, which is otherwise slow in the reverse direction to allow coordination. For this reason, an active and reliable communication channel is essential at least within the microgrid, between PCC and µGCB, so communication redundancy may be required. For faults outside the microgrid, the backup protection may operate faster or slower than the main protection when the communication channel is offline, depending on the location, impedance, and type of the fault.

3.5.4.2. Island mode

Following a planned transition to the island mode, the microgrid feeder becomes radial as load and fault currents can only flow in one direction, as shown in Figure 3.18. Thus, non-directional time-overcurrent protection coordination can be performed between the fuses within the microgrid and the relay at µGCB.

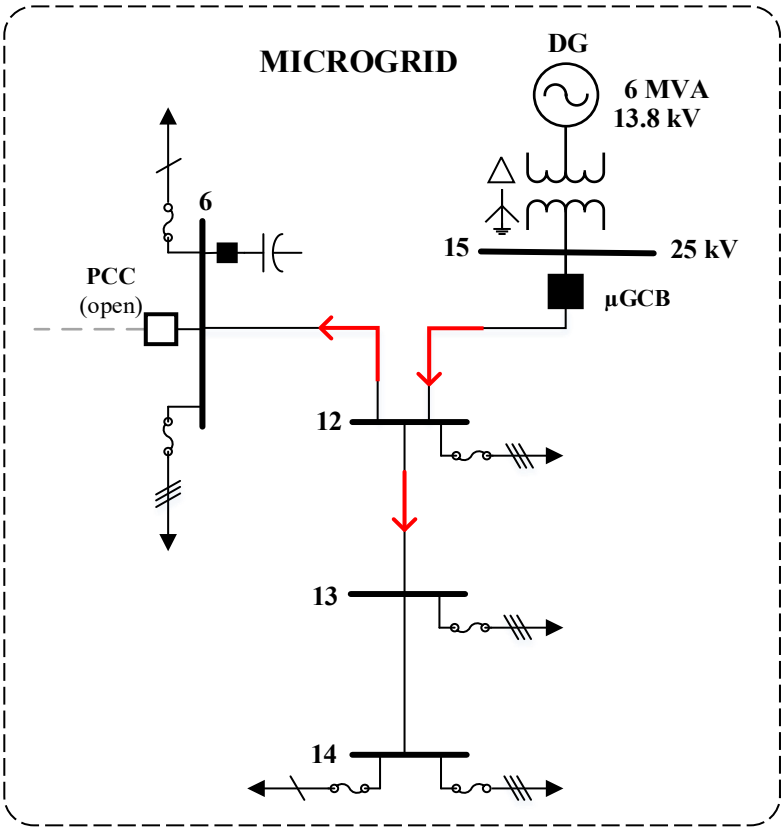

Figure 3.18. Microgrid feeder topology during island mode.

Additionally, during certain emergency situations, such as unavailability of the EPS, or protection operation while in the grid-connected mode, the microgrid may be allowed to island with the pre-established portion of utility load beyond the point of common coupling depicted in Figure 3.19. In this scenario, the boundaries of the microgrid are extended temporarily, and thus, additional protection elements must be considered in the protection scheme. The events after which the extended island may occur and how the microgrid control system handles them are covered in more details in Section 3.6. Note that RCL3 and RCL4 are open to avoid the load, totalling 5.6 MVA, exceeds the generation capacity within the island.

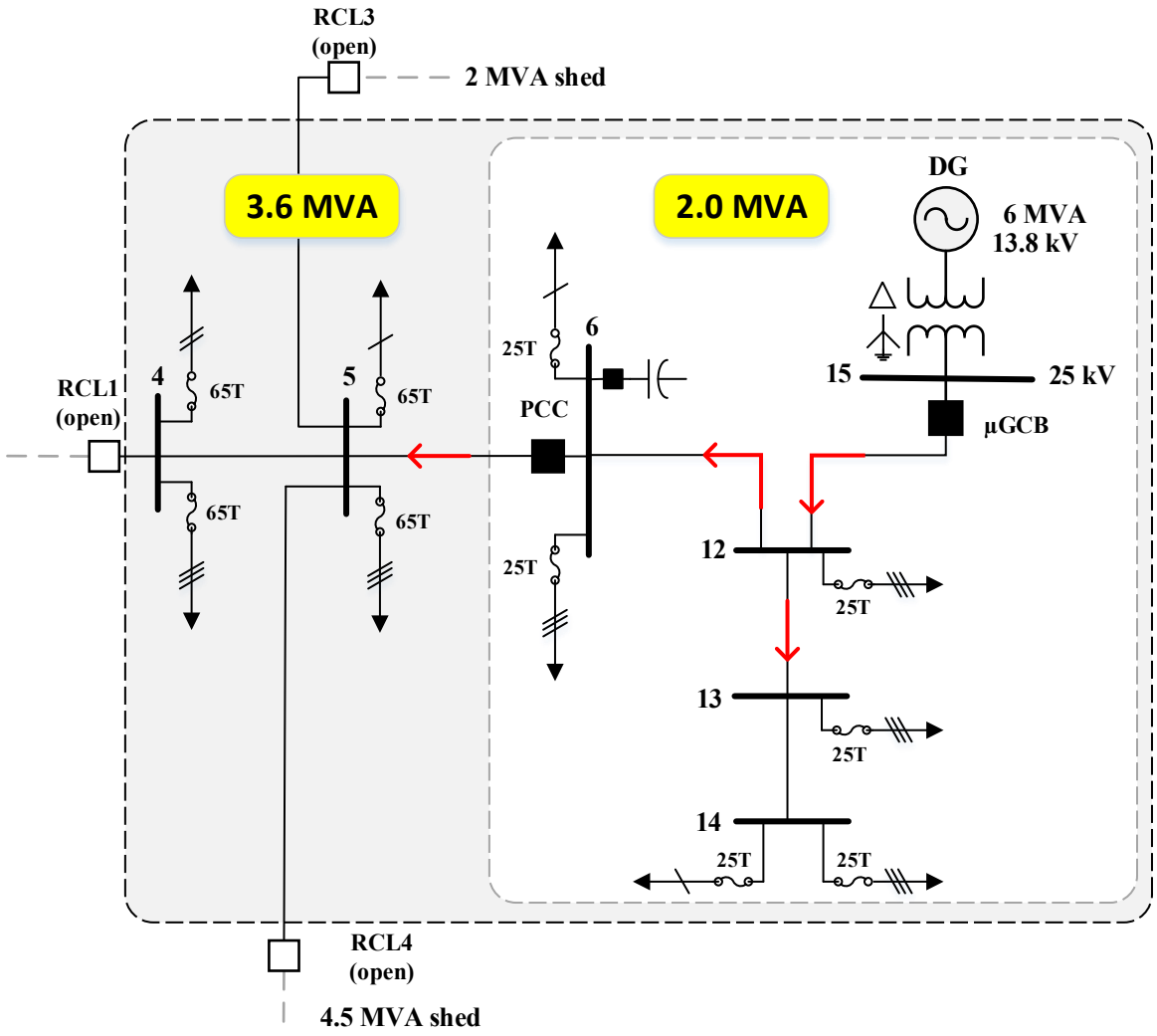

Figure 3.19. Extended microgrid boundaries during emergency operation.

In the island mode, either planned or unplanned, the short-circuit levels are significantly reduced when compared to the grid-connected mode. Therefore, adaptive overcurrent protection is required for the relays at µGCB and the PCC to coordinate properly with the fuses within the island for diminished fault currents [58]–[60]. Figure 3.20 depicts the time-overcurrent coordination between the protection devices in the island mode. In this topology, bolted faults range from 300 A to 1200 A depending on the location and type of the fault. Granted this, for any fault occurring beyond the common coupling (utility infrastructure), the relay at PCC must operate in a fuse-saving scheme with the fuses in the utility side of the island (65T); this allows the 50/51 protection at PCC to operate within 1 second for any fault while also allowing fast coordination with the relay at µGCB, which serves as a backup with a minimum CTI of 0.2 second. On the other hand, for faults

occurring within the microgrid, to the right of the point of common coupling, the relay at µGCB operates in a fuse-blowing scheme with the fuses in the zone (25T). All bolted faults within the microgrid are cleared within 1 second.

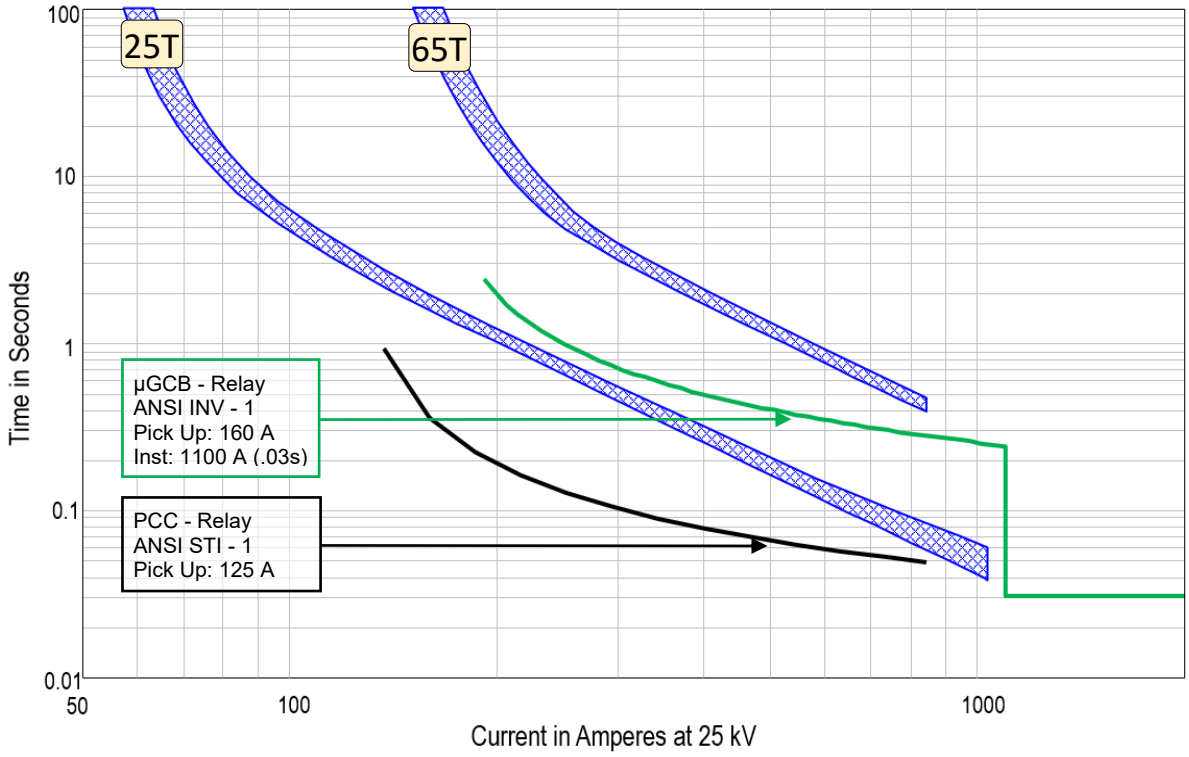

Figure 3.20. Protection coordination for the island mode (planned and unplanned).

It is worth noting that during planned or unplanned transitions to the island mode that result in the formation of the grid depicted in Figure 3.18, adaptive protection is only applied to the relay at µGCB and no changes are made to the relay at PCC. A summary of the phase and ground protection settings for the island mode are reported in Appendix C.

3.6. Microgrid Control System

To ensure the adequacy of the standalone operation of the microgrid as well as its interoperability with the EPS in the grid-connected mode, the functional requirements of the microgrid control system must be established as described in Section 3.3. For the feeder studied in this chapter, the proposed microgrid control system (MGCS) consists in a decision-making and monitoring module embedded in a CPU featuring bi-directional communication capability with multiple devices via a remote terminal unit (RTU) as shown in Figure 3.21. In this application, the RTU serves both as

an analog and digital input/output data interface between the supervised and controlled devices and the MGCS, as well as a gateway for communications [61].

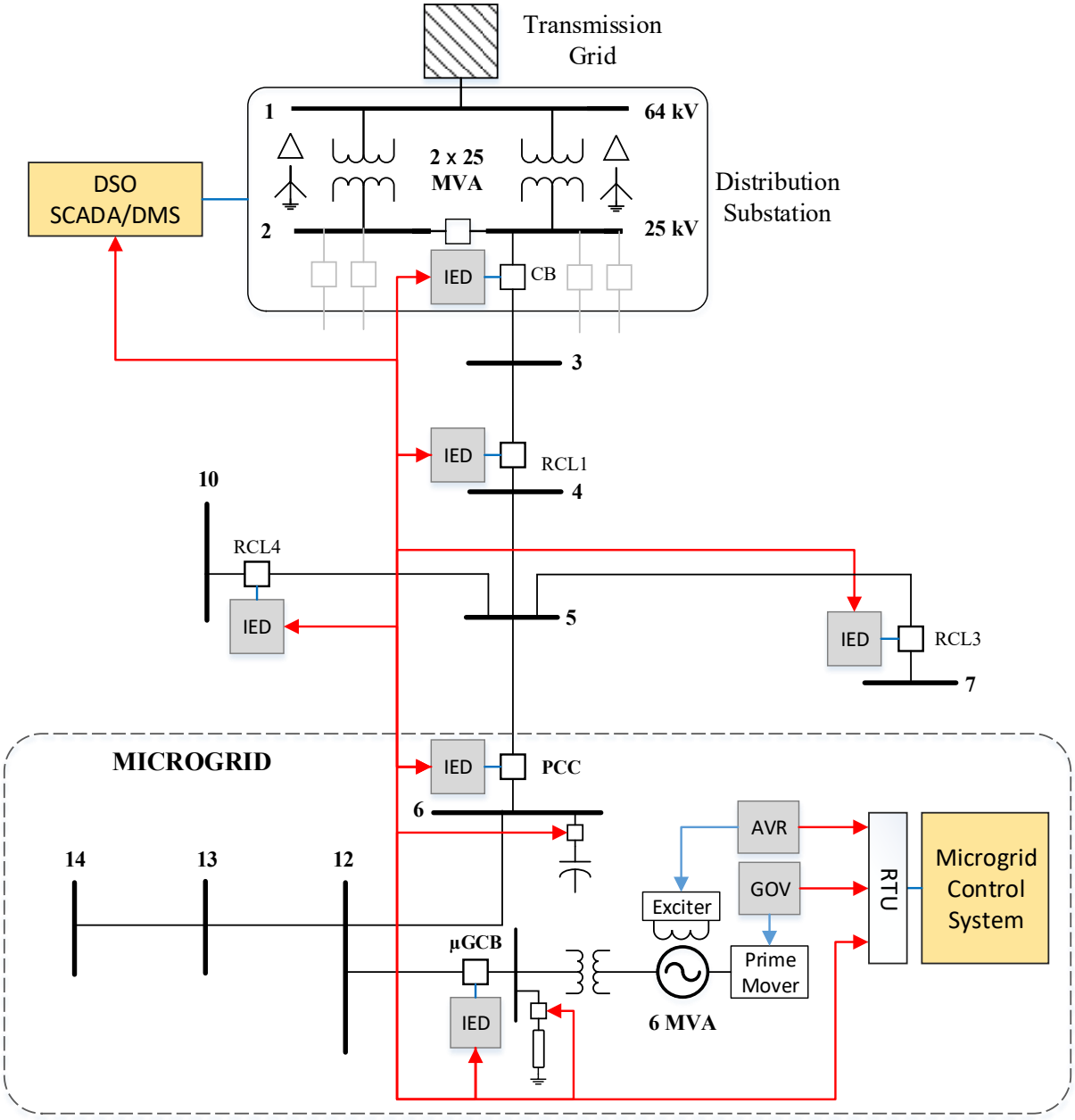

Figure 3.21. Architecture of the microgrid control system.

In this architecture, the MGCS is able to monitor and command local devices, including the machine governor control and its automatic voltage regulator (AVR) as well as the remote protection devices deployed along the feeder, interconnected to one another in the same local area network (LAN) through a shared optical fiber channel. Furthermore, this communication channel

serves as a link between the DSO and the MGCS, for bi-directional exchange of information and requests. In the next sections, the functional specifications of the microgrid control system are defined in accordance with IEEE Std. 2030.7 [14]. For communication compatibility, the MGCS must also be IEC 61850 compliant.

3.6.1. Specification of the dispatch functions

As discussed in Section 3.3.1, the dispatch function is in charge of commanding the generation within the microgrid based on predefined settings, known as dispatch rules, applied to the DERs and other dispatchable elements such as capacitor banks, within the microgrid, soon after a transition between operation modes has occurred or upon external request. Normally, these rules are established upon contractual agreement between the microgrid or the DER operator/owner and the DSO, especially for the grid-connected mode. Granted this, to define the dispatch rules, the functional requirements of the DG must be delimited first.

As per IEEE Std. 1547 [15], the synchronous machine in the DG station can be classified in category B, assigned to DERs fully capable of regulating voltage, and reactive power while in the grid-connected mode. In this context, as a category B DER, the synchronous machine in the microgrid under study must be able to operate in either of the following modes when operating in parallel with the grid:

- Active power-reactive power mode (PQ or watt-var mode).
- Voltage-active power mode (PV or volt-watt mode).

Other operating modes, such as constant power factor mode, constant reactive power mode and voltage-reactive power mode (QV or volt-var mode) are also mandatory for category B DERs as per IEEE 1547 recommendation; however, dispatch rules based on these modes are not required for this application. For the island mode, voltage regulation can be performed by reactive power sharing control (closed-loop control to reach voltage setpoint) whereas frequency regulation can be achieved by means of isochronous control (constant speed control) as specified in IEEE Std. 1547.4 [62]. Table 3.2 summarizes a set of practical dispatch rules for the operation of the synchronous machine for grid-connected and the island mode. Note that the settings for each rule can be modified anytime when required by the DSO.

Table 3.2. Default dispatch rules and settings for the DG based on the microgrid operation mode.

Dispatch Rule Code	Rule Objective	Microgrid Operation Mode	DG Operation Mode	P_{DG}	Q_{DG}	$V_{control}$
DRGC1	Fixed Active Power Export	Grid-connected mode	PV	$k \cdot P_{rated}$ $0.1 \leq k \leq 0.9$	n/a	1.00 p.u. @ bus 15
DRGC2	No Active Power Export	Grid-connected mode	PV	$P\ @\ PCC \approx 0$	n/a	1.00 p.u. @ bus 15
DRGC3	Variable Power Export/Import	Grid-connected mode	PQ	$P_{min} \leq P \leq P_{rated}$	$Q_{\text{maxabs}} \leq Q \leq Q_{maxinj}$	n/a
DRGC4	No Export/ Pre-island	Grid-connected mode	PQ	$P\ @\ PCC \approx 0$	$Q\ @\ PCC \approx 0$ Capacitor Bank OFF	n/a
DRGC5	No Export/ Pre-island	Grid-connected mode	PQ	$P\ @\ RCL1 \approx 0$	$Q\ @\ RCL1 \approx 0$ Capacitor Bank OFF	n/a
DRIM1	Local Voltage – frequency control	Island mode	SL[(1)]	$P_{load}\ @\ 60\ Hz$	$Q\ @\ V_{control}$	1.00 p.u. @ bus 15
DRIM2	Local Voltage – frequency control	Island mode (emergency)	SL	As required by the transition functions during unintentional transitions to island mode.		
DRIM3	Remote Voltage – frequency control (synchronization)	Island mode	SL	Allows voltage and frequency control with different parameters to those in DRIM1 for reconnection to the main grid		

(1) Slack mode (SL): DG operates as reference machine with isochronous and reactive power sharing control.

Figure 3.22 depicts the time-domain simulation performed on EMTP-RV for the operation of the dispatch function during a planned transition from the grid-connected mode to the island mode. Before the islanding request is received by the MGCS, the DG output was set to 80% (4.8 MW) at nominal voltage (dispatch rule DRGC1, $k = 0.8$). In this condition, the active power export from the microgrid to the utility measured at 2.8 MW at the PCC. Soon after the request is approved, the dispatch rule is switched to DRGC4, reducing the power export through the PCC to 0. Finally, after steady state has been reached, the point of common coupling is opened, attaining a seamless transition between operation modes.

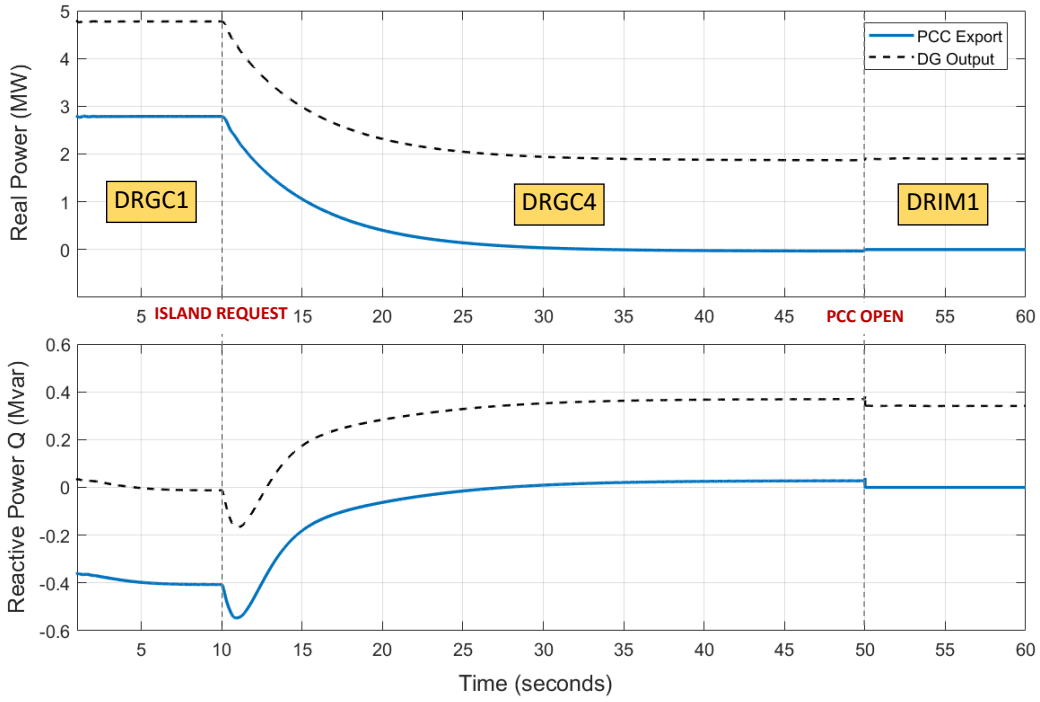

Figure 3.22. Operation of the dispatch function during intentional transitions to the island mode.

It must be considered that before authorizing a request to execute a specific dispatch rule, the current microgrid operation mode must be properly calculated in the MGCS by circuit breaker status monitoring. For instance, dispatch rules intended for the island mode can only be put into effect if either the PCC or RCL1 (for extended island) are open while the DG is operational.

3.6.2. Specifications of the transition functions

As discussed in previous sections, the transition function in the MGCS executes a sequence of actions to attain a seamless transition between operation modes. These actions are specific for each type of transition to ensure the microgrid properly adapts to the new grid conditions, such as load

and short-circuit levels. This process takes place from the moment a transition is requested or estimated (for unplanned transitions) until steady-state operation is achieved. Additionally, as the transition function has the highest hierarchy in the MGCS, it may also command the dispatch function during transitions. In the following sections, the specific actions for each transition type are presented.

3.6.2.1. Grid-connected mode to island mode (intentional)

For intentional or planned transitions from the grid-connected mode to the island mode, the transition function must progressively adjust the operating conditions in the microgrid to avoid significant transients after disconnection from the main grid. Thus, fast power quality mitigation actions are not required. The sub functions and actions included in the transition function for the MGCS depicted in Figure 3.21 is listed Table 3.3.

Table 3.3. Subfunctions included in the transition function module.

Subfunction	Action	Target Devices
Request Processing	Initiates the islanding process upon external request. - Island 1: Microgrid (standalone) - Island 2: Extended Island (emergency)	n/a
Communication Test	Checks the communication link between the MGCS and the actuating IEDs in the feeder for remote command by ping testing or GOOSE messaging.	IED: PCC, RCL1, RCL3 and RCL4 Capacitor Bank CB
Dispatch Adjusting	Transmits a command to the dispatch function to prepare the DG for the transition.	AVR and GOV (via dispatch function)
Import/Export calculation	Calculates or retrieves the exported or imported power at the islanding device.	IED: PCC or RCL1
Power Flow Check	Allows the disconnection of the islanding device when the power at the islanding device is below the minimum threshold (5% of machine rated power) within a preestablished timeout setting (1 minute).	n/a
Remote tripping	Generates and transmits a tripping command for the circuit breakers (through their IEDs) involved in the islanding process.	IED: PCC, RCL1, RCL3 and RCL4 Capacitor Bank CB
Protection Reconfiguration	Updates the protection settings of the applicable IEDs within the islanded circuit as part of the adaptive protection strategy.	IED: µGCB, PCC

Note that as many of the subfunctions required for planned transitions are reliant on a healthy communication channel, the latter must be checked first before proceeding with the islanding sequence. As the MGCS and the protection IEDs in the feeder are in the same Internet-protocol-based local area network, the health of the communication link and reachability between them may be verified by a ping test or a GOOSE messaging test [63], [64].

Figure 3.23 shows the sequential execution of the sub functions included in the transition module in the MGCS. In normal conditions, this process should be completed in few seconds depending on the current DG output and the load as illustrated previously in Figure 3.22.

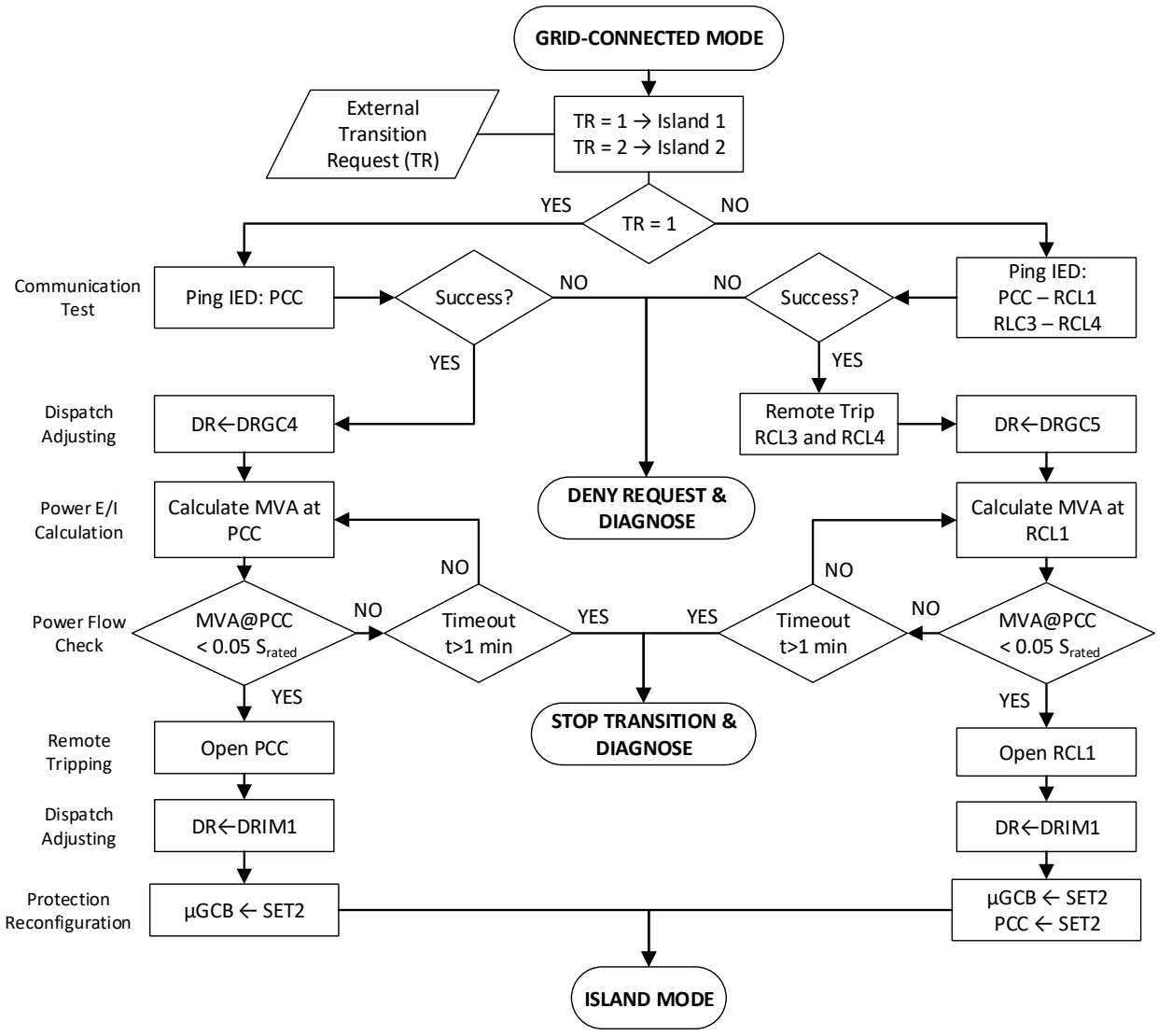

Figure 3.23. Sequence of actions for planned islanding.

3.6.2.2. Grid-connected mode to island mode (unintentional)

Power disturbances in the utility side may cause a sudden and inadvertent disconnection of the microgrid from the area EPS. In this scenario, the operating conditions in the microgrid (e.g., power import/export at PCC) may not be adequate at the moment of disconnection. As a result, significant power quality issues and transients might arise as a consequence of the load-generation unbalance and the generator controllers rapidly attempting to restore it.

As discussed previously, the most common cause of unintentional islanding is protection operation. For the microgrid under study, unintentional islanding involving microgrid load only will occur for faults in zone 2 as shown in Figure 3.24, as these must be normally cleared by RCL1 and PCC, breaking the path of parallel operation between the utility and the microgrid. This situation may lead to voltage and frequency regulation issues within the microgrid, mainly caused by load-generation unbalance and DG under or over excitement.

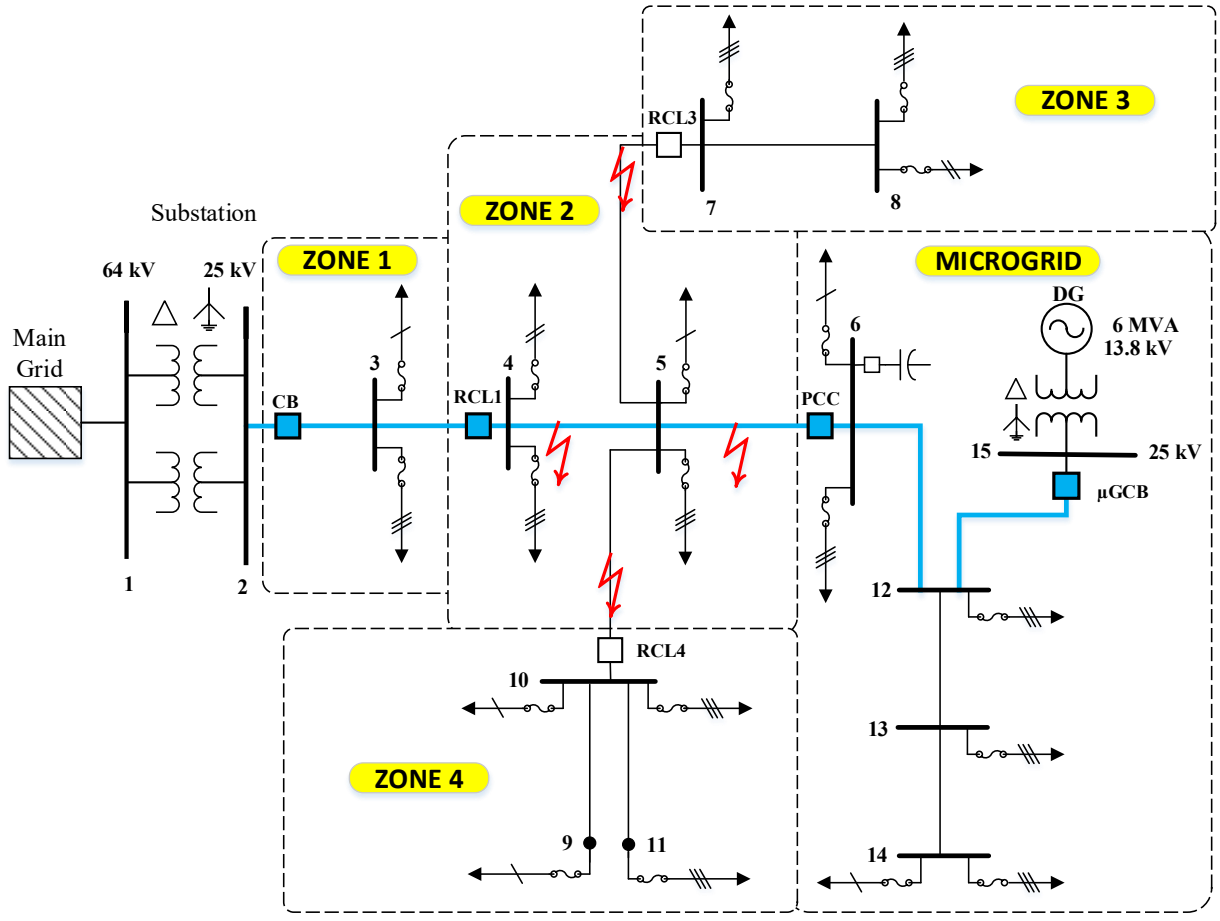

Figure 3.24. Protection zones in the grid-connected mode.

Additionally, other island configurations encompassing utility load can be unintentionally formed due to protection operation in other zones. For instance, an island encircling the microgrid and load in zones 2, 3 and 4 will be formed immediately after protection tripping for faults in zone 1, normally cleared by CB and RCL1. On the other hand, the load in zone 1 may be included in the islanded portion if the feeder head-end CB is tripped by bus 2 differential protection for faults in the utility substation. In all these cases, the generation-load unbalance is unsustainable as the DG capacity is insufficient to match the load, even in a minimum-demand scenario.

To tackle these problems, a series of specific actions must be taken by the MGCS via the transition function to ensure island viability while mitigating any power quality issues that may ensue. The execution of these actions is triggered by the islanding detection algorithm, a module within the MGCS that oversees the inadvertent formation of islands. This module contains two core detection techniques, a fast, remote method serving as main islanding detector and a local, passive detection method as a backup for the first.

The remote detection method consists in real-time switch-state and DG status monitoring taking advantage of the communication infrastructure between the MGCS and the islanding circuit breakers and reclosers through their corresponding IEDs. The advantage of this method is the high islanding detection speed (< 2 cycles) with virtually zero non-detection zone (NDZ) as long as the communication between devices is available [65]. Additionally, the exact island condition may be estimated through a lookup table as shown in Table 3.4 for which specific actions may be taken.

Table 3.4. Lookup table for possible island configurations

Island Code	Islanding Device Status					Zones Islanded	Maximum Islanded Load
	CB	RCL1	PCC	μGCB	DG		
ISL1	n/r*	n/r	0	1	1	Microgrid Only	2 MVA
ISL2	n/r	0	1	1	1	Microgrid and Zone 2, 3 and 4	12.1 MVA
ISL3	0	1	1	1	1	Microgrid and Zone 1,2, 3 and 4	12.7 MVA

* n/r denotes a circuit breaker status that is not required for decision making in the MGCS.

On the other hand, the local passive method (backup islanding detection) uses a multilevel Rate of Chance of Frequency relay (ROCOF, ANSI function 81R) at the DG station to measure the variation of frequency over time when unintentional islanding has occurred. Although this detection technique has a higher NDZ [50], it is effective for scenarios during which the unintentional island results in power mismatch. Thus, islanding conditions ISL2 and ISL3 can be detected without difficulty regardless of the DG output at the moment of disconnection. However, detection of ISL1 may be compromised during unintentional islanding if the DG matches the microgrid load after the transition. Therefore, most island configurations may be detected if the power export or import at the PCC is different from zero. For this reason, this condition is only advisable if communication between the MGCS and PCC is available so that unintentional islanding of the microgrid only could be always detected by the primary method. The settings for the ROCOF relay are presented in Table 3.5. These settings were defined based on time-domain simulation using EMTP-RV for unintentional islanding events caused by different fault types at multiple locations along the feeder. The third-level setting, ROCOF-3, requires at least 1 MVA exported to the main grid at the PCC for islanding detection.

Table 3.5. Settings for the ROCOF relay.

Level	df/dt (Hz/s)	Time (s)	Island Condition
ROCOF-1	-1.5	0.15	ISL2 – ISL3
ROCOF-2	-1	0.50	ISL2 – ISL3
ROCOF-3	+1.25	0.20	ISL1

The selected settings allow the ROCOF relay to detect unintentional islanding conditions within 2 seconds, complying with IEEE Std 1547, Clause 8.1 [15] while also avoiding false detection during the transient period from fault occurrence to protection tripping. The signals generated upon detection are handled by the MGCS for decision making.

In certain conditions, power quality issues regarding voltage and frequency regulation may arise following an unintentional islanding event. Normally, the settings of the governor and automatic voltage control are updated by the dispatch function upon islanding detection to allow voltage and frequency regulation as in planned transitions. In most cases, this is sufficient to ride through the power disturbance until steady state is reached within the island. However, in some circumstances,

this disturbance may compromise the viability of the island, causing operation of over/under voltage or frequency protection, finally forcing DG to shutdown. Figure 3.25 shows the response of the AVR and isochronous control of the DG for an unintentional islanding event caused by tripping of the point of common coupling following a bolted three-phase fault in zone 2. Before the fault occurs ($t = 1\ s$), the DG was dispatching 80% of its capacity (4.8 MW) with a total 2.8 MW exported to the main grid through the PCC and the capacitor bank in node 6 was online. As it can be observed, voltage and frequency in the island are restored to normal values in a few seconds after the unintentional islanding event takes place. However, as the AVR attempts to rapidly recover nominal conditions after a significant voltage sag and in an unbalanced island scenario, a voltage overshoot exceeding 120% of the DG rated value for about occurs.

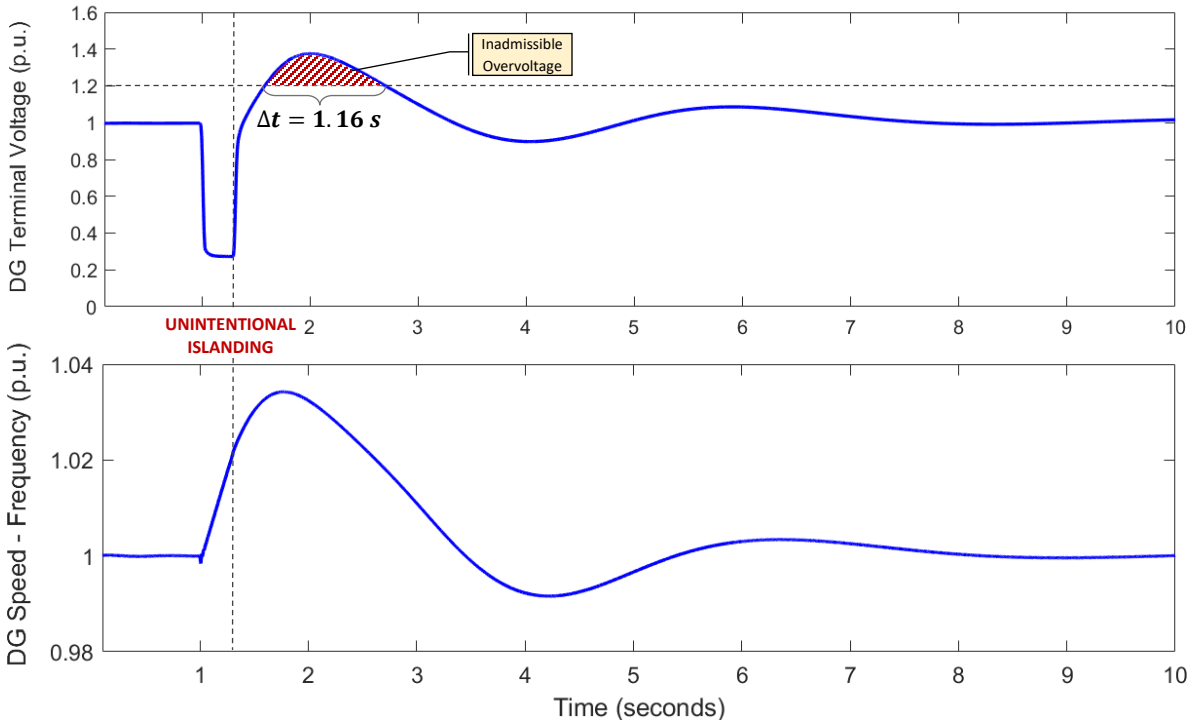

Figure 3.25. Island voltage and frequency following an unintentional islanding event.

Although IEEE Std. 1547 requires the overvoltage protection settings to allow the DG to ride through temporary voltage disturbances above 1.10 p.u., it also mandates to cease its operation for voltage magnitudes above 1.20 p.u. within 10 cycles (160 ms.). In this context, the islanding condition presented in Figure 3.25 is unviable as the DG should be shutdown.

To avoid losing the microgrid load during unintentional islanding caused by external faults, the transition function for this study case also includes an overvoltage mitigation module (OVMM) supported by additional components in the microgrid. First, a supervisory undervoltage relay function (ANSI function 27U) is included in the MGCS to allow the detection of voltage sags in the DG terminal. This function serves as an indicative of a possible external fault that may result in unintentional islanding. This helps the MGCS execute specific preemptive mitigating actions before the separation from the main grid occurs. Additionally, to temporarily compensate for the power mismatch resulting from unintentional islanding events, a significant factor in the appearance of inadmissible overvoltages, a breaking resistor bank is also incorporated to the microgrid. This shunt bank, consisting of three 500 Ω resistors connected in star, has the capability of drawing 1.25 MW at 25 kV. This bank is physically connected to the HV bus of the DG transformer and can be remotely switched on and off by the MGCS as required. Table 3.6 summarizes the additional subfunctions required for the overvoltage mitigation module within the transition function.

Table 3.6. Transition subfunctions for overvoltage mitigation.

Subfunction	Action	Target Devices
Voltage Sag Detection	Uses relay function 27U to generates a logic signal whenever the DG terminal voltage falls below 0.5 p.u. for at least 50 ms.	n/a
Update EDR (Preemptive)	Updates the emergency dispatch rule DRIM2 to temporarily reduce the DG voltage setpoint to 0.90 p.u. for 30 seconds. If no island is detected within 2 seconds of voltage sag detection, voltage setpoint is restored to 1 p.u. in 3 seconds.	AVR (via dispatch function)
Remote Capacitor Tripping (Preemptive)	Capacitor bank at node 6 is disconnected remotely.	Capacitor Bank
Breaking Resistor Switch On/Off	The breaking resistor bank (RS1) is connected for 15 seconds when voltage crosses 0.95 p.u.	RB1
Process Interruption	Allows the overvoltage mitigation process to stop immediately using interruption-based programming. Voltage setpoint is restored to 1 p.u..	n/a

For islanding conditions ISL2 and ISL3, overvoltage magnitudes above the permissible values are unlikely to occur as load is significantly larger that generation capacity. Thus, upon discrimination

of these specific scenarios, the OVMM must be interrupted to avoid unnecessary actions to be taken. Moreover, as these island configurations are not viable, a straight-forward load shedding strategy must be executed to hold as much load as possible within the DG capability. Granted that, whenever ISL2 or ISL3 are detected, a remote tripping command is transmitted to RCL1, RCL3 and RCL4 to isolate the load in the microgrid and the one in zone 2 for a total maximum load of 5.6 MVA, corresponding to 93% of DG rated power. This configuration corresponds to the extended island presented in Figure 3.19. However, if remote tripping fails, the trip is then transferred to PCC to island the microgrid only. The operation logic of the transition function including the OVMM is depicted in Figure 3.26.

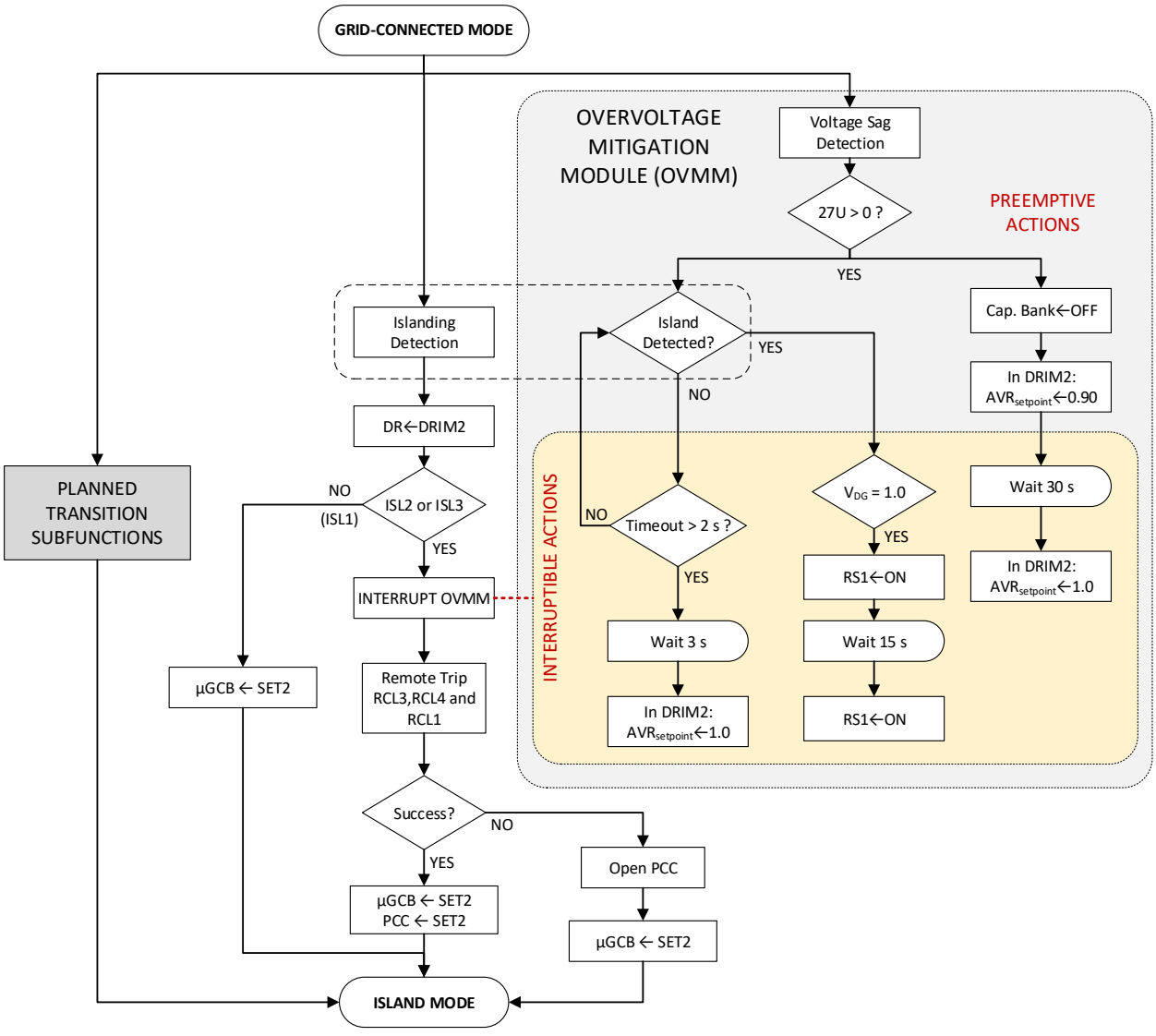

Figure 3.26. Transition function with unintentional islanding handling.

Figure 3.27 shows the performance of the OVMM during an unintentional islanding event with similar conditions to the one presented previously in Figure 3.25. In this scenario, after the islanding occurs, the voltage crosses the 1.10 p.u. threshold for less than 0.5 second without overshooting beyond 1.15 p.u. It must be taken into account that IEEE Std.1547 recommends overriding the DG overvoltage protection for at least 1 second for temporary overvoltage magnitudes between 1.10 p.u. and 1.15 p.u.; thus, the DG should be able to ride through the disturbance without being forced to shutdown.

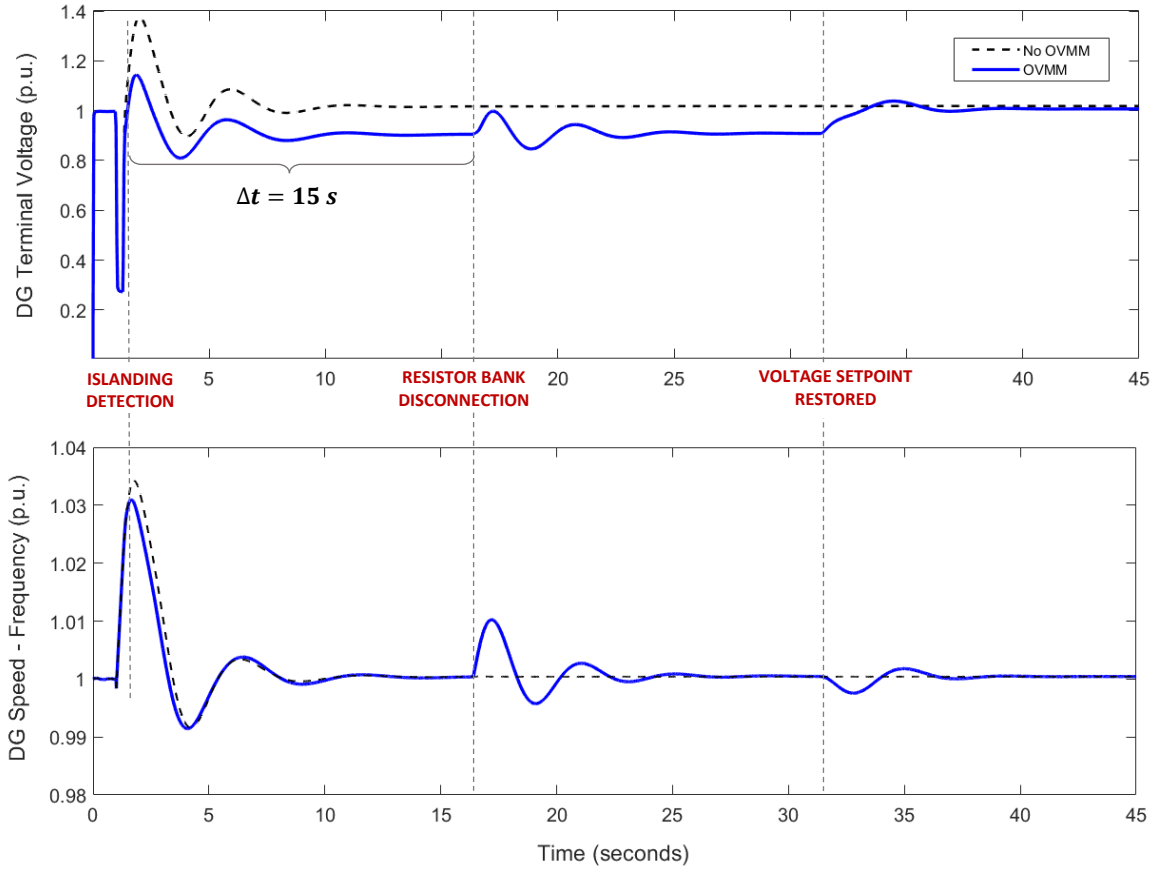

Figure 3.27. Mitigation of impermissible overvoltage magnitudes during unintentional islanding.

3.6.2.3. Island mode to grid-connected mode

Transitions from the island mode to the grid-connected can only be initiated upon external request. Therefore, it is assumed that these transitions are always planned or scheduled beforehand. For the reconnection of the microgrid to the area EPS, an automatic synchro-check relay (ANSI function 25) is required at the paralleling devices, either PCC for the microgrid island or RCL1 for the extended microgrid configuration. This relay authorizes the MGCS to transmit a remote closing

command to the corresponding reconnection circuit breaker through their IED when the synchronism conditions are within the limits listed in Table 3.7, recommended in IEEE Std.1547 for synchronization of DG units with a rated power larger than 1.5 MVA with the area EPS.

Table 3.7. Synchronization parameter limits.

Parameter	Unit	Value
Frequency difference (Δf)	Hz	0.1
Voltage difference (ΔV)	%	3.0
Phase Angle Difference ($\Delta\phi$)	Degree	10

If these conditions are not met simultaneously, the transition function must first allow the remote voltage and frequency matching control in the microgrid via the dispatch function (dispatch rule DRIM3) to match those in the main grid at the point of connection (PCC or RCL1). After frequency matching, a slip frequency $\Delta f = \pm 0.025$ Hz may be used to reduce phase angle difference at a rate of 10 degrees per second. Figure 3.28 shows the voltage at the PCC during a re-synchronization with $\Delta V = 0.012$ p.u., $\Delta f = 0.001$ Hz and $\Delta\phi = 5°$. As it can be noted, after the re-connection ($t = 5\ s$), the resulting voltage step does not exceed 0.55% of rated voltage from the utility standpoint, and 1% from the microgrid standpoint. This also complies with IEEE Std. 1547 (clause 4.10.4) that requires a voltage step less than 3% of the rated value if the point of common coupling is located at the MV level.

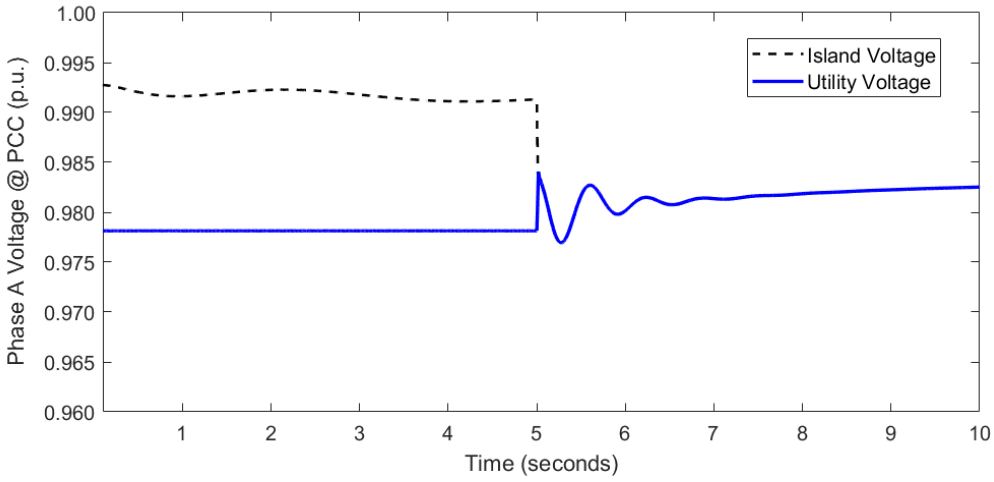

Figure 3.28. Voltage at the point of common coupling during reconnection to the main grid.

3.7. Summary

In this Chapter, a brief discussion on the microgrid concept, including a description of the microgrid operation modes, its technical challenges and functional requirements is presented. Subsequently, the specifications for a protection system and the functional requirements for a microgrid controller are defined for a benchmark MV feeder comprising a microgrid with a synchronous-machine-based distributed generator. Later, the implementation and performance of the microgrid control system in the benchmark network during transitions between operating modes is tested using time-domain simulations in the EMTP-RV software. The benchmark network, and the islanding strategy presented in this chapter are used in Chapter 4 to assess the impact of microgrid islanding on service restoration during CLPU conditions.

Chapter 4

EFFECT OF MICROGRID ISLANDING ON CLPU

4.1. Framework for Benchmarking

In this chapter, the physical load model presented in Section 2.6.3 is scripted in MATLAB and used to analyze the impact of unplanned microgrid islanding on service restoration times under the severe CLPU conditions that may ensue following extended outages during typical Canadian winter conditions. To accomplish this, the distribution feeder containing the microgrid, in conjunction with the islanding strategy presented in Chapter 3 is used as a benchmark network with its load adjusted to physically reflect the progressive loss of diversity that occurs during prolonged service interruptions amid significantly low outdoor temperatures. The selected criteria to assess the level of impact focuses on the estimation of restoration times, and event-based reliability indices including energy not supplied (ENS) and its costs.

4.1.1. Load and CLPU parameters

As defined in Section 2.6.3, apart from the physical characteristics of the heating elements and the average Canadian dwellings in which they are installed, the weather conditions play a critical role in the load behavior during normal conditions and CLPU. Additionally, as there is no information in reference [53] on the number of customers connected to the feeder for the benchmark network, this must be estimated first as this parameter is also required for the construction of the physical CLPU model. In this context, two daily temperature profiles are considered for this work.

The first temperature profile consists of a severe winter day in southern Canada with extremely low temperatures (below -30 °C) [66] as shown in Figure 4.1. With this profile, the number of customers is determined by matching the maximum load of the resulting load profile obtained in with the CLPU model scripted in MATLAB with the system peak load (12.3 MW) reported in [53], based on the assumption that the latter was measured when the heating load was at its maximum during normal operating conditions.

The second profile is used for benchmarking and it corresponds to a scalation of the first profile to 60% to reflect a more recurrent winter day in the same geographic location with an average daily minimum temperature of -20.7 °C [67].

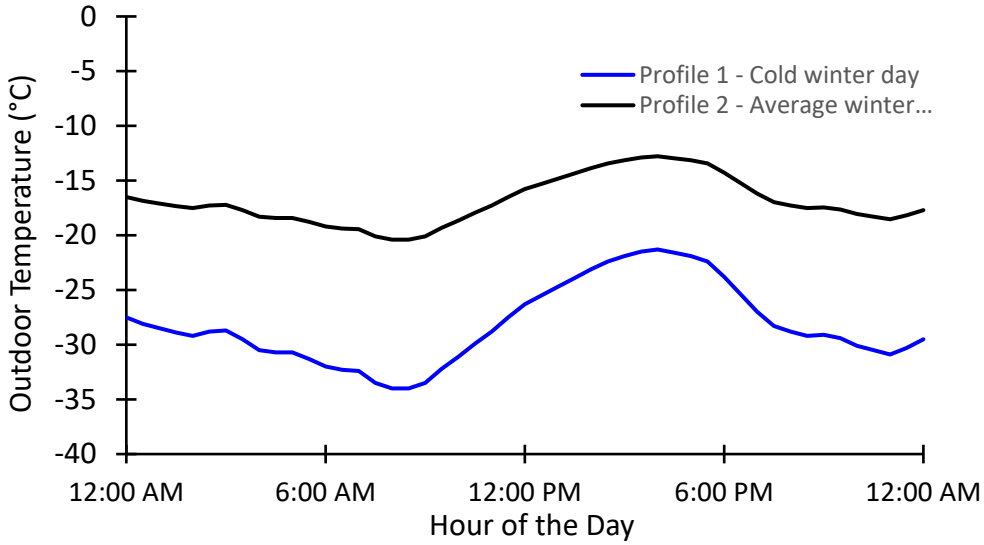

Figure 4.1. Daily temperature profiles for estimation of the peak load and benchmarking.

Figure 4.2 depicts the resulting load profile for the feeder, obtained for a total of 1420 residential customers for the coldest day using the physical load model with the parameters listed in Appendix A. In these weather conditions, the load peaks at 12.3 MW, equaling the total load reported in [53]. This load profile does not include power losses which reach 0.57 MW during the system peak load.

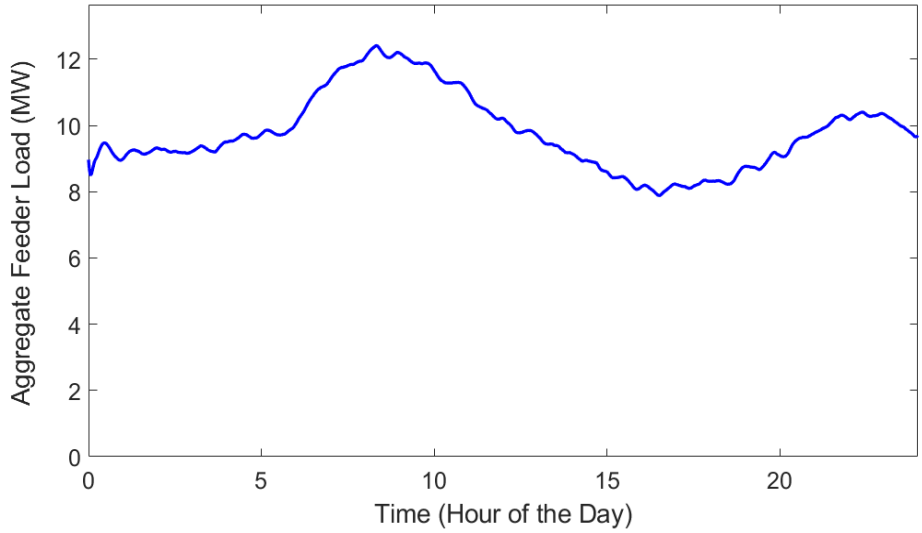

Figure 4.2. Aggregate feeder load for the coldest winter day.

Additionally, the number of customers in each of the zones shown in Figure 3.15 are required for the calculation of the ENS and the restoration times. To estimate these numbers, the physical model given in Section 2.6.3 is used to calculate and match the approximate instantaneous load in each zone with the aggregate load reported in [53] at the system peak shown in Figure 4.2. As the load is considered to have a large resistive heating component, a power factor of 0.99 (lagging) is assumed [53]. The results are listed in Table 4.1.

Table 4.1. Number of customers in each zone.

Zone	Nodes	Total Load (MW)	Number of customers
1	3	0.567	65
2	4,5	3.516	415
3	7,8	1.835	215
4	9,10,11	4.389	500
5 - Microgrid	6,12,13,14	1.958	225

4.1.2. Outage time and duration

As discussed in Chapter 2, the outage duration has a direct relationship with the CLPU magnitude and duration. Hence, four different outage durations are considered for all the cases studied in this chapter, namely a 30-minute outage, and 1, 2 and 3-hour outages. As the outage duration is strictly associated with fault location and reparation time only, it does not include any additional time delay required for the sectionalized feeder restoration strategy discussed in Section 2.5.1. Furthermore, the outage is assumed to occur at 3 PM (15h00), after the coldest part of the day has elapsed. Outages occurring during colder periods will cause a faster rate of loss of diversity, and thus, outage duration will have less relevance.

4.1.3. Assessment criteria

To measure the impact of the proposed unintentional microgrid islanding strategy on service restoration during CLPU conditions, several event-based indices are defined for this research work. These metrics include restoration times, the ENS during the interruption, and its corresponding costs to the utility. Since this study is limited to the winter season and the effect of the heating load behavior on CLPU, other common long-term reliability indices are not considered.

4.1.3.1. Peak CLPU current

The peak CLPU current is the maximum current magnitude measured at the first recloser or circuit breaker to be closed where the risk of nuisance tripping is higher during the sectionalized feeder restoration. These magnitudes are obtained from MATLAB simulations of the physical model for the proposed outage scenarios and are expressed as a percentage of the phase pickup setting of the relay located at the same device accordingly with the protection settings defined in Section 3.5.4. To determine whether a CLPU current magnitude that is above the pickup setting of the affected relay could cause its tripping, the protection scheme implemented in EMTP-RV is used for testing.

4.1.3.2. Restoration Time

The restoration time, $t_{restoration}$, measures the time required to re-establish service after the fault that originally caused the outage has been cleared, repaired, or removed. Normally, if all of the loads lost during the outage can be restored at once, $t_{restoration}$ is equal to zero. If the CLPU during restoration of a portion of the load caused protection operation, $t_{restoration}$ is the minimum additional time delay, rounded up to a 15-minute interval, required before energizing the adjacent feeder section to allow diversification of others previously restored to avoid nuisance tripping.

4.1.3.3. Total interruption duration

The total interruption duration, $t_{interruption}$, measures the time elapsed between protection tripping until service has been restored for all the customers in a specific zone. In general terms, the interruption duration for a particular feeder section can be calculated as the sum of the outage duration and its restoration time.

4.1.3.4. Energy not supplied (ENS)

The total energy not supplied by the system to a single or multiple feeder sections for the assumed interruption periods can be calculated using Equation (4.1), where P_i is the instantaneous load in kW for a time interval Δt of one minute (1/60 hour) obtained from the daily load profile generated in MATLAB assuming continuous service in the affected zone during the same interruption period. The ENS index is calculated for the outage duration and for the additional restoration time as well.

$$ENS = \sum_{i=1}^{n} P_i \Delta t \tag{4.1}$$

Subsequently, the cost of the ENS during the interruption is estimated by multiplying this index by the average electricity rate for residential users in Canada, equal to 0.1488 $/kWh, calculated for the average consumption in the major cities of Canada [68].

4.2. Base Case: Islanding Prohibited

For the base case, it is assumed that the MV feeder presented in Figure 4.3 is operated in a conventional fashion; thus, the DG is not allowed to island, and it is immediately shutdown or disconnected upon fault or islanding detection. As the microgrid is prohibited from supporting the main grid during the outage, all of the load located downstream of the fault clearing device is lost and considered in the cold load pickup model for restoration. Moreover, only permanent faults occurring within zones 1 and 2 are considered as these will result in unintentional microgrid islanding, analyzed in the upcoming sections. In addition, fault clearing in zones 1 and 2 causes a loss of at least 95% of the feeder load.

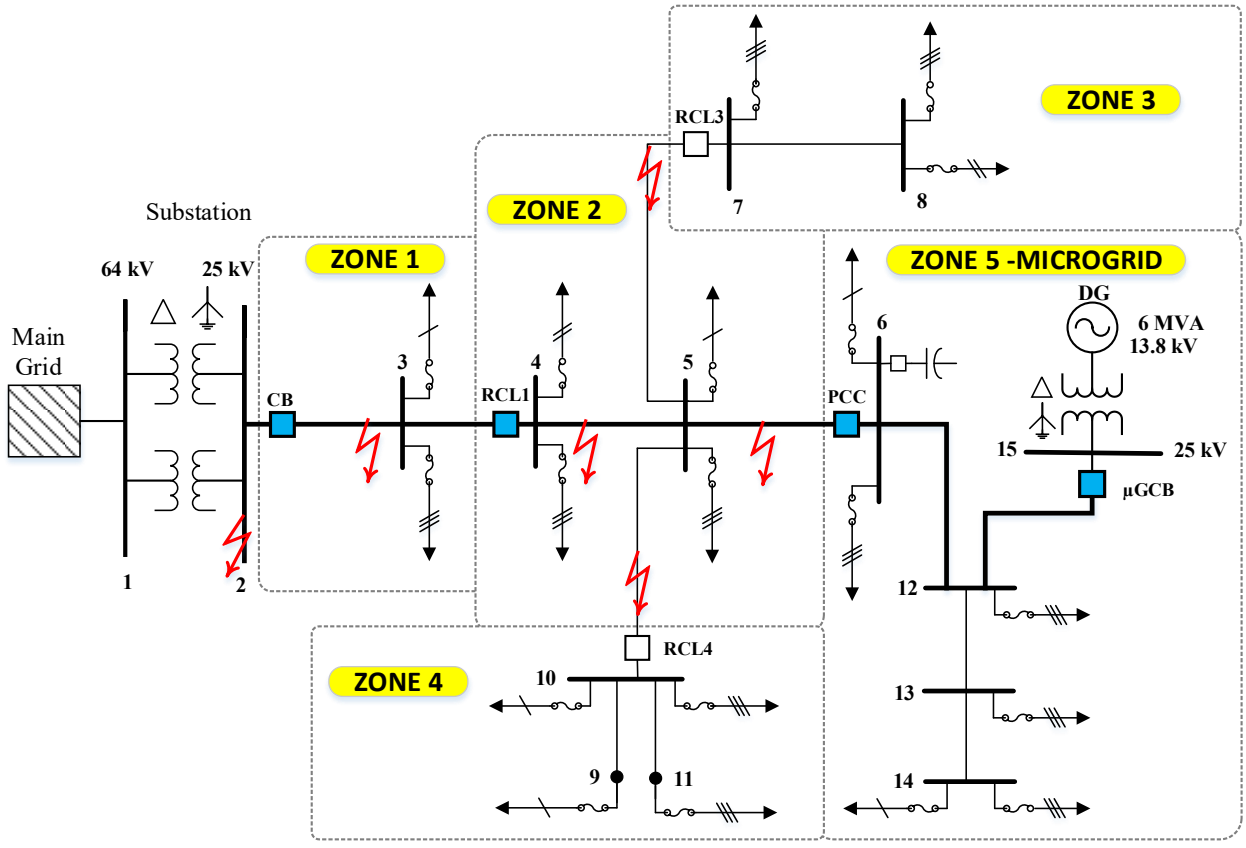

Figure 4.3. Fault locations causing a loss of at least 95% of the feeder load.

Figure 4.4 shows the CLPU current measured at RCL1 while attempting to simultaneously restore service following the outage durations specified in Section 4.1.2 following permanent faults in zone 2. To illustrate the CLPU effects, the protections in CB and RCL1 were locked out from operating during restoration. As it can be noted, when the interruption lasts more than one hour, the CLPU current during restoration temporarily crosses the phase pickup setting at RCL1 (450 A). In this scenario, the recloser will trip in 5 to 40 seconds depending on the outage duration, impeding the simultaneous restoration of the load. Hence, service must be re-established by feeder sectionalizing (restoration by sections) to allow diversification of the load as discussed in Section 2.5.1. Likewise, if zone 1 is lost, the subsequent simultaneous restoration of 100% of the feeder load will also lead to the nuisance tripping of CB or RCL1; however, since the load beyond RCL1 must be restored by parts and the load encompassed in zone 1 is relatively low (65 customers), no additional time is necessary other than the required to energize the load beyond RCL1.

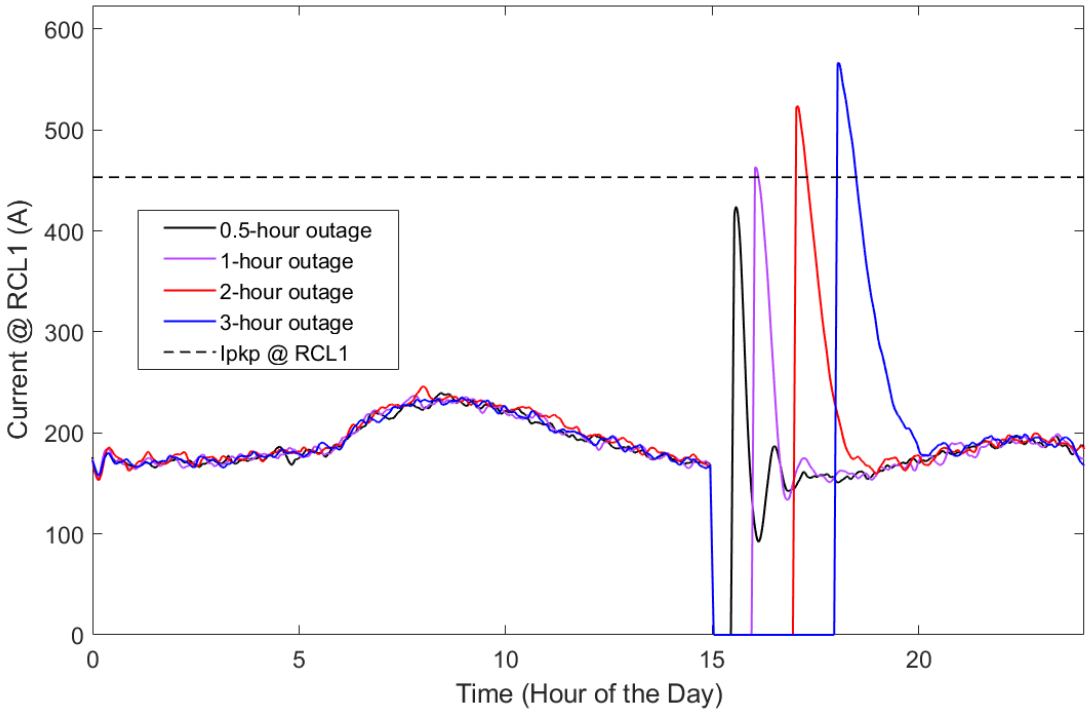

Figure 4.4. Current profile at RCL1 while attempting to restore all loads simultaneously.

To initiate the sectionalized restoration of the feeder assuming the fault has been repaired or removed, the involved reclosers and circuit breakers of the non-faulted sections must be manually or remotely opened first. In this context, the following sequence is considered: first, zones 1,2 and 4 can always be simultaneously restored without any intentional delay regardless of the outage

duration by closing CB, RCL1 and RCL4 while RCL3 and PCC remain open. Depending on the duration of the outage, zones 3 and 5 may also be restored along with the other zones by closing RCL3 or PCC, respectively. However, for the outages lasting longer than 1 hour, a minimum intentional delay before restoring these zones must be taken into account to allow diversification of the previously restored groups and avoid nuisance tripping of CB or RCL1. The minimum restoration times for each outage duration are shown in Table 4.2.

Table 4.2. Minimum time delay for sectionalized restoration of the feeder.

Outage Duration (hours)	$t_{restoration}$ Stage 1 - Zone 5 (hours)	$t_{restoration}$ Stage 2 - Zone 3 (hours)	Longest $t_{interruption}$ (hours)	Peak Current (% of I_{pkp} @ $RCL1$)
0.5	0	0	0.50	95%
1.0	0.25	0	1.25	89%
2.0	0.50	0	2.50	97%
3.0	0.50	0.75	3.75	92%

Figure 4.5 to Figure 4.8 depict the current profile measured at RCL1 and the corresponding contribution of the zones with delayed restoration for the feeder sectionalizing strategy shown in Table 4.2. As can be observed, in neither outage scenario does the peak CLPU current cross the pickup threshold at RCL1 as a result of the reduction of the cumulative effect of the highly undiversified load at this point. Hence, the nuisance tripping of RCL1 can be avoided and service can be re-established at the expense of prolonging the interruption time of the radial tail-end sections of the feeder, in this case zones 3 and 5 (microgrid). It must be pointed out that the reclosers or circuit breakers in charge of restoring smaller clusters of loads, such as RLC3 for zone 3 or PCC for zone 5, are less prone to nuisance tripping during restoration as a fewer number of customers translates into a less diversified load in normal conditions for which pickup settings are defined. If protection tripping occurred while restoring small groups, further sectionalizing may be required.

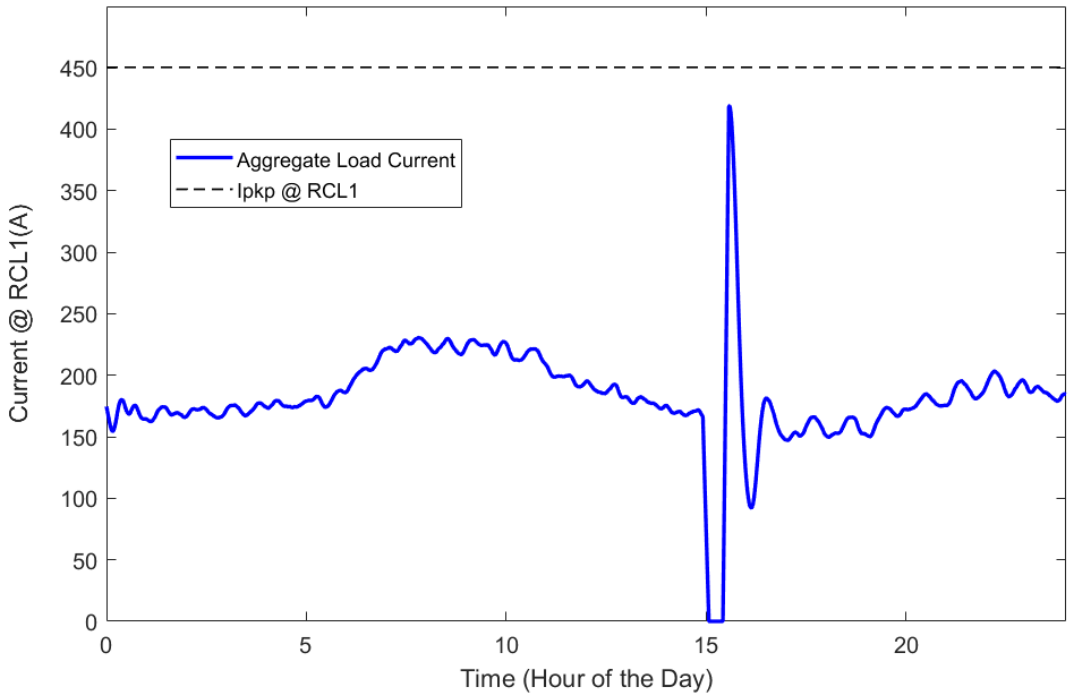

Figure 4.5. CLPU current measured at RCL1 during the simultaneous restoration of 1355 residential customers for the 0.5-hour outage scenario (base case).

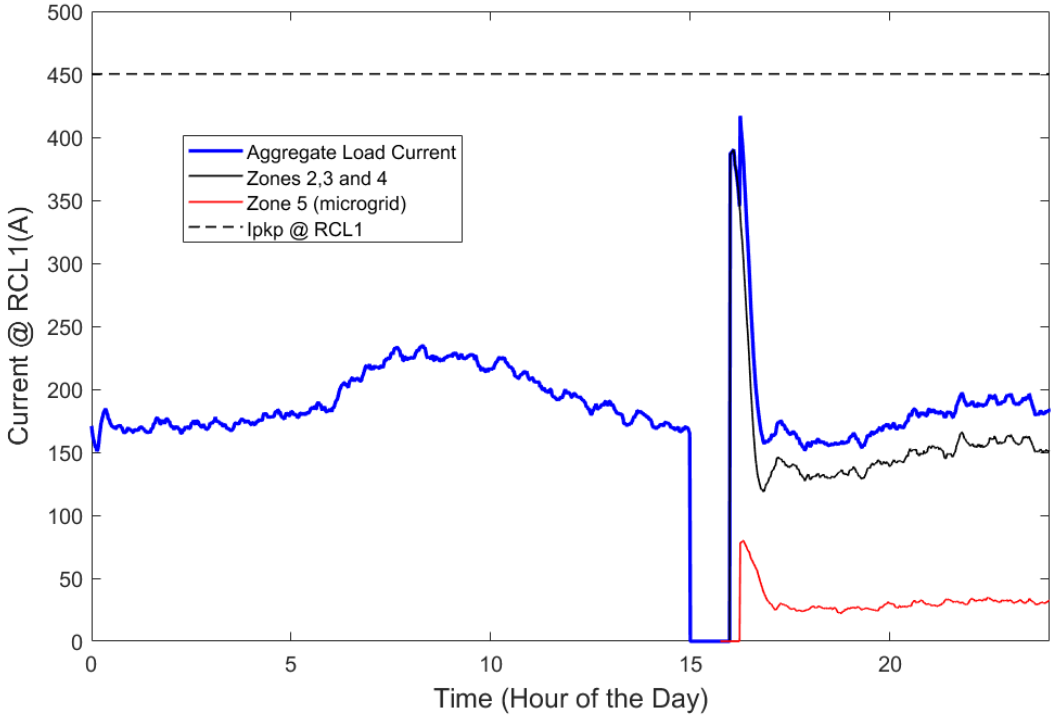

Figure 4.6. CLPU current measured at RCL1 during sectionalized feeder restoration for the 1-hour outage scenario (base case).

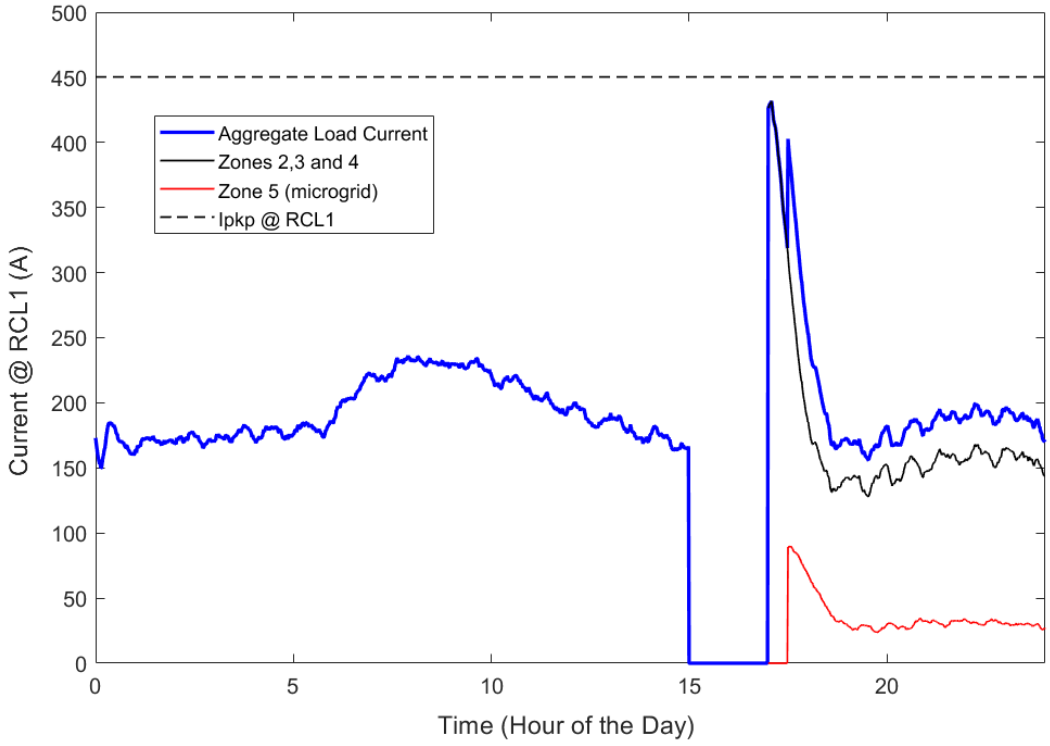

Figure 4.7. CLPU current measured at RCL1 during sectionalized feeder restoration for the 2-hour outage scenario (base case).

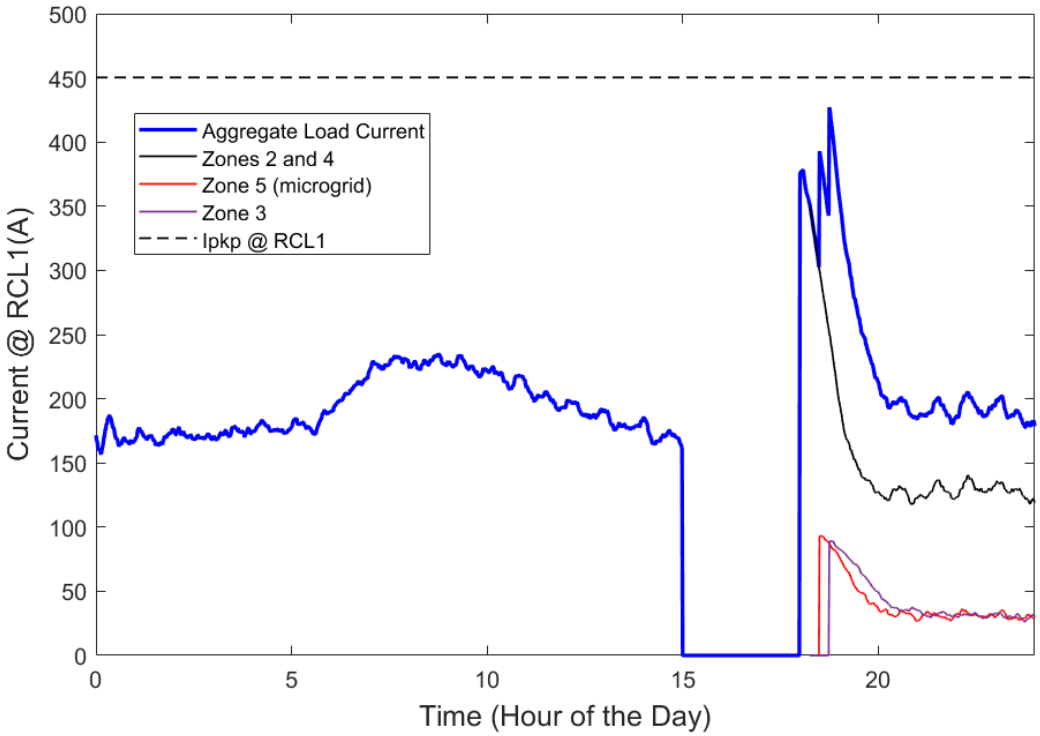

Figure 4.8. CLPU current measured at RCL1 during sectionalized feeder restoration for the 3-hour outage scenario (base case).

The total ENS during the interruptions listed in Table 4.2 is broken down in Table 4.3. As it can be observed, the largest ENS component corresponds to the outage period regardless of its duration. Hence, the cost of the ENS to the utility comes primarily from the outage itself. However, as the outage duration increases, up to 7% of the total ENS is the result of the restoration time required for the diversification process.

Table 4.3. ENS and its associated costs for the base case: islanding prohibited.

Outage Duration (hours)	ENS_{outage} (kWh)	$ENS_{restoration}$ Stage 1 (kWh)	$ENS_{restoration}$ Stage 2 (kWh)	ENS_{total} (kWh)	$Cost$ ($)
0.5	3,642.20	0.0	0.0	3,642.20	541.96
1.0	7,033.55	303.31	0.0	7,336.86	1,091.72
2.0	13,593.00	585.34	0.0	14,178.34	2,109.74
3.0	20,562.44	582.83	839.10	21,752.72	3,236.80

Additionally, as can be observed in Figure 4.9, the ENS and its corresponding costs per event vary linearly with the outage duration. In this scenario, the correlation between the two variables yields an average slope equal to 7 MWh not supplied per hour including the ENS during the outage and the ENS during restoration altogether. On the other hand, the ENS during restoration has a slight exponential correlation with the duration of the outage. This is expected as the longer the outage is, the more time and stages are required to restore the totality of the load. Additionally, for the longest outage events (1, 2 and 3 hours), longer time delays should be allowed for pre-diversification of the load during the suggested sectionalized restoration strategy, opposed to the shortest one (1 hour) for which the load can be restored simultaneously.

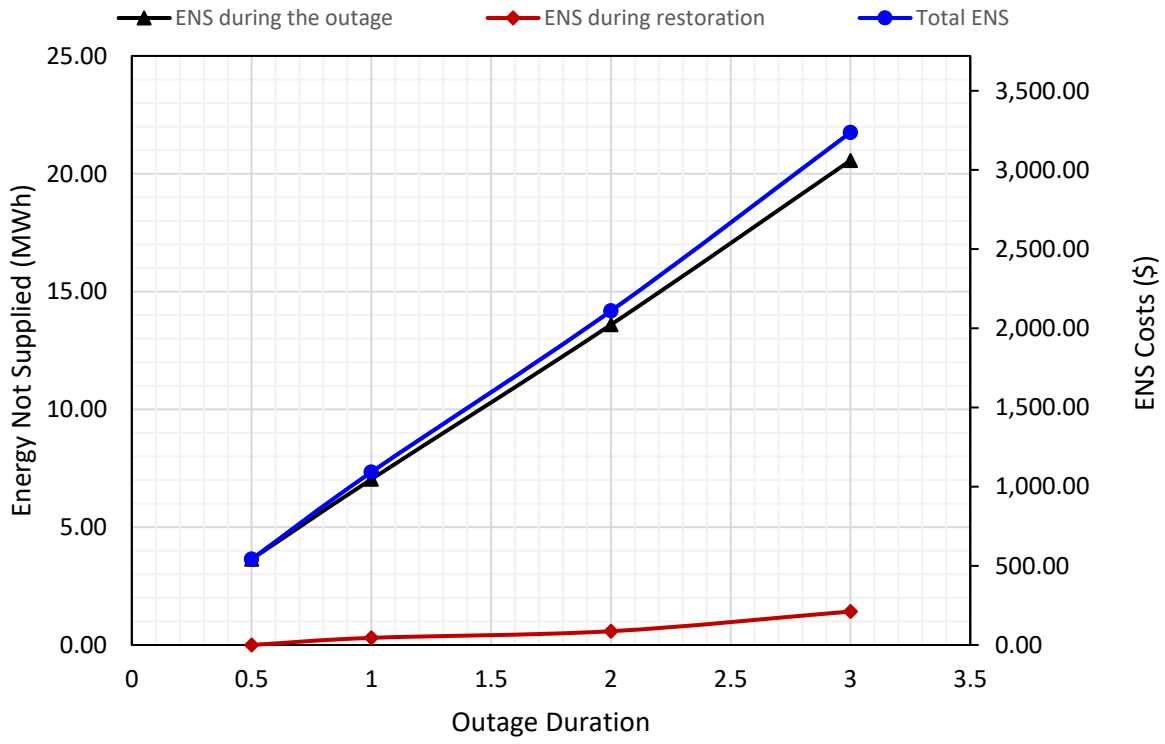

Figure 4.9. Variation of the ENS and ENS costs with the outage duration for the base case.

As microgrid islanding is prohibited in this case, the ENS and the corresponding costs presented in Table 4.3 represent the worst-case scenario in an outage-event basis. In the following sections, the impact of the microgrid on the same variables is analyzed depending on the permitted microgrid boundaries during unintentional islanding.

4.3. Case 2: Microgrid Islanding

In this case, the microgrid is only allowed to island with the load delimited within its original boundaries for the fault locations depicted in Figure 4.10. In this scenario, the 225 customers in zone 5 do not lose supply during the outages specified in Section 4.1.2 as opposed to the base case. Hence, this load is not considered for the CLPU and ENS calculation. On the other hand, the load of up to 1195 customers is lost during the outage depending on the fault location. The impact on restoration times for this case is shown in Table 4.4.

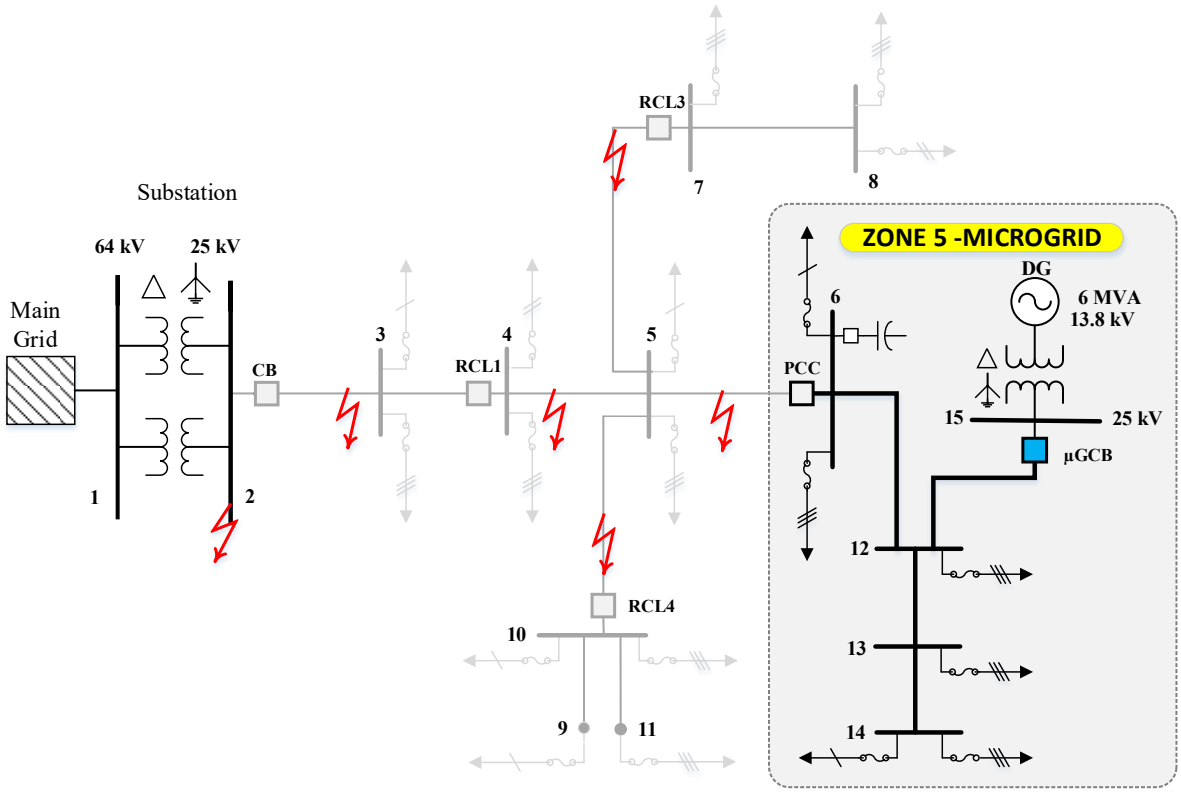

Figure 4.10. Unintentional island configuration for case 2.

Table 4.4. Minimum time delay for sectionalized restoration of the feeder for case 2.

Outage Duration (hours)	$t_{restoration}$ Stage 1 - Zone 5 (hours)	$t_{restoration}$ Stage 2 - Zone 3 (hours)	Longest $t_{interruption}$ (hours)	Peak Current (% of I_{pkp} @ $RCL1$)
0.5	Not lost	0.0	0.5	80%
1.0	Not lost	0.0	1.0	85%
2.0	Not lost	0.0	2.0	96%
3.0	Not lost	0.25	3.25	89%

From the results presented in Table 4.4, it can be concluded that maintaining the microgrid load during the outage allows the immediate restoration of the totality of lost load for outages up to 2 hours long while also permitting a faster restoration of zone 3 for the 3-hour outage as depicted in Figure 4.12 to Figure 4.15. Additionally, as the diversity of a small portion of the load remains unaffected during the outage, the maximum CLPU current for the 0.5, 1 and 3-hour outage decreases approximately 10% when compared to the base case as shown in Figure 4.11. Conversely, for the 2-hour outage, the peak CLPU current is similar in both cases, but as feeder

sectionalizing is not required in case 2, restoration is faster than in the base case. It is important to mention that in order to proceed with the restoration of zone 3, the microgrid does not need to be re-synchronized to the main grid in advance.

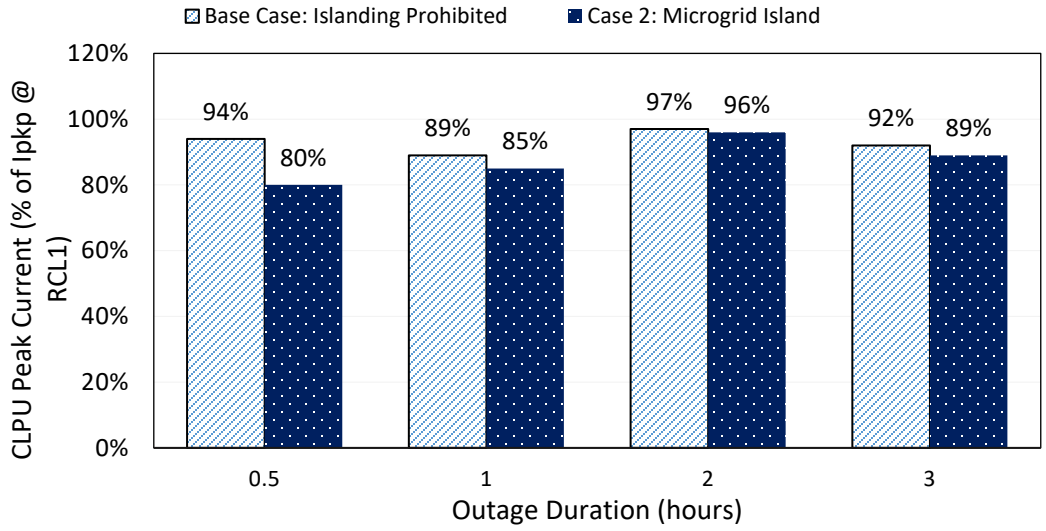

Figure 4.11. Variation of the CLPU current magnitude with the outage duration for the base case and case 1.

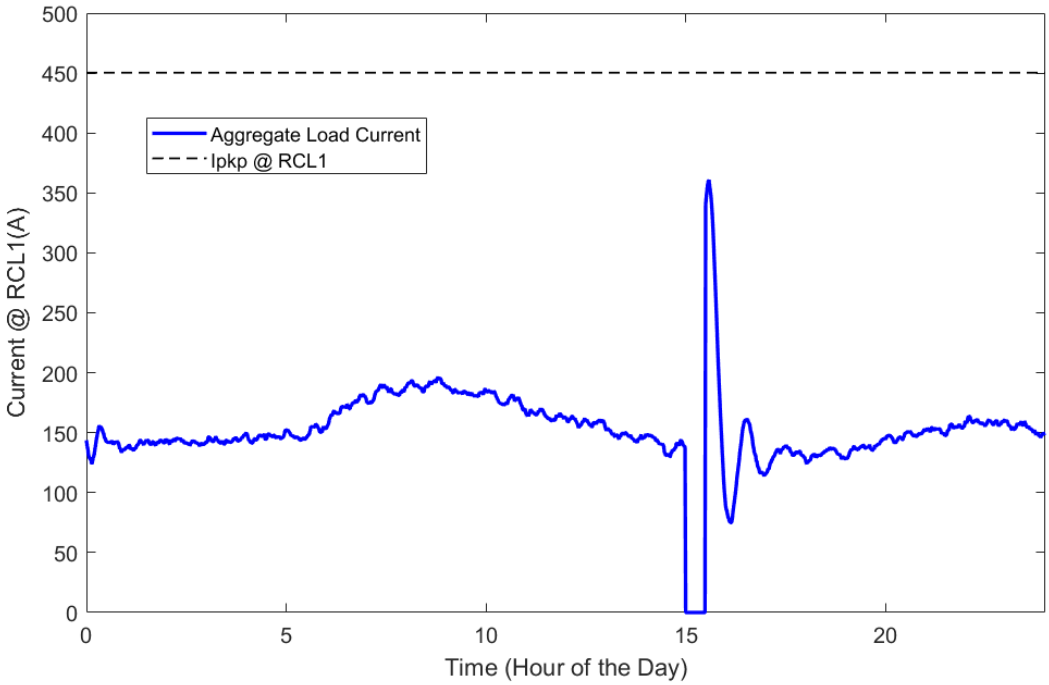

Figure 4.12. CLPU current measured at RCL1 during the simultaneous restoration of zones 2, 3 and 4 while zone 5 (microgrid) is islanded for a 0.5-hour outage (case 2).

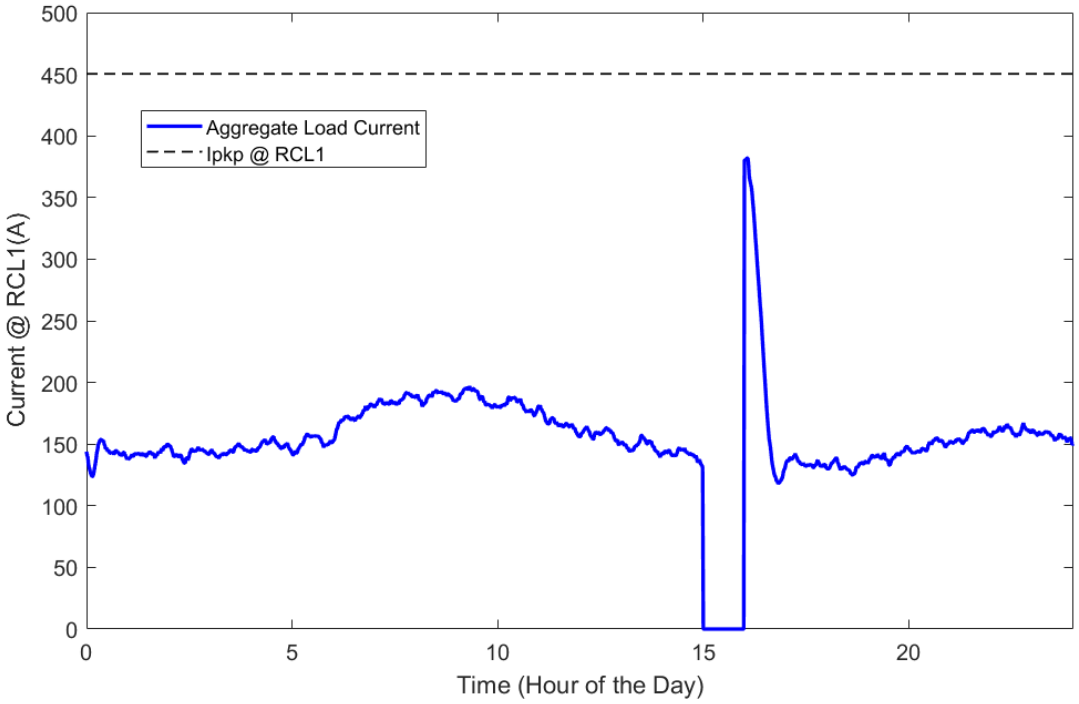

Figure 4.13. CLPU current measured at RCL1 during the simultaneous restoration of zones 2, 3 and 4 while zone 5 (microgrid) is islanded for a 1-hour outage (case 2).

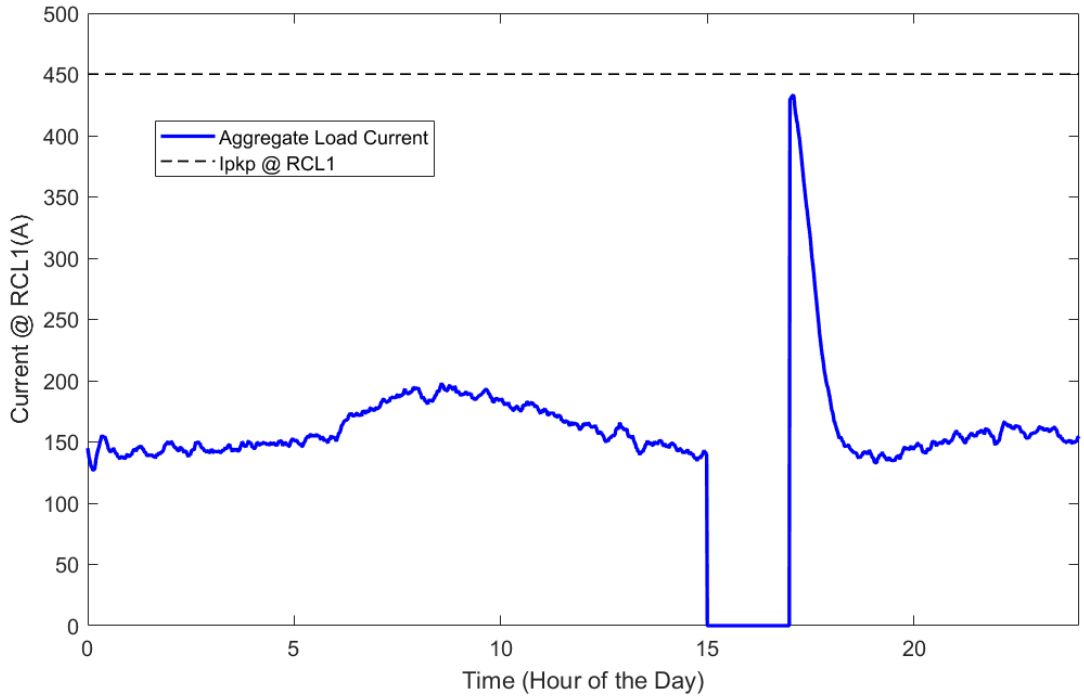

Figure 4.14. CLPU current measured at RCL1 during the simultaneous restoration of zones 2, 3 and 4 while zone 5 (microgrid) is islanded for a 2-hour outage (case 2).

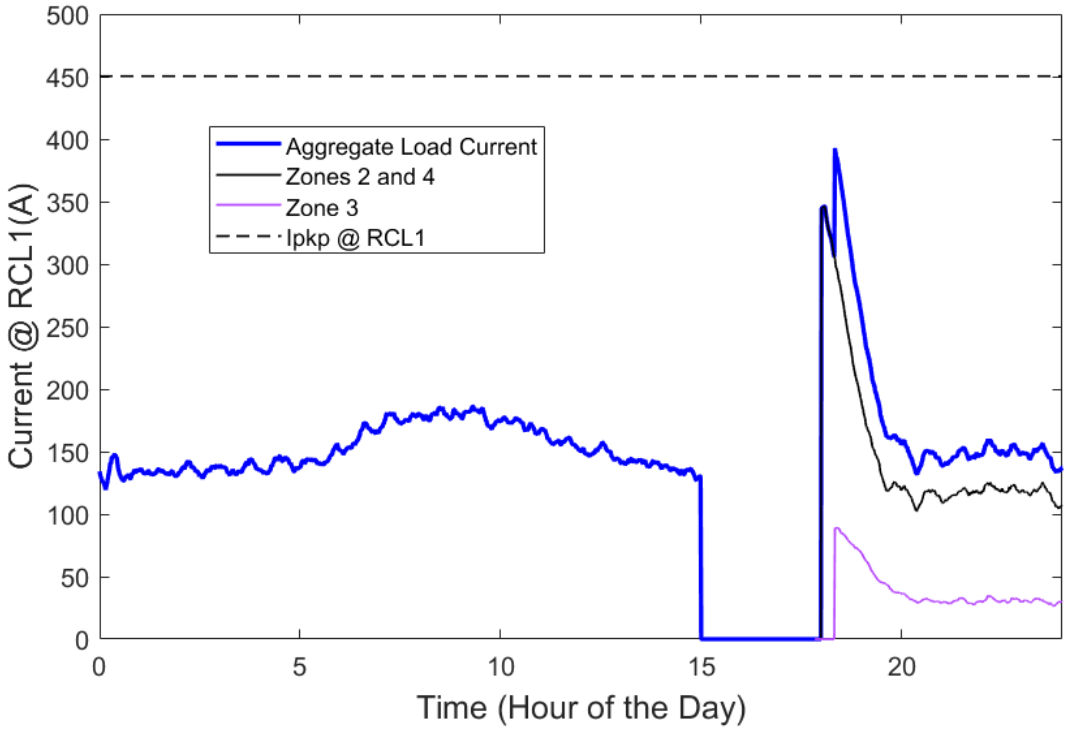

Figure 4.15. CLPU current measured at RCL1 during the sectionalized restoration of zones 2, 3 and 4 while zone 5 (microgrid) is islanded for a 3-hour outage (case 2).

Table 4.5 shows the ENS for case 2 according to the restoration strategy shown in Table 4.4. In this scenario, the ENS and associated costs decrease approximately 20% when compared to the base case as the 225 customers in the microgrid do not lose supply during any of the outage events. Additionally, there is no ENS incurred during restoration for the outages with durations shorter than 2 hours, whereas for the 3-hour outage, the ENS during represent only 1.5% of the total ENS, 80% less when compared to the base case.

Table 4.5. ENS and its associated costs for case 2: microgrid island only.

Outage Duration (hours)	ENS_{outage} (kWh)	$ENS_{restoration}$ Stage 1 (kWh)	$ENS_{restoration}$ Stage 2 (kWh)	ENS_{total} (kWh)	$Cost$ ($)
0.5	3,128.72	n/a	0.0	3,128.72	465.55
1.0	5,804.40	n/a	0.0	5,804.40	863.69
2.0	11,374.16	n/a	0.0	11,374.16	1,692.48
3.0	17,050.25	n/a	271.98	17,322.23	2,577.55

Additionally, the ENS and the outage duration also have a linear correlation similar to the base case as illustrated in Figure 4.16. However, in this scenario, the average slope is smaller than in the base case, equaling to 5.6 MWh not supplied per hour during the outage as the ENS during restoration is null except for the 3-hour outage. This means that the average ENS per hour is 1.4 MWh less when compared to the base case On the other hand, the ENS during restoration maintains a slight exponential correlation with the outage duration as the outage events shorter than 2 hours allow the simultaneous restoration of the totality of the load, but the 3-hour outage still needs to be restored by feeder sectionalizing although the only stage required to do so is shorter and encompasses less load when compared to the same scenario of the base case.

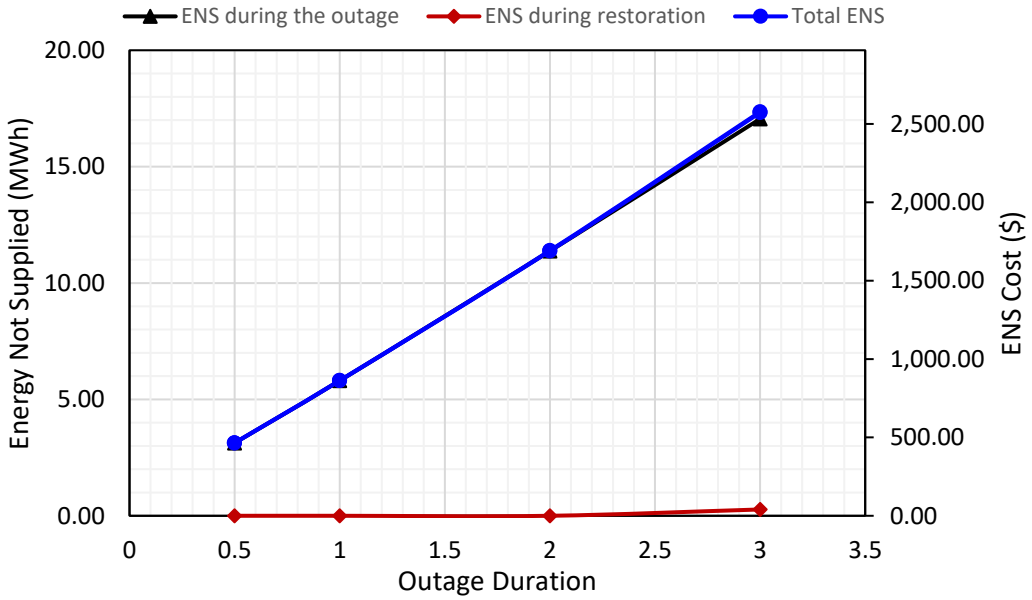

Figure 4.16. Variation of the ENS and ENS costs with the outage duration for case 2.

4.4. Case 3: Emergency extended island

In this case, the microgrid is permitted to extend its boundaries during unplanned islanding to include the utility load in zone 3 for permanent faults in zone 1 as illustrated in Figure 4.17. As a result, a continuous supply is maintained for 640 customers, otherwise lost in the base case. However, the load in zones 3 and 4, totalling 715 customers, must be shed to maintain a balanced island within the DG capability as described in Section 3.6.2.2. It is important to mention that zones 3 and 4 are also lost if the microgrid islanding (case 2) or no islanding at all (base case) configurations were permitted, so there is not a different effect to the customers in these zones due

to the load shedding. In this context, only 780 customers in total, including the 65 in zone 1, are considered for the CLPU calculation.

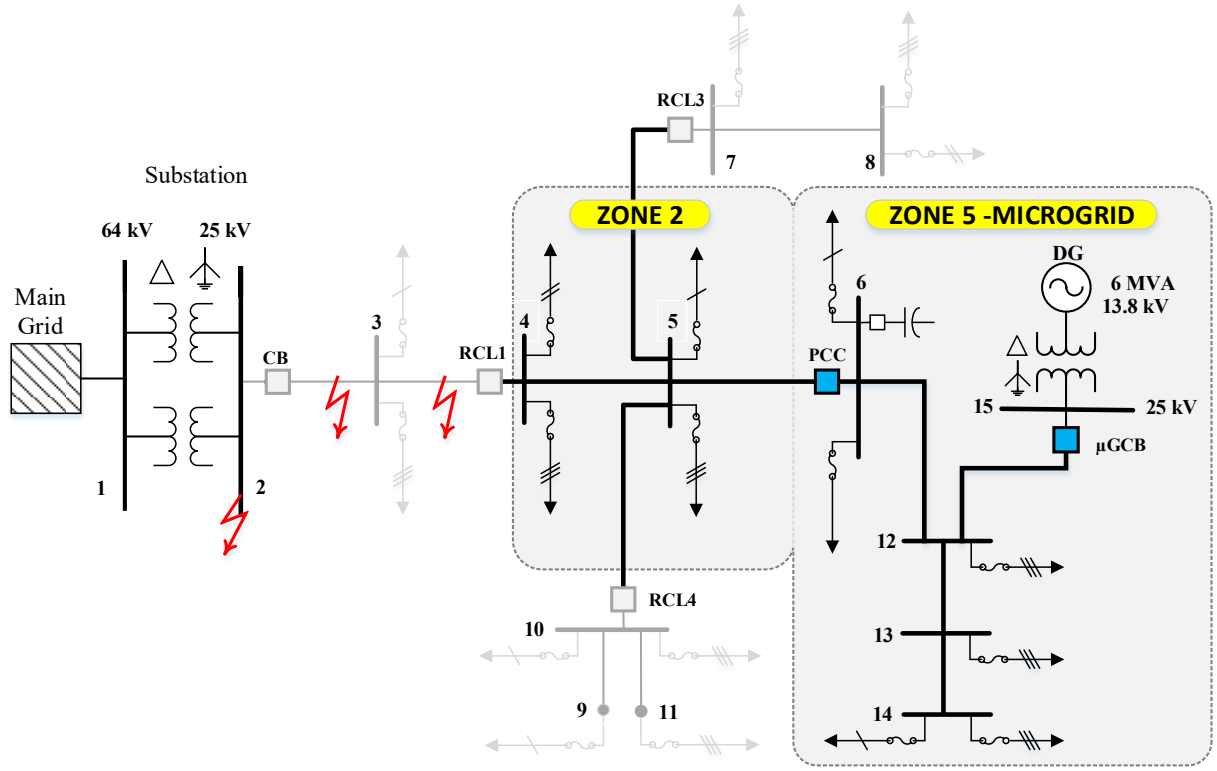

Figure 4.17. Emergency island configuration for case 3.

For restoration under these conditions, the following steps are taken: First, after the fault in zone 1 has been repaired or removed, CB is closed and zone 1 alone is immediately restored. Soon after, RCL1 is closed without intentional delay additional to the time required until synchronism conditions are met. Subsequently, with the available capacity of the EPS, RCL3 and RCL4 can be closed considering that zone 2 is already energized and with its load diversity unaffected during the outage. Note that the restoration of zones 3 and 4 cannot be completed if the island is not re-synchronized to the main grid first.

As discussed previously, the cumulative effect of the undiversified load for this case occurs as a result of the simultaneous restoration of zones 3 and 4 after the transition between the microgrid island mode and the grid-connected mode is completed. Thus, the impact of CLPU for this case is measured at RCL1, which acts as the re-synchronizing device, assuming that the loads in zones 2 and 5 (microgrid) are supplied by the DG operating in a fixed PQ mode at the moment of

reconnection. Thus, it can be assumed that the power import/export through RCL1 is 0 the instant before RCL3 and RCL4 are closed. The results for this case are shown in Table 4.6.

Table 4.6. Minimum time delay for sectionalized restoration of the feeder for case 3.

Outage Duration (hours)	$t_{restoration}$ Stage 1 Zone 1 (hours)	$t_{restoration}$ Stage 2 Zone 3 & 4 (hours)	Longest $t_{interruption}$ (hours)	Peak Current (% of I_{pkp} @ CB)
0.5	0	0	0.50	52%
1.0	0	0	1.00	58%
2.0	0	0	2.00	64%
3.0	0	0	3.00	71%

From the results obtained for this case, it can be seen that no additional time is required for service restoration when the extended microgrid islanding is allowed to form. Hence, service can be restored instantaneously for zones 1, 3 and 4 regardless of the outage durations tested; nonetheless, it is important to mention that this application is limited to outages caused by permanent faults in zone 1 unlike case 2, where faults in zone 2 are included.

Regarding the maximum CLPU current, there is an average reduction of 30% for the outages up to 2 hours long and 20% for the 3-hour outage when compared to case 2 as shown in Figure 4.18. This reduction is the result of a reduced cumulative effect of the undiversified load at RCL1 as only 715 are restored simultaneously from the utility side, opposed to the maximum of 1355 and 1100 customers restored in the base case and case 2 scenarios, respectively. The peak currents presented in Table 4.6 are calculated considering that the undiversified load of the 65 customers in zone 1 does not accumulate at RCL1 but in CB instead. Figure 4.19 to Figure 4.22 depict the current profile at RCL1 during the restoration of zones 3 and 4.

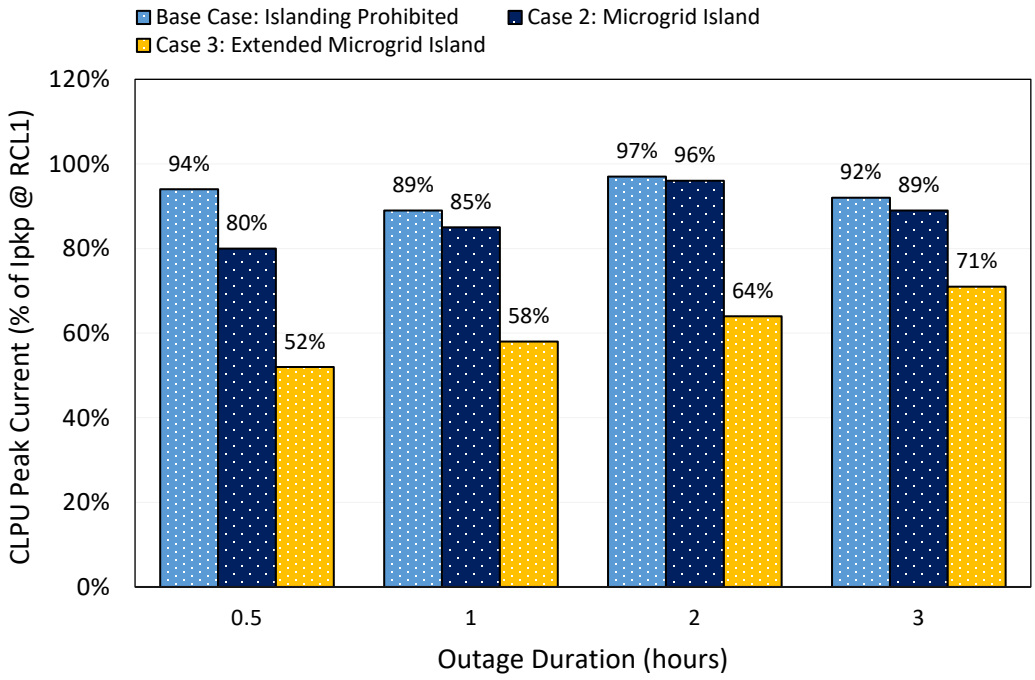

Figure 4.18. Variation of the CLPU current magnitude with the outage duration for the base case and case 1 and case 2.

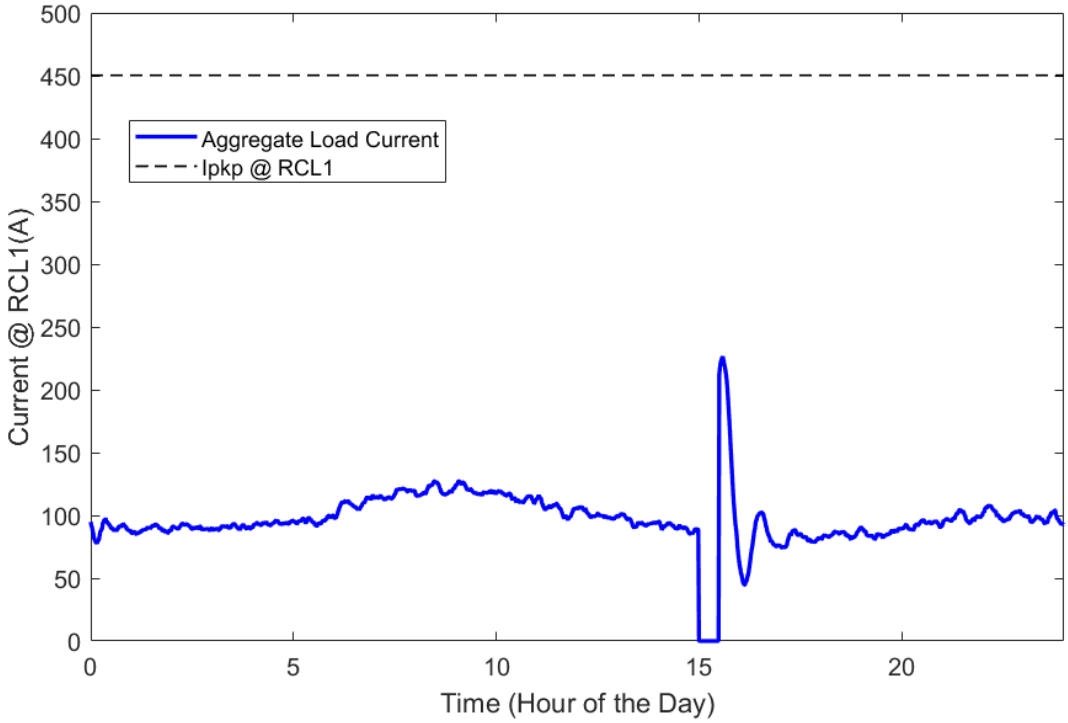

Figure 4.19. CLPU current at RCL1 during the restoration of zones 3 and 4 for the 0.5-hour outage (case 3).

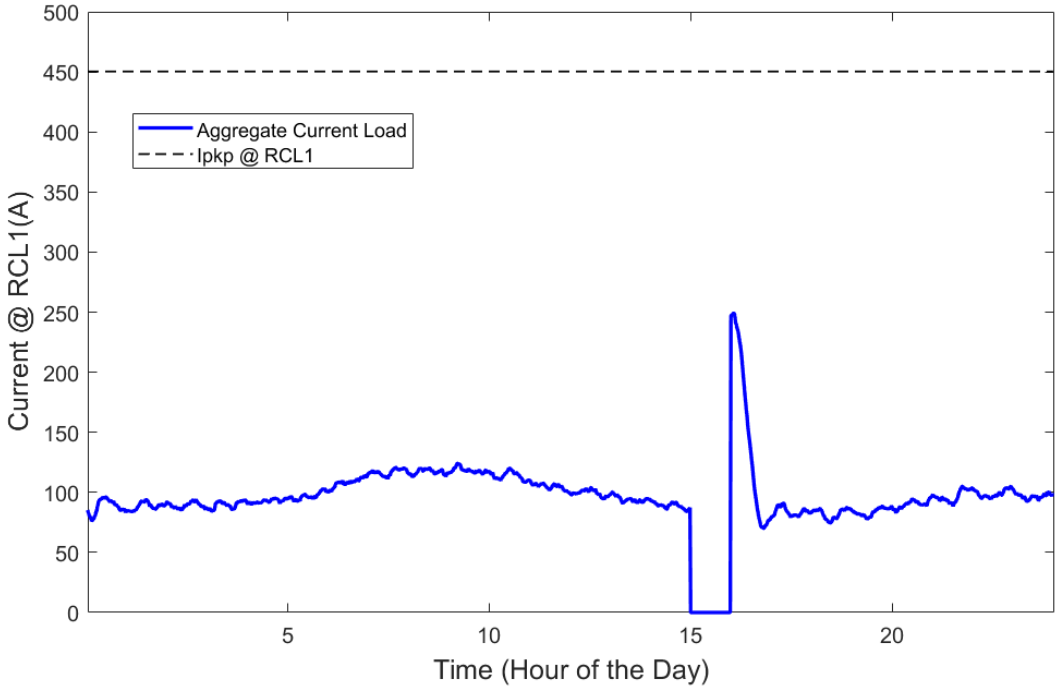

Figure 4.20. CLPU current at RCL1 during the restoration of zones 3 and 4 for the 1-hour outage (case 3).

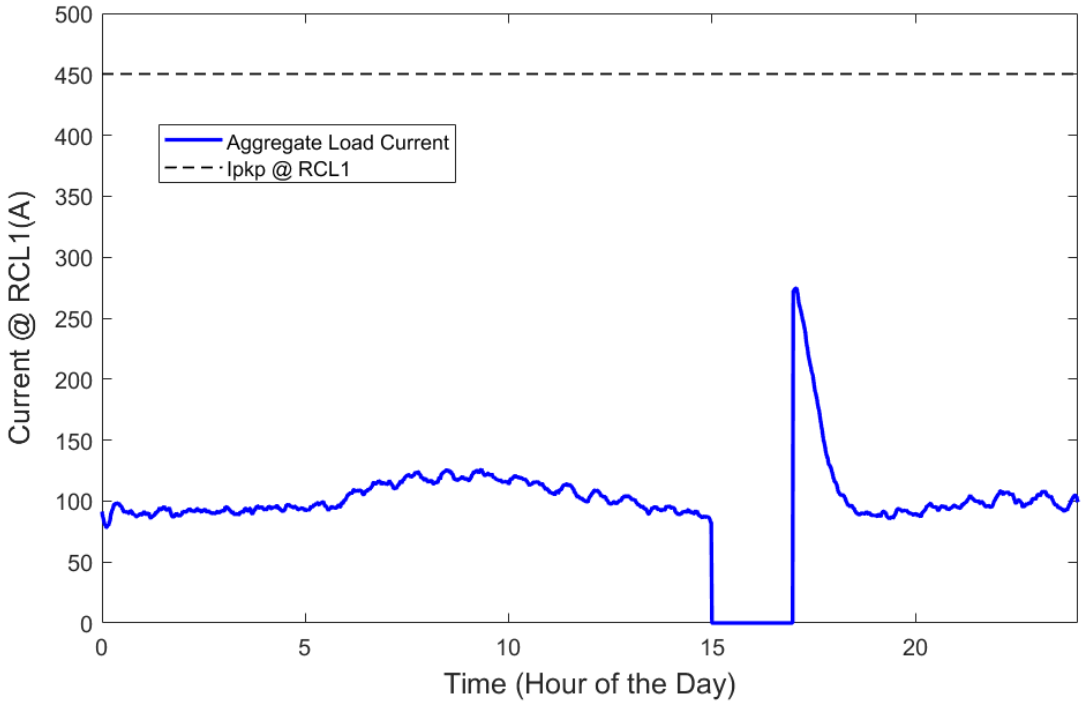

Figure 4.21. CLPU current at RCL1 during the restoration of zones 3 and 4 for the 2-hour outage (case 3).

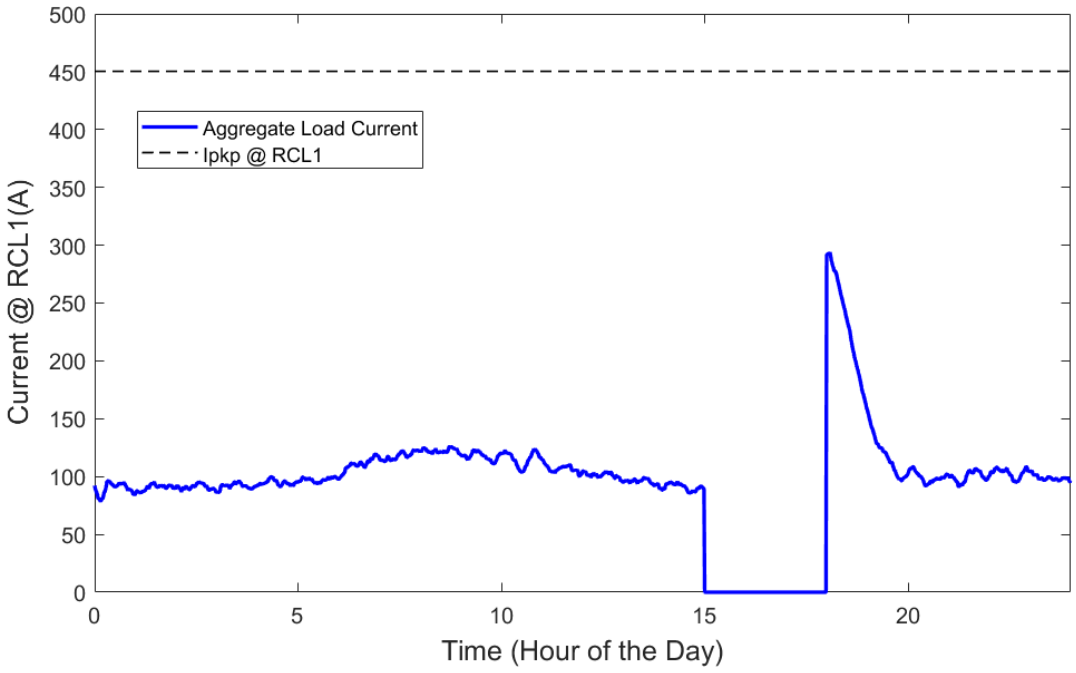

Figure 4.22. CLPU current at RCL1 during the restoration of zones 3 and 4 for the 3-hour outage (case 3).

Since a larger portion of the feeder load remains supplied during the outage compared to the previous cases, the ENS and its corresponding costs are significantly lower in this scenario as shown in Table 4.7. This reduction is approximately 35% when compared to case 2, and 50% when compared to the base case. Furthermore, as no supplementary time is required for diversification of zone 1, no additional costs are incurred during restoration.

Table 4.7. ENS and its associated costs for case 3: extended (emergency) island.

Outage Duration (hours)	ENS_{outage} (kWh)	$ENS_{restoration}$ Stage 1 (kWh)	$ENS_{restoration}$ Stage 2 (kWh)	ENS_{total} (kWh)	$Cost$ ($)
0.5	2,047.29	0.0	0.0	2,047.29	304.64
1.0	4,083.46	0.0	0.0	4,083.46	607.62
2.0	7,798.80	0.0	0.0	7,798.80	1,160.46
3.0	11,636.54	0.0	0.0	11,636.54	1,731.52

Furthermore, in this case, the ENS also varies linearly with the outage duration similar to the base case and case 2 as shown in Figure 4.23. However, in this scenario, the average slope is the smallest between the three cases, equaling to 3.8 MWh lost per hour during an outage. This translates into 1.8 MWh not supplied per hour less when compared to the case 2 and 3.2 MWh not supplied per hour less when compared to the base case.

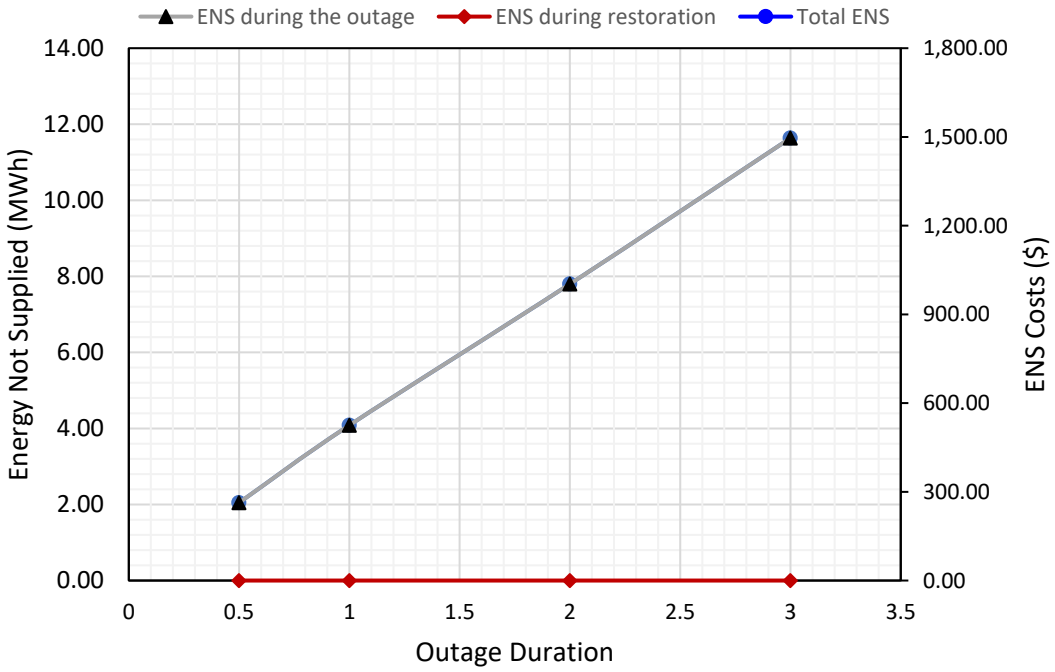

Figure 4.23. Variation of the ENS and ENS costs with the outage duration for case 3.

4.5. Analysis and Discussion of the Results

The examination of the results presented in Sections 4.2, 4.3, and 4.4 for the three cases considered for this study makes it evident that the unplanned microgrid islanding strategy proposed in Chapter 3 has a positive impact on the restoration times as maintaining continuous service for a larger number of customers during the assumed outage scenarios, significantly reduces the cumulative effect of the loss of load diversity at the feeder head-end devices at which restoration is attempted. Consequently, the peak magnitude of the CLPU current is reduced, and thus, the time delay before energizing a feeder section required to allow diversification of others restored in advance can be shortened or neglected. This becomes particularly apparent in Case 3, for which no pre-diversification time is required regardless of the outage durations tested. It is important to point out that longer restoration times can translate into longer interruptions, especially for the customers

grouped in the radial, tail-end sections of the feeder, normally restored during the last stages after extended outages as depicted in Figure 4.24. The hatched portion of the columns for cases 1 and 2 corresponds to the customers encircled in zones 3 and 5, considered in the sectionalized restoration strategy.

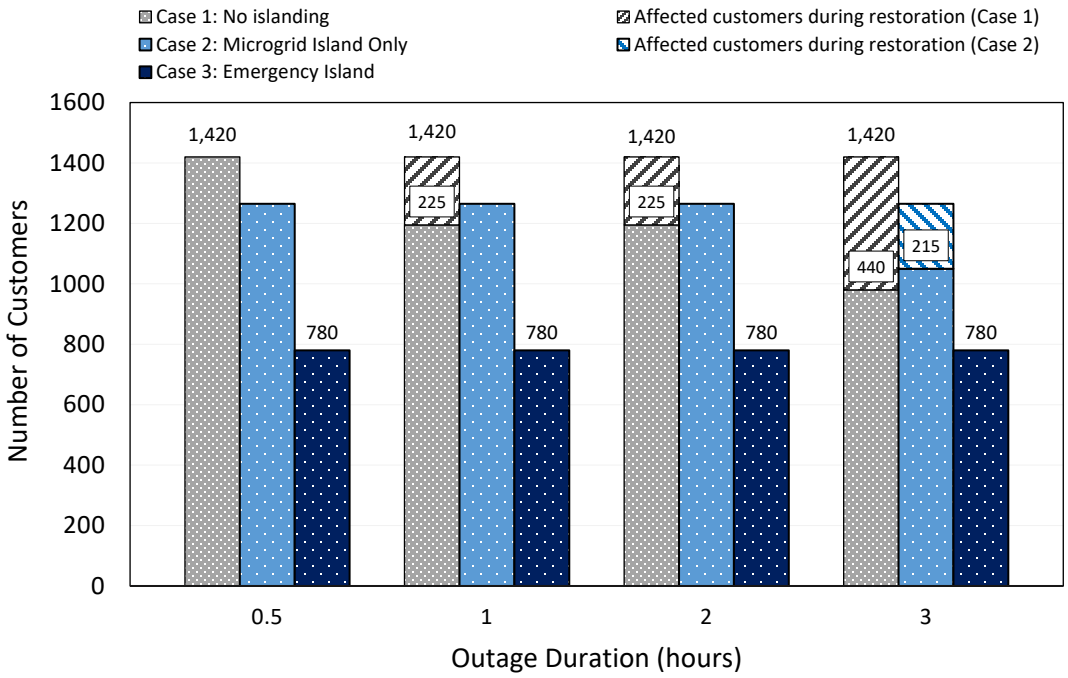

Figure 4.24. Number of customers affected in each case for the pre-defined outage durations for permanent faults in zone 1.

Figure 4.25 shows the peak CLPU current expressed in terms of the pickup setting at RCL1 for all the cases. For illustrative purposes, the current measured at RCL1 during the attempt to simultaneously restore the load when islanding is prohibited is also included in the bar chart. It can be appreciated that there is a reduction of the peak current from case to case as more customers are included in the islanding strategy. Once more, this is clearer for case 3 for which the peak CLPU magnitudes are the lowest of the three cases, reaching and average of 60% of the pickup current at RCL1 for the outages lasting less than two hours and 70% for the 3-hour outage. On the other hand, there is no significant change in the peak current magnitude from the base case to case 2. However, it must be noted that in case 2, sectionalized restoration is not required for the outages lasting less than 2 hours, and only a short time delay for zone 3 is required for the 3-hour outage, opposed to the base case where not only restoration by parts is required for the outages longer than 1 hour, but also involves zone 3 and the microgrid load as well.

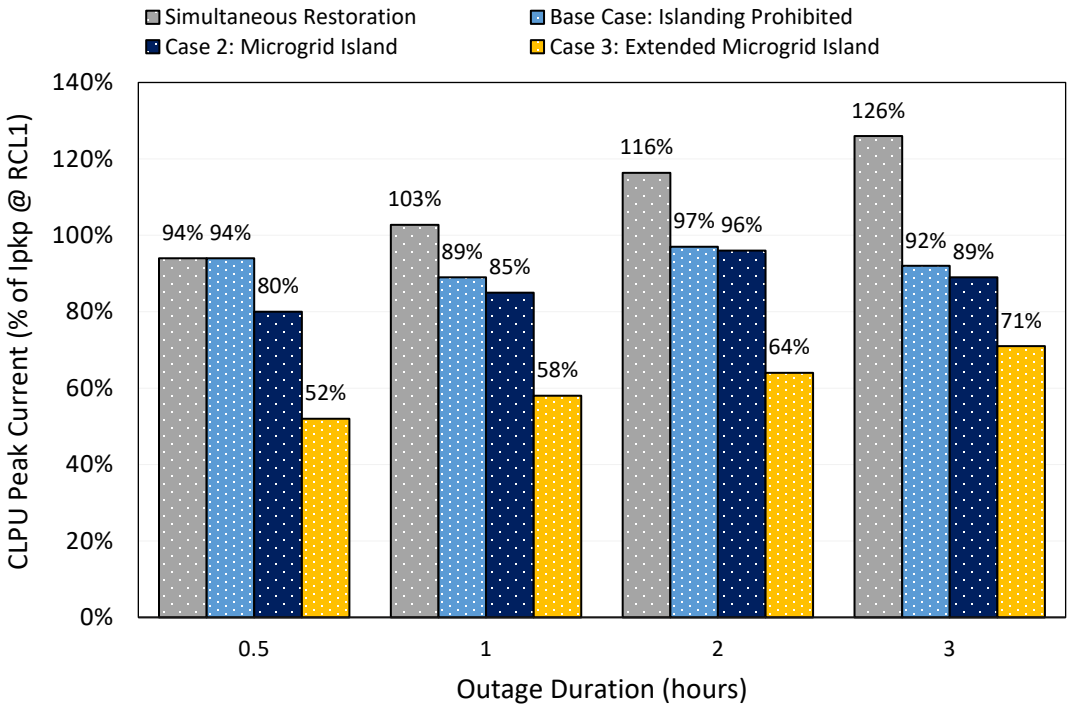

Figure 4.25. Variation of the CLPU current magnitude with the outage duration expressed in terms of the relay pickup setting at RCL1 for the three cases. Currents above 100% lead to nuisance tripping of RCL1.

On the other hand, with a larger portion of load unaffected during the outage when islanding is permitted (cases 2 and 3), there is also an effect on the ENS during the interruption. Through observation of Figure 4.26, when the microgrid is permitted to island with its designated loads (Case 2), the ENS and its associated costs reduce to 80% of the values indicated in the base case. Furthermore, if the microgrid is permitted to extend its island as shown in Case 3, The ENS and associated costs reduce to 55% of the original base case. As mentioned previously, this reduction is only associated to a single event, should multiple outages occur, the benefit of the microgrid islanding and the maintenance of the load diversification will only multiply the cost savings benefit.

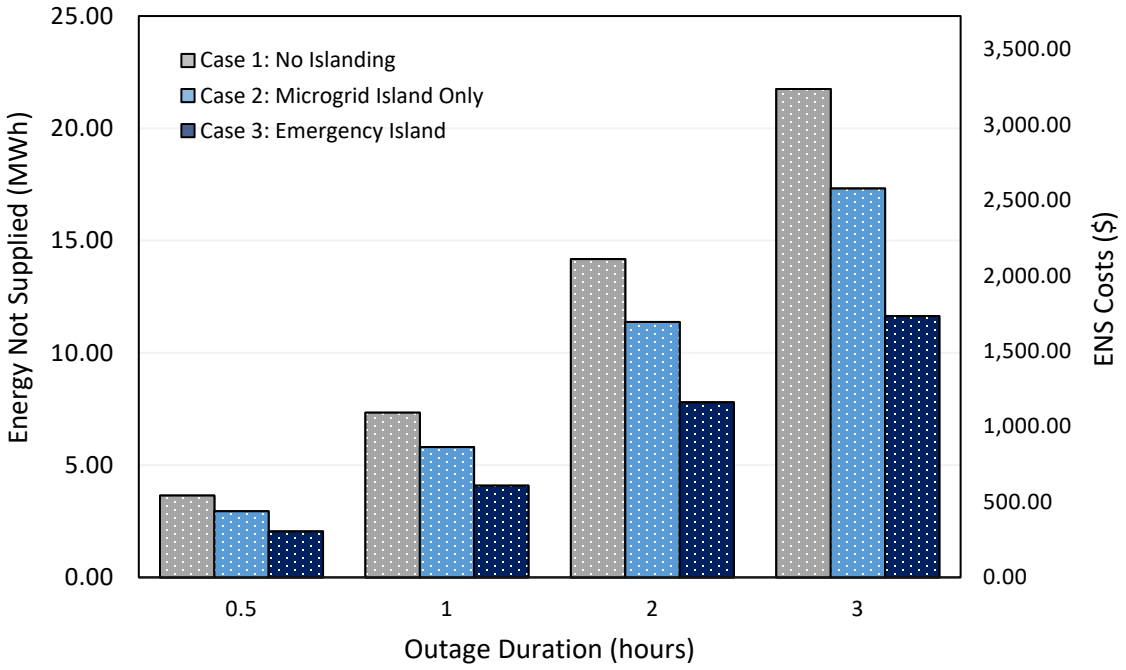

Figure 4.26. ENS and its average costs for each case for the defined outage scenarios.

It is worth noting that most utilities use a tiered rate for the residential consumer sector based on monthly consumption. Therefore, the actual ENS cost, and thus, the savings resulting from microgrid islanding could be higher than the one presented in this chapter if a higher electricity rate is considered or if the outage occurs when the monthly consumption of most of the serviced customers have climbed to higher-rated tiers during their billing period. For instance, Saskpower, the principal electric utility in the province of Saskatchewan, charges residential users supplied by diesel generation $0.5253 for every kWh above 650 kWh/month, opposed to the base tier with a rate of 0.1422 $/kWh [69]. Nonetheless, the average rate introduced in Section 4.1.3.4, calculated for the average residential consumption in the major cities of Canada, serves as a reasonable rate for comparison purposes.

4.6. Summary

In this chapter, the physical load model presented in Chapter 2 is used to evaluate the effect of the unintentional microgrid islanding strategy proposed in Chapter 3 on service restoration after prolonged interruptions during severe CLPU conditions in the Canadian winter season. To accomplish this, multiple simulations for the load model are performed in MATLAB for different microgrid configurations and outage scenarios during a typical winter day. Subsequently, a

restoration sequence based on the feeder sectionalizing strategy is proposed for the cases during which nuisance protection tripping occurs. Later, from the load profiles obtained from these simulations for each outage scenario and network configuration, the energy not supplied (ENS) and its associated costs for the outage events are estimated. Finally, a comparison between the results obtained for all the islanding scenarios is presented and discussed.

Chapter 5

SUMMARY AND CONCLUSIONS

5.1. Summary

The configuration of the typical distribution system, originally conceived for radial operation with a single source, has been transitioning from passive into active as the incorporation of small-scale distributed generation (DG) is becoming more usual, driven by climate-change concerns and energy market liberalization. This has brough about a great deal of technical challenges to utilities which usually resort to rigid operation practices with the purpose of averting unintentional islanding and the potential power quality issues that may ensue as a consequence. However, with the extensive research on distributed generation that has been carried out over the recent years, the technical gap limiting complex application, such as the implementation of the microgrid concept, continues to narrow, allowing distributed generation to have a more flexible integration with the grid.

A microgrid is an independent controllable entity that comprises load and distributed generation that unlike traditional distribution systems can operate both connected to the grid or as a power island as needed. This allows the distributed generation to support the main grid during outages and power disturbances while maintaining and adequate power quality at all times. In this work, a microgrid islanding strategy is proposed for a MV feeder comprising a synchronous-machine DG to attain a superior interoperability between the grid components for multiple network configurations and operation scenarios. To achieve this, an adaptive, communication-assisted protection scheme is designed to accommodate the DG, and the functional requirements for a microgrid control system are specified to ensure a seamless transition between the microgrid operating modes.

Finally, to exemplify the potential benefits of microgrid islanding, the problems caused by cold load pickup (CLPU) during service restoration are also investigated. In pursuit of this, a detailed overview of the CLPU phenomenon is provided, including its causes and adverse effects on distribution systems. Later, an aggregate physical load model for distribution feeders that replicates the effect of the progressive loss of load diversity that occurs following extended outages is presented. This model is used to assess the impact of the proposed microgrid islanding strategy for the benchmark network on service restoration times, and on the energy not supplied during outages caused by permanent faults in distribution feeders.

Before introducing the microgrid concept, a brief overview of the operation and protection of traditional distribution systems is provided in Chapter 1. Additionally, the adverse effects and technical challenges that distributed generation causes in distribution systems are introduced.

In Chapter 2, a detailed overview of the cold load pickup phenomenon is provided, covering its components, causes and adverse effects on distribution systems. Moreover, a recompilation of several CLPU models intended for power system planning and operation studies is presented, giving particular attention to the aggregate physical modelling of thermostat-controlled residential load.

In Chapter 3, the microgrid concept is introduced, including the fundamentals of microgrid operation and control. Subsequently, the specifications for a protection system and the functional requirements for a microgrid controller are defined in the framework of IEEE Std 2030.7 for a MV distribution network containing a microgrid with a synchronous-machine-based distributed generator to comply with IEEE Std 1547. The performance of the proposed protection and control approach for the study case is evaluated for multiple fault locations along the feeder and for planned and unplanned transitions between the microgrid operation modes using time-domain simulations in the EMTP-RV program.

In Chapter 4, multiple MATLAB simulations of the physical load model presented in Chapter 2 are used to evaluate the effect of the unintentional microgrid islanding strategy proposed in Chapter 3 on service restoration under the severe CLPU conditions that arise after extended outages. For the restoration scenarios resulting in nuisance protection tripping as a consequence of CLPU, a feeder sectionalizing restoration sequence is proposed. Later, a quantitative assessment focusing on the estimation of restoration times, the energy not supplied during the interruptions

and its associated costs is presented for all the possible island configurations and for multiple outage scenarios during a typical winter day in Canada.

5.2. Conclusions

The following conclusions can be derived from this research work:

1. Although CLPU is a common phenomenon in all distribution systems, the problems it may cause becomes more prominent and challenging to address in geographic locations with a high penetration of electric HVAC load, such as space heating. Normally, as this type of thermostat-controlled load is more sensitive to temperature variations, its diversity is easily affected during system outages, causing considerable current spikes during restoration, especially amid extreme weather conditions.

2. The aggregate physical load model used in this research work provides a more accurate representation of the behavior of the load diversity than other more simplistic models commonly used as reference among utilities that oftentimes lead to errors in the estimation of the CLPU parameters. Additionally, even though this model is intended for residential load, it may also be used for CLPU estimation in feeders with different compositions as the residential-like loads such as space and water heating are found in all consumer sectors while other types of loads, such as large industrial machinery, do not typically contribute to CLPU.

3. Complex applications in distribution systems, including those involving unconventional operation of distributed generation, such as microgrids, require state-of-the-art computational technology. However, the foundation for future-proof distribution networks, capable of achieving a high degree of automation and interoperability between its components is without a doubt a reliable and fast communication infrastructure as it allows the maximum exploitation of all the available but disperse resources in the grid.

4. The communication-assisted pilot relaying scheme presented in this research work for the protection of a MV distribution feeder containing synchronous machine based distributed generation, is a fast, sensitive, and selective method for fault detection and clearing where the presence of intermediate loads and laterals taps in each protection zone impedes the use

of other unit protection schemes, such as differential protection, while also provides protection backup to other upstream and downstream devices.

5. The most critical component for the integration of a microgrid in the distribution level is the microgrid control system, whose functional requirements must be thoroughly specified accordingly with the intended application for which it is designed. To accomplish this, it is necessary to identify all the grid resources available to the control system, so that it can ensure a seamless operation of the microgrid for different feeder configurations during both steady-state and emergency scenarios, such inadvertent islanding.

6. The microgrid islanding strategy presented in this research work, including the temporary extension of its boundaries for certain power disturbances in the main grid, proves to be effective in reducing the service restoration times during severe CLPU conditions while also reducing the number of customers affected during sustained supply interruptions, improving the overall system reliability and service continuity.

7. By allowing the microgrid in the benchmark network to island in different configurations depending on the fault location while in the grid-connected mode, the interruption costs can be decreased up to 50% when compared to the scenario where no islanding is permitted. This reaffirms the idea that investment in infrastructure that allows a better integration of the distributed energy resources with the grid can have a positive economic impact on utilities, resulting in long-term savings while improving the overall system reliability.

REFERENCES

[1] T. A. Short, *Electric Power Distribution Handbook, Second Edition*, Second edition. CRC Press, 2014.

[2] *Electrical Transmission and Distribution Reference Book*. ABB power T & D Company Incorporated, 1997.

[3] J. L. Blackburn and T. J. Domin, *Protective Relaying: Principles and Applications, Fourth Edition*. CRC Press, 2015.

[4] "The Authoritative Dictionary of IEEE Standards Terms, Seventh Edition," *IEEE Std 100-2000*, pp. 1–1362, Dec. 2000, doi: 10.1109/IEEESTD.2000.322230.

[5] "IEEE Standard for Inverse-Time Characteristics Equations for Overcurrent Relays," *IEEE Std C37.112-2018 (Revision of IEEE Std C37.112-1996)*, pp. 1–25, Feb. 2019, doi: 10.1109/IEEESTD.2019.8635630.

[6] P. M. Anderson, *Power System Protection*. Wiley, 1998.

[7] J. C. Das, *Power system protective relaying*. CRC Press Taylor & Francis Group, 2018.

[8] "IEEE Standard for Interconnection and Interoperability of Distributed Energy Resources with Associated Electric Power Systems Interfaces," *IEEE Std 1547-2018 (Revision of IEEE Std 1547-2003)*, pp. 1–138, Apr. 2018, doi: 10.1109/IEEESTD.2018.8332112.

[9] M. H. Bollen and F. Hassan, *Integration of distributed generation in the power system*, vol. 80. John wiley & sons, 2011.

[10] A. Girgis and S. Brahma, "Effect of distributed generation on protective device coordination in distribution system," in *LESCOPE 01. 2001 Large Engineering Systems Conference on Power Engineering. Conference Proceedings. Theme: Powering Beyond 2001 (Cat. No.01ex490)*, Jul. 2001, pp. 115–119, doi: 10.1109/LESCPE.2001.941636.

[11] K. A. Wheeler, S. O. Faried, and M. Elsamahy, “Assessment of distributed generation influences on fuse-recloser protection systems in radial distribution networks,” in *2016 IEEE/PES Transmission and Distribution Conference and Exposition (T D)*, May 2016, pp. 1–5, doi: 10.1109/TDC.2016.7519917.

[12] M. A. Zamani, “Protection and Control of Active Distribution Networks and Microgrids,” *Electronic Thesis and Dissertation Repository*, Nov. 2012, [Online]. Available: https://ir.lib.uwo.ca/etd/1046.

[13] C. J. Mozina, “A Tutorial on the Impact of Distributed Generation (DG) on Distribution Systems,” in *2008 61st Annual Conference for Protective Relay Engineers*, Apr. 2008, pp. 591–609, doi: 10.1109/CPRE.2008.4515083.

[14] “IEEE Standard for the Specification of Microgrid Controllers,” *IEEE Std 2030.7-2017*, pp. 1–43, Apr. 2018, doi: 10.1109/IEEESTD.2018.8295083.

[15] “IEEE Standard for Interconnection and Interoperability of Distributed Energy Resources with Associated Electric Power Systems Interfaces,” IEEE. doi: 10.1109/IEEESTD.2018.8332112.

[16] G. E. Company, *Distribution Data Book: A Collection of Fundamental Data Pertaining to the Elements Of, and the Loads On, Distribution Systems*. 1972.

[17] C. L. Brooks, J. W. Sanders, and B. W. Kennedy, “A Method for Evaluating the General Load and Loss Effects of Demand-Side Management on the T D Delivery System,” *IEEE Transactions on Power Systems*, vol. 2, no. 3, pp. 700–706, Aug. 1987, doi: 10.1109/TPWRS.1987.4335197.

[18] D. L. Nickel and H. R. Braunstein, “Distribution Transformer Loss Evaluation: II - Load Characteristics and System Cost Parameters,” *IEEE Transactions on Power Apparatus and Systems*, vol. PAS-100, no. 2, pp. 798–811, Feb. 1981, doi: 10.1109/TPAS.1981.316932.

[19] D. Fink and H. W. Beaty, *Standard Handbook for Electrical Engineers*. McGraw Hill Professional, 2006.

[20] IEEE PES-PSRC Working Group Report, "Cold Load Pickup Issues," IEEE Power Engineering Society, 2009.

[21] N. Saker, M. Petit, J. Vannier, and J.-L. Coullon, "Cold Load Pick-Up with Electrical Space Heating Loads Under Demand Response Actions," Jun. 2011.

[22] S. Lefebvre and C. Desbiens, "Residential load modeling for predicting distribution transformer load behavior, feeder load and cold load pickup," *International Journal of Electrical Power & Energy Systems*, vol. 24, no. 4, pp. 285–293, May 2002, doi: 10.1016/S0142-0615(01)00040-0.

[23] M. Nagpal, Delmee, Gilles, A. El-Khatib, K. Stich, D. Ghangass, and A. Bimbhra, "A Practical and Cost Effective Cold Load Pickup Management Using Remote Control," presented at the Western Protection Relay Conference, Spokane, Washington, USA, Oct. 2014.

[24] V. Kumar, I. Gupta, and H. Gupta, "An Overview of Cold Load Pickup Issues in Distribution Systems," *Electric Power Components and Systems - ELECTR POWER COMPON SYST*, vol. 34, pp. 639–651, Jun. 2006, doi: 10.1080/15325000500419219.

[25] W. W. Lang, M. D. Anderson, and D. R. Fannin, "An Analytical Method for Quantifying the Electrical Space Heating Component of a Cold Load Pick Up," *IEEE Transactions on Power Apparatus and Systems*, vol. PAS-101, no. 4, pp. 924–932, Apr. 1982, doi: 10.1109/TPAS.1982.317158.

[26] Natural Resources Canada, "Keeping the Heat In," Office of Energy Efficiency - NRCAN, 2012.

[27] N. G. Chondrakis and F. V. Topalis, "Influence of cold starting on the life of T5 fluorescent tubes and CFLs," in *2009 35th Annual Conference of IEEE Industrial Electronics*, Nov. 2009, pp. 3530–3536, doi: 10.1109/IECON.2009.5415165.

[28] R. Wilde, "Effects of Cold Load Pickup at the Distribution Substation Transformer," *IEEE Trans. on Power Apparatus and Syst.*, vol. PAS-104, no. 3, pp. 704–710, Mar. 1985, doi: 10.1109/TPAS.1985.319007.

[29] F. Edstrom, J. Rosenlind, K. Alvehag, P. Hilber, and L. Soder, "Influence of Ambient Temperature on Transformer Overloading During Cold Load Pickup," *IEEE Transactions on Power Delivery*, vol. 28, no. 1, pp. 153–161, Jan. 2013, doi: 10.1109/TPWRD.2012.2219079.

[30] J. Aubin, R. Bergeron, and R. Morin, "Distribution transformer overloading capability under cold-load pickup conditions," *IEEE Transactions on Power Delivery*, vol. 5, no. 4, pp. 1883–1891, Oct. 1990, doi: 10.1109/61.103685.

[31] The Electric Power Research Institute, "Green Circuits: Distribution Efficiency Case Studies," EPRI, Technical Report 1023518, Oct. 2011.

[32] "Transmission System Map," BC Hydro, B.C., Canada, 2015.

[33] W. M. Strang *et al.*, "Distribution Line Protection Practices - Industry Survey Results," *IEEE Transactions on Power Delivery*, vol. 10, no. 1, pp. 176–186, Jan. 1995, doi: 10.1109/61.368400.

[34] "Distribution Feeder Protection." General Electric Grid Solutions, [Online]. Available: https://www.gegridsolutions.com/multilin/resource/feeder/uniflip_publication/document.pdf.

[35] E. Agneholm and J. Daalder, "Cold load pick-up of residential load," *Transmission and Distribution IEE Proceedings - Generation*, vol. 147, no. 1, pp. 44–50, Jan. 2000, doi: 10.1049/ip-gtd:20000058.

[36] C. Hachmann, G. Lammert, L. Hamann, and M. Braun, "Cold load pickup model parameters based on measurements in distribution systems," *IET Generation, Transmission & Distribution*, vol. 13, no. 23, pp. 5387–5395, Oct. 2019, doi: 10.1049/iet-gtd.2018.6524.

[37] R. Wilde, "The Effects of Cold Load Pickup on Distribution Transformers," *IEEE Trans. on Power Apparatus and Syst.*, vol. PAS-100, no. 5, pp. 2433–2437, May 1981, doi: 10.1109/TPAS.1981.316768.

[38] F. Edstrom, J. Rosenlind, P. Hilber, and L. Soder, "Modeling Impact of Cold Load Pickup on Transformer Aging Using Ornstein-Uhlenbeck Process," *IEEE Transactions on Power Delivery*, vol. 27, no. 2, pp. 590–595, Apr. 2012, doi: 10.1109/TPWRD.2012.2185521.

[39] C. Ucak and A. Pahwa, "An analytical approach for step-by-step restoration of distribution systems following extended outages," *IEEE Transactions on Power Delivery*, vol. 9, no. 3, pp. 1717–1723, Jul. 1994, doi: 10.1109/61.311189.

[40] D. Higham, "An Algorithmic Introduction to Numerical Simulation of Stochastic Differential Equations," *SIAM Review*, vol. 43, pp. 525–546, Sep. 2001, doi: 10.1137/S0036144500378302.

[41] D. Athow and J. Law, "Development and applications of a random variable model for cold load pickup," *IEEE Transactions on Power Delivery*, vol. 9, no. 3, pp. 1647–1653, Jul. 1994, doi: 10.1109/61.311198.

[42] P. S. Dolan, M. H. Nehrir, and V. Gerez, "Development of a Monte Carlo based aggregate model for residential electric water heater loads," *Electric Power Systems Research*, vol. 36, no. 1, pp. 29–35, Jan. 1996, doi: 10.1016/0378-7796(95)01011-4.

[43] C. J. Mozina, "Impact of Smart Grids and Green Power Generation on Distribution Systems," *IEEE Transactions on Industry Applications*, vol. 49, no. 3, pp. 1079–1090, May 2013, doi: 10.1109/TIA.2013.2253292.

[44] G. Pepermans, J. Driesen, D. Haeseldonckx, R. Belmans, and W. D'haeseleer, "Distributed generation: definition, benefits and issues," *Energy Policy*, vol. 33, no. 6, pp. 787–798, Apr. 2005, doi: 10.1016/j.enpol.2003.10.004.

[45] K. D. Brabandere, K. Vanthournout, J. Driesen, G. Deconinck, and R. Belmans, "Control of Microgrids," in *2007 IEEE Power Engineering Society General Meeting*, Jun. 2007, pp. 1–7, doi: 10.1109/PES.2007.386042.

[46] H. Kuang, S. Li, and Z. Wu, "Discussion on advantages and disadvantages of distributed generation connected to the grid," in *2011 International Conference on Electrical and Control Engineering*, Sep. 2011, pp. 170–173, doi: 10.1109/ICECENG.2011.6057500.

[47] Working Group C6.22, *Microgrids 1 Engineering, Economics & Experience*. CIGRE, 2015.

[48] C. Marnay *et al.*, "Microgrid Evolution Roadmap," in *2015 International Symposium on Smart Electric Distribution Systems and Technologies (EDST)*, Sep. 2015, pp. 139–144, doi: 10.1109/SEDST.2015.7315197.

[49] M. Farrokhabadi *et al.*, "Microgrid Stability Definitions, Analysis, and Examples," *IEEE Transactions on Power Systems*, vol. 35, no. 1, pp. 13–29, Jan. 2020, doi: 10.1109/TPWRS.2019.2925703.

[50] P. Mahat, Zhe Chen, and B. Bak-Jensen, "Review of islanding detection methods for distributed generation," in *2008 Third International Conference on Electric Utility Deregulation and Restructuring and Power Technologies*, Apr. 2008, pp. 2743–2748, doi: 10.1109/DRPT.2008.4523877.

[51] A. Khamis, H. Shareef, E. Bizkevelci, and T. Khatib, "A review of islanding detection techniques for renewable distributed generation systems," *Renewable and Sustainable Energy Reviews*, vol. 28, pp. 483–493, Dec. 2013, doi: 10.1016/j.rser.2013.08.025.

[52] C. R. Reddy, B. S. Goud, B. N. Reddy, M. Pratyusha, C. V. V. Kumar, and R. Rekha, "Review of Islanding Detection Parameters in Smart Grids," in *2020 8th International Conference on Smart Grid (icSmartGrid)*, Jun. 2020, pp. 78–89, doi: 10.1109/icSmartGrid49881.2020.9144923.

[53] E. Abbasi *et al.*, "Typical Canadian Medium Voltage Benchmark Network Model for Integration of Distributed Energy Resources," presented at the 2016 CIGRÉ Canada Conference, Vancouver, Canada, Oct. 2016.

[54] S. H. Horowitz and A. G. Phadke, *Power System Relaying*. John Wiley & Sons, 2013.

[55] J. Horak, "Directional overcurrent relaying (67) concepts," in *59th Annual Conference for Protective Relay Engineers, 2006.*, Apr. 2006, p. 13 pp.-, doi: 10.1109/CPRE.2006.1638701.

[56] “IEEE Standard Electrical Power System Device Function Numbers, Acronyms, and Contact Designations,” *IEEE Std C37.2-2008 (Revision of IEEE Std C37.2-1996)*, pp. 1–48, Oct. 2008, doi: 10.1109/IEEESTD.2008.4639522.

[57] “IEEE Recommended Practice for Implementing an IEC 61850-Based Substation Communications, Protection, Monitoring, and Control System,” *IEEE Std 2030.100-2017*, pp. 1–67, Jun. 2017, doi: 10.1109/IEEESTD.2017.7953513.

[58] A. Oudalov and A. Fidigatti, “Adaptive network protection in microgrids,” *Int. Journal of Distributed Energy Resources*, vol. 5, pp. 201–226, Jan. 2009.

[59] K. A. Wheeler, S. O. Faried, and M. Elsamahy, “A microgrid protection scheme using differential and adaptive overcurrent relays,” in *2017 IEEE Electrical Power and Energy Conference (EPEC)*, Oct. 2017, pp. 1–6, doi: 10.1109/EPEC.2017.8286150.

[60] M. R. Islam and H. A. Gabbar, “Analysis of Microgrid protection strategies,” in *2012 International Conference on Smart Grid (SGE)*, Aug. 2012, pp. 1–6, doi: 10.1109/SGE.2012.6463969.

[61] S. Chowdhury, S. P. Chowdhury, and P. Crossley, *Microgrids and Active Distribution Networks*. The Institution of Engineering and Technology, 2009.

[62] “IEEE Guide for Design, Operation, and Integration of Distributed Resource Island Systems with Electric Power Systems,” *IEEE Std 1547.4-2011*, pp. 1–54, Jul. 2011, doi: 10.1109/IEEESTD.2011.5960751.

[63] W. Huang, “A practical guide of troubleshooting IEC 61850 GOOSE communication,” in *2017 70th Annual Conference for Protective Relay Engineers (CPRE)*, Apr. 2017, pp. 1–8, doi: 10.1109/CPRE.2017.8090009.

[64] M. Van Rensburg, D. Dolezilek, and J. Dearien, “Case Study: Using IEC 61850 Network Engineering Guideline Test Procedures to Diagnose and Analyze Ethernet Network Installations,” presented at the PAC World Africa Conference, Johannesburg, South Africa, Nov. 2015.

[65] O. Rintamaki and K. Kauhaniemi, “Applying modern communication technology to loss-of-mains protection,” in *CIRED 2009 - 20th International Conference and Exhibition on Electricity Distribution - Part 1*, Jun. 2009, pp. 1–4, doi: 10.1049/cp.2009.0966.

[66] I. Maqsood, M. R. Khan, G. H. Huang, and R. Abdalla, “Application of soft computing models to hourly weather analysis in southern Saskatchewan, Canada,” *Engineering Applications of Artificial Intelligence*, vol. 18, no. 1, pp. 115–125, Feb. 2005, doi: 10.1016/j.engappai.2004.08.019.

[67] Government of Canada, “Canadian Climate Normals 1981 to 2010 - Saskatoon Diefenbaker Int’l A. Station,” Sep. 25, 2013. https://climate.weather.gc.ca/climate_normals/index_e.html (accessed Jan. 14, 2021).

[68] Natural Resources Canada, “Electricity Facts,” Oct. 06, 2017. https://www.nrcan.gc.ca/science-data/data-analysis/energy-data-analysis/energy-facts/electricity-facts/20068 (accessed Jan. 31, 2021).

[69] Saskpower, “2021 Power Supply Rates.” https://www.saskpower.com/Accounts/Power-Rates/Power-Supply-Rates (accessed Jan. 31, 2021).

APPENDIX A

STATISTICAL DATA FOR PHYSICAL COMPONENTS

Table A.1. Typical parameters for space heating load **[22]**

Variable	Name	Unit	Mean	Standard Deviation
Q_{sh}	Total heating Capacity	kW	12	n/a
$1/R_b$	Building Equivalent Thermal Conductance	$kW/°C$	0.121	0.032
R_bC_b	Building Equivalent Time	h	30.63	5
ΔT	Thermostat Deadband	$°C$	0.55	n/a
$T_{setpoint-day}$	Thermostat Setpoint during the day	$°C$	19.4	0.55
$T_{setpoint-night}$	Thermostat Setpoint during the night	$°C$	18.3	0.55

Table A.2. Typical parameters for water heating load **[22]**

Variable	Name	Unit	Mean	Standard Deviation
Q_{sh}	Total heating capacity	kW	4.5	n/a
$1/R_{wh}$	Water equivalent thermal conductance	$kW/°C$	0.0027	n/a
C_{wh}	Water heater equivalent thermal mass	$kWh/°C$	0.351	n/a
ΔT_{wh}	Thermostat deadband	$°C$	1.11	n/a
T_{ref}	Water heater thermostat Setpoint	$°C$	65	n/a
N_u	Average number of hot water usage per day (for W_D(t) calculation)	-	11.27	4.14
V_{24}	Mean daily water consumption (for W_D(t) calculation)	l	200	62.9

APPENDIX B

DATA FOR ELECTRICAL AND CONTROL COMPONENTS

Table B.1. Loads for the MV benchmark network.

Node	**3**	**4**	**5**	**6**	**7**	**8**
Single Phase (kVA)	A: 81	A: 212 C: 306	A: 361	A: 137 B: 80 C: 44	-	A: 191 C: 186
Three Phase (kVA)	492	784	1981	226	1329	176
Node	**9**	**10**	**11**	**12**	**13**	**14**
Single Phase (kVA)	-	B: 61	-	-	-	B: 119
Three Phase (kVA)	2459	1071	927	688	336	370

Table B.2. Electrical and Mechanical Data for the Synchronous Machine.

Parameter	**Unit**	**Value**	**Parameter**	**Unit**	**Value**
Rated Power	MVA	6	X'_d	p.u.	0.345
Rated Voltage	kV	13.8	X'_q	p.u.	0.70
# of poles	-	4	T'_{d0}	s	4.17
Frequency	Hz	60	T'_{q0}	s	1.20
Inertia Constant	s	3.12	X''_d	p.u.	0.264
X_d	p.u.	1.236	X''_q	p.u.	0.211
X_q	p.u.	0.75	T''_{d0}	s	0.03
X_l	p.u.	0.155	T''_{q0}	s	0.19

Table B.3. Governor control parameters (IEEEG3).

Parameter	Variable	Unit	Value
Gate servomotor time constant	T_G	s	0.2
Pilot servo valve time constant	T_P	s	0.05
Dashpot time constant	T_R	s	2
Water inertia time constant	T_W	s	0.5
Maximum gate speed (opening)	U_o	p.u./s	0.3
Maximum gate speed (closing)	U_c	p.u./s	-0.3
Maximum gate opening	P_{max}	p.u.	0.9
Minimum gate opening	P_{min}	p.u.	0
Permanent Droop	σ	p.u.	0.005
Temporary Droop	δ	p.u.	0.01
Turbine Coefficient	A_{11}	p.u.	1.3
Turbine Coefficient	A_{13}	p.u.	1.0
Turbine Coefficient	A_{21}	p.u.	1.0
Turbine Coefficient	A_{23}	p.u.	1.1

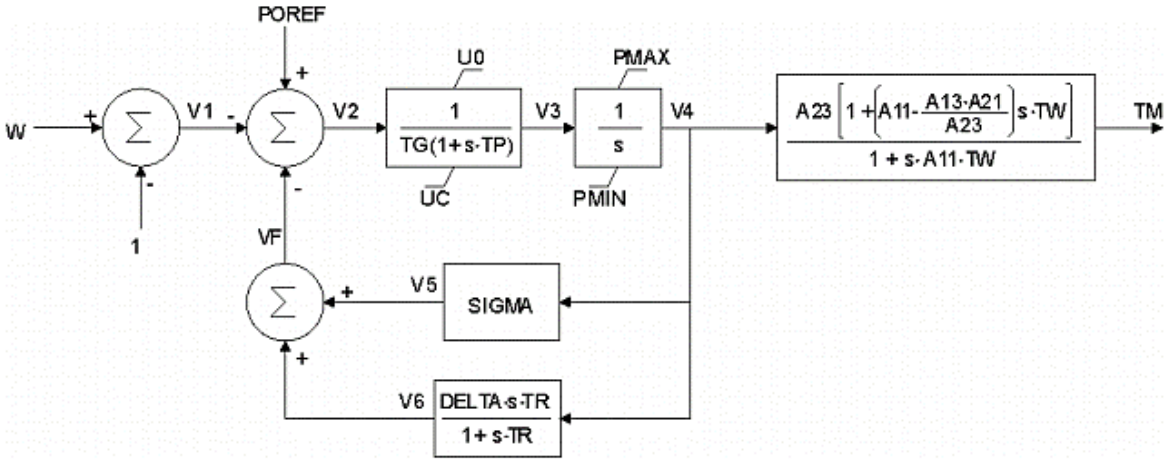

Figure B. 1. IEEEG3 Speed Governing Model

Table B.4. Exciter control parameters (SEXS).

Parameter	Variable	Unit	Value
Time Constant	T_A	s	0.2
Time Constant	T_B	s	0.05
Time Constant	T_E	s	2
Gain	K	-	0.5
Maximum field voltage output	E_{max}	p.u.	0.3
Minimum field voltage output	E_{min}	p.u.	-0.3

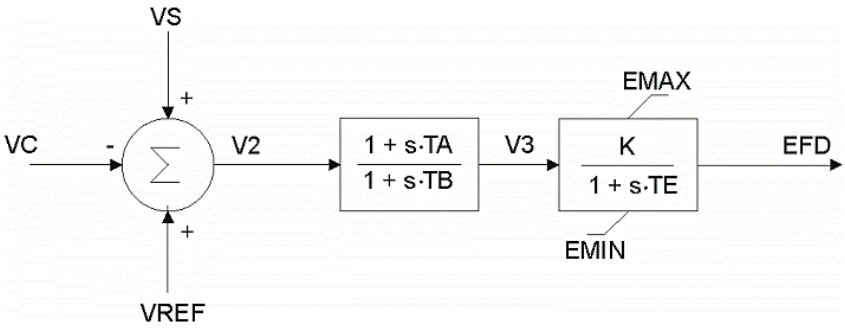

Figure B. 2. Simplified Excitation System (SEXS)

Table B.5. Power System Stabilizer parameters (PSS1A).

Parameter	Variable	Unit	Value
PSS Gain	K_S	-	2.7
Transducer time constant	T_R	s	0
Washout time constant	T_W	s	10
PSS signal conditioning frequency filter	A_1	p.u.	0
PSS signal conditioning frequency filter	A_2	p.u.	0
Lead/lag time constant	T_1	s	1
Lead/lag time constant	T_2	s	0.5
Lead/lag time constant	T_3	s	2
Lead/lag time constant	T_4	s	0.15

Table B.5. Power System Stabilizer parameters (PSS1A) (continued)

Parameter	Variable	Unit	Value
Maximum PSS voltage output	V_{stmax}	p.u.	0.9
Minimum PSS voltage output	V_{stmin}	p.u.	-0.9

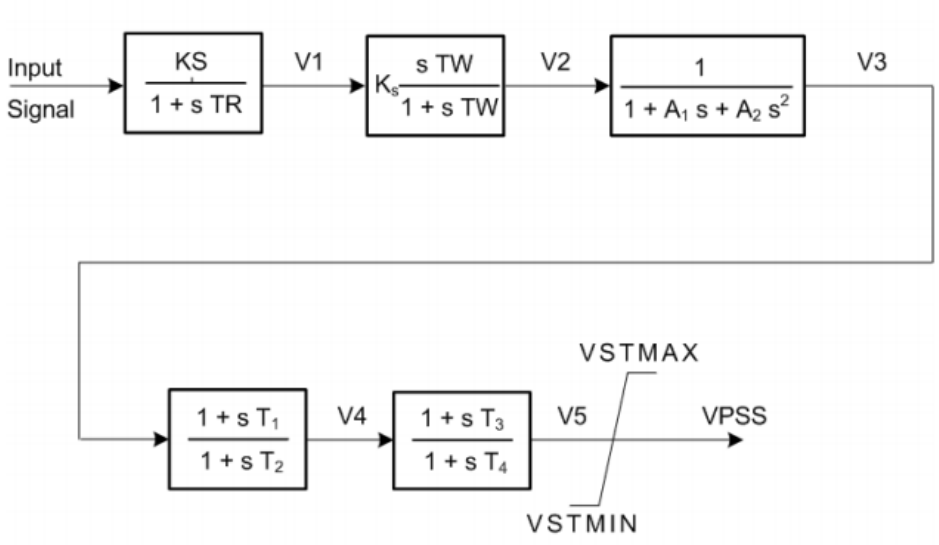

Figure B. 3. Power System Stabilizer PSS1.

APPENDIX C

PROTECTION SETTINGS

Table C.1. SET 1 – Protection settings for the grid-connected mode.

		FORWARD		**REVERSE**	
Device	**Function**	**Phase Setting**	**Ground Setting**	**Phase Setting**	**Ground Setting**
IED CB	51P/N	IEC VI - 0.10 I_{pkp}: 550 A	IEC INV - 0.20 I_{pkp}: 225 A	ANSI STI – 1 I_{pkp}: 5 A	ANSI STI – 1 I_{pkp}: 10 A
	50P/N	I_{inst}: 2800A t_{delay}: 0.05 s	I_{shtime}: 1500 A t_{delay}: 0.2 s I_{inst}: 1800 A t_{delay}: 0.05 s	n/a	n/a
IED RCL1	51P/N	ANSI VI - 1 I_{pkp}: 450 A	ANSI INV - 2 I_{pkp}: 200 A	ANSI VI – 2 I_{pkp}: 50 A	IEC VI – 0.4 I_{pkp}: 25 A
	50P/N	I_{inst}: 2500 A t_{delay}: 0.05 s	n/a	n/a	n/a
IED PCC	51P/N	ANSI STEI - 0.4 I_{pkp}: 100 A	IEC INV - 0.05 I_{pkp}: 45 A	ANSI STI-5 I_{pkp}: 160 A	ANSI INV-3 I_{pkp}: 70 A
	50P/N	n/a	n/a	n/a	I_{inst}: 700 A t_{delay}: 0.30 s
IED µGCB	51P/N	n/a	n/a	ANSI STI-6 I_{pkp}: 200 A	IEC INV-0.3 I_{pkp}: 100 A
	50P/N	n/a	n/a	I_{inst}: 800 A t_{delay}: 0.05 s	I_{inst}: 900 A t_{delay}: 0.15 s

Table C. 2. SET 2 – Protection settings for the microgrid island mode.

Device	**Function**	**Phase Setting**	**Ground Setting**
IED μGCB	51P/N	ANSI INV - 1 I_{pkp}: 160 A	ANSI STI - 5 I_{pkp}: 60 A
	50P/N	I_{inst}: 1100 A t_{delay}: 0.05 s	n/a
IED PCC	51P/N	ANSI STI - 1 I_{pkp}: 125 A	ANSI STI - 1 I_{pkp}: 60 A
	50P/N	n/a	n/a